Charge Transport Properties in Disordered Organic Semiconductors: Monte Carlo Simulation

Seyfan Kelil

Dissertation Submitted to the Graduate Programs
In Partial Fulfillment of the Requirements
For the Degree of Doctor of Philosophy in Physics

College of Natural and Computational Sciences
Department of Physics
University of Addis Ababa
Addis Ababa, Ethiopia

Addis Ababa University
School of Graduate Studies
College of Natural and Computational Science
Department of Physics

The undersigned hereby certify that they have read and recommend to the School of Graduate Studies for acceptance a thesis entitled "**Charge Transport Properties in Disordered Organic Semiconductors: Monte Carlo Simulation**" by **Seyfan Kelil** in partial fulfillment of the requirements for the degree of **Doctor of Philosophy in Physics**.

Dated: June 2021

Approved by the Examination Committee:

	Name	Signature	Date
Advisor:	_____,	_____,	_____
Internal Examiner:	_____,	_____,	_____
External Examiner:	_____,	_____,	_____
Chairman:	_____,	_____,	_____

ADDIS ABABA UNIVERSITY

Date: **June 2021**

Author: **Seyfan Kelil**

Title: **Charge Transport Properties in Disordered Organic Semiconductors: Monte Carlo Simulation**

Department: **Physics**

Degree: **Ph.D.** Convocation: **June** Year: **2021**

Signature of Author

For those family and friends of mine who have unlimited potential but can not attend the school.

Table of Contents

List of Figures

List of Publications and Presentations

A. Articles in Professional Journals

1. Effects of localization length and spatial disorder on a charge carrier mobility in organic disordered semiconductors

   Seyfan Shukri and Lemi Deja AIP Advances 11, 095118 (2021) https://doi.org//10.1063//5.0061868 (Published)

2. Charge carriers density, temperature and electric field dependence of the charge carrier mobility in disordered organic semiconductors in low density region.

   Seyfan kelil Shukri and Lemi Demeyu Deja Condensed Matter condensedmatter-1408725 (Accepted for Publication)

B. Presentations at Professional Meetings

1. Seyfan Kelil and Lemi Demeyu, The effect of electric field on charge transport in disordered organic semiconductors: Monte Carlo simulation, Ethiopian Physical Society (EPS) Annual Conference, Adama, 15 – 16 February, 2019.

2. Seyfan Kelil and Lemi Demeyu, Charge Transport Properties in Disordered Organic Semiconductors: Monte Carlo Simulation, Eastern Africa School on Electronics Structure Methods and Application, Addis Ababa, 1 – 5 July, 2019

3. Seyfan Kelil and Lemi Demeyu, The Effect of Spatial Disorder on Charge Transport in Disordered Organic Semiconductors: Monte Carlo Simulation, Regional

African School of Electronic Structure Methods and Applications (RASESMA) with ABINT, Kigali, Rwanda, 27– 31 January, (2020).

Acknowledgements

First of all, I would like to thank my advisor Dr. Lemi Demmeyu for helping me since we began working together. Thanks for being always a great source of ideas, open to discussion, and helping me to do better. I would also like to thank Dr. Mulugeta Bekele and Dr. Tatek Yergou for their comments and suggestions during the seminar and progress report presentation.

I would also like to acknowledge the International Program in Physical Science (IPPS), at Uppsala University, for their support computing facilities at our laboratory and providing financial support for participating in schools of Complex quantum systems out of equilibrium in many-body physics and beyond which held in Yerevan (Armenia) on June 3 to 7, 2019 and Regional African School of Electronic Structure Methods and Applications (RASESMA) with ABINT which held in Kigali (Rwanda) on January 27 to 31, (2020). I am also thankful to JigJig University for their sponsorship to study at Addis Ababa University (AAU). Finally, I would like to thank Addis Ababa University (AAU) for providing financial support for the study.

My heartfelt gratitude goes to my wife, Semira Negash Gemechu, and sweet daughters, Wania Seyfan and Dania Seyfan, for their endless wishes to my success and extensive moral throughout my study. Special acknowledgment is also extended to my friend Kelil Aliy who helped me a lot, especially in commenting on this work for providing some material for this study and financial support.

A special thanks to my family. Words can not express how grateful I am to Kelil Shukri, Mulu Bekele, Negash Gemechu, Sunsuna Tola, and Abdi Kelil.

Finally, I would like to thank a statistical and computational group of Addis Ababa University especially Dr. Solomon Negash, Dr. Anley Gisese, Mesay Tilahun, Fikre Jida, and Dr. Tolossa Dima. I could not think this dissertation finished without you.

Abstract

In this thesis, we have used a Monte Carlo simulation technique to study the charge carrier mobility as a function of charge carrier density and electric field in disordered organic semiconducting materials using the lattice model. Our simulations reveal that the charge carrier mobility versus charge carrier density at lower charge carrier density and disorder is constant. In contrast, at higher disordered and lower charge carrier density, the charge carrier mobility increases with charge carrier density. Therefore, the effect of the disorder parameter ($\hat{\sigma} = \frac{\sigma}{k_B T}$) on the charge carrier mobility is more pronounced than the charge carrier density at lower charge carrier density. We studied a charge carrier mobility as a function of the electric field for the case of the regular grid and spatial disorder lattice site with different lattice site spacing parameter r and the ratio of localization length to the lattice parameter (i. e, α/b). We show that a charge carrier mobility increases with an electric field for the case of the regular grid and spatial disorder lattice site of lower or equal values of lattice site spacing r to the ratio of α/b. But, at a higher value of lattice site spacing r to the ratio of α/b, the electric field dependence of charge carrier mobility for spatial disordered lattice sites differs from that of the regular grid case. We observed that both a localization length and lattice parameter are relevant for the electric field variation of charge carrier mobility in both the regular grid and spatial disordered lattice sites at lower or equal values of lattice site spacing r to the ratio of α/b cases. However, at higher values of the lattice site spacing r relative to the ratio of α/b, the only parameter

responsible for the electric field dependence of charge carrier mobility is the localization length of disordered organic semiconducting materials.

Chapter 1

Introduction

1.1 Conjugated polymers

1.1.1 History

A polymer is a substance composed of molecules characterized by multiple repetition of one or more species of atoms or groups of atoms (constitutional repeating units) linked to each other in amounts sufficient to provide a set of properties that do not vary markedly with the addition of one or a few of the constitutional repeating units. Each repeating unit is known as a monomer. A molecule with only a few constitutional repeating units is called an oligomer or small molecule. Unlike a polymer the physical properties of an oligomer vary with the addition or removal of one or a few constitutional repeating units to or from its molecule. Organic polymers can, in general, be classified as saturated and unsaturated on the basis of the number and type of the carbon valence electrons involved in the chemical bonding between consecutive carbon atoms and other neighboring atoms along the main chain of the polymers. In the case when all the four valence electrons are involved in valence bonding the polymers are classified as saturated, whereas in the case when only three of the four carbon valence electrons are involved in covalent bonding the polymers are classified as unsaturated [1]. Since all the four valence electrons of the carbon atoms are used up in covalent bonds the saturated polymers are insulators which are classified as synthetic polymers [2, 3]. Because of this, polymers were considered uninteresting from

the point of view of electronic materials prior to the discovery of conducting polymers, despite their use for insulating electric current conducting wires. Their mechanical and chemical properties had also been used mainly for industrial purposes.

The main research had focused on such ordinary polymers until 1960s. After that their suitability for electronic applications gaind increasing attention. The first observations of electric conduction in organic materials dated back by more than half a century and were first made on crystals of small organic molecules [4–9] and later on small organic molecules embedded in a polymer matrix [10]. A very important step forward in the field of organic conducting polymers was made by accident after 1960s. In the early 1970s Hideki Shirakawa of the Tokyo Institute of Technology was working to make the organic polymer from polyacetylene gas. However, during an experiment a visiting student, supervised by Shirakawa, by mistake added thousand times more catalyst than that was normally used. The result was not the usual polymer, but a peculiar stretchable film, the simplest conjugated polymer, which was not electrically conductive. After sometime the metallic reflective film inspired the interest of Alan G. MacDiarmid, who visited the Tokyo Institute of Technology to give lectures, whether it could be used as a possible candidate for his goal to make a nonmetallic electrical conducting substance, a "synthetic metal". For the accomplishment of his purpose and also further studies on the fortuitous result, he invited Shirakawa to work at the University of Pennsylvania, and so Shirakawa joined the group of Alan G. MacDiarmid and Alan J. Heeger in 1976. This group have shown major breakthrough in the area of conducting polymers which occurred later in 1977 when iodine or arsenic pentafluoride was doped to an intrinsically insulating organic polymer, polyacetylene. And it was discovered that polyacetylene, which has an intrinsic conductivity lower than $10^{-5}\ \Omega^{-1}cm^{-1}$, could be made highly conducting of conductivity $\sim 10^{3}\ \Omega^{-1}cm^{-1}$, by doping it with acceptors such as iodine or arsenic pentafluoride [11]. It was also found that polyacetylene can be doped with donors usually alkali metals and that conductivities larger than $100\ \Omega^{-1}cm^{-1}$ were obtained [11, 12]. Allan J. Heeger,

Alan G. MacDiarmid, and Hideki Shirakawa [13] received the Nobel Prize in chemistry in 2000 for the discovery of electrical charge–carrier transport in conjugated polymers in 1977 and the development of these conducting polymers [11, 14]. Following the discovery mentioned above many other conducting polymers such like polythiophene (PTh) and poly(para-phenylene vinylene) [PPV] were prepared. This discovery induced a lot of research and especially the interest revived at the end of the 1980s as a result of the demonstration of high performance electroluminescent organic multi-layer structures of vacuum-sublimed dye films [15,16]. Moreover, the discovery of electro luminescence (EL) from diodes based on the conjugated polymer poly(para-Phenylene Vinylene) (PPV) [17] initiated a lot of activities in the field of conjugated polymers, certainly because of the commercial applications. The first established electronic application of organic materials was xerography [18]. The main advantages of conjugated polymers over inorganic semiconductors are their flexibility, light weight and ease of processability. Although a number of problems associated with organic transistors remain to be solved, it now appears increasingly likely that organic thin film transistors will find use in a range of commercial, industrial, and military applications. Such applications might include flexible flat panel displays, smart cards, smart inventory tags, supermarket shelf-edge labels, and intelligent sensory arrays.

1.1.2 Electronic structure of conjugated polymers

The π-conjugated organic materials are either small molecules or polymers. Ideally, conjugated polymers are infinitely long linear systems regularly built from repeat units containing π electrons extended along the infinite length of the chain [19]. The chemical structure of some of the most studied conjugated polymers; polyacetylene, poly(para-phenylene vinylene) [PPV], polythiophene and that of the small molecule pentacene are displayed in Figure 1.1.

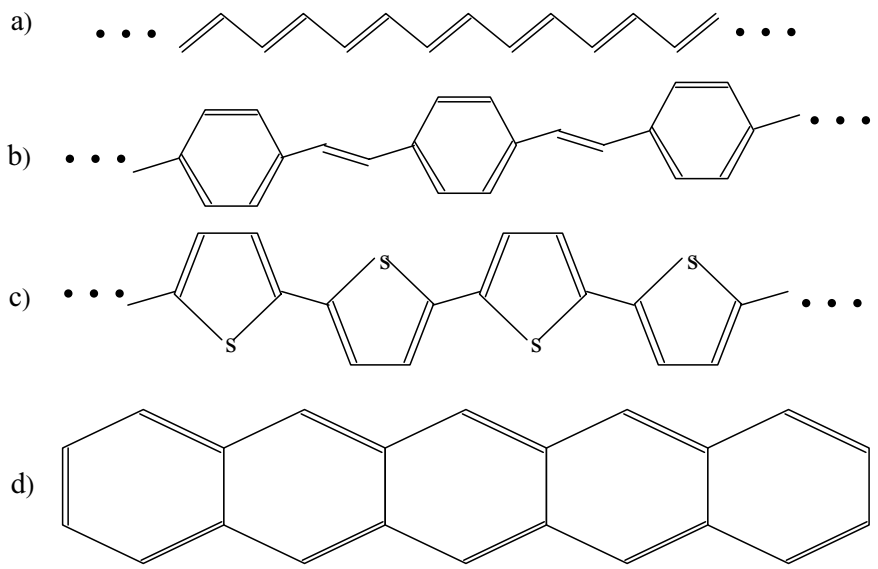

Figure 1.1: Chemical structure of some common conjugated polymers: a) polyacetylene, b) poly(para-phenylene vinylene) [PPV], c) polythiophene, and d) the small molecule pentacene.

Polyacetylene is the simplest and first studied classic example of conjugated polymers. Poly(para-phenylene vinylene) was the active material used in the first polymer light-emitting diodes [17]. The soluble derivatives of PPV, which can be spin cast from organic solutions, are well studied and widely used materials due to their suitability for various applications. Polythiophenes exhibit broad optical absorption and high conductivity. Substituted polythiophenes such as poly(3-hexylthiophene) [P3HT] have been used to build efficient electronic devices. The small molecule Pentacene is widely used in organic thin-film transistors [20]. It is a family of molecules described by the standard formula $C_{4n+2}H_{2n+4}$, where $n = 1, 2, 3, 4, 5$ correspond to benzene, naphtalene, anthracene, tetracene and pentacene molecules.

We mentioned in the previous section that the main building block of organic polymers is carbon atom. We also mentioned that the electronic properties of the polymers are determined on the basis of the number of valence electrons involved in bonding the carbon

atom with other carbon atoms and other elements in the neighbors. Carbon atom has six electrons of electric configuration $[1s^2 2s^2 2p^2]$. The four outer electrons participate in the bonding but the two inner ones do not participate in the bonding. The number of electrons on p orbitals used in the hybridization process determine the type of polymer and its chemical as well as structural properties. In simple compounds like methane, CH_4 or ethane, C_2H_6 experimental evidence shows that the properties of 2s electrons are similar to that of the 2p electrons. This is justified by thinking that one of the 2s electrons is promoted to a 2p state by taking up some energy, then the 2p orbitals and the remaining 2s orbital create four tetrahedral equal orbits and form sp^3 hybrids. The energy required for this hybridization is compensated by the energy gained while forming tetrahedral bonds. Each hybridized orbital contains a single unpaired electron, which can pair with a single 1s electron from hydrogen to form a bond known as σ bond. Here, all the outer electrons of the carbon atom are used up in bonding. It is also possible for one s and two p orbitals to form three sp^2 hybridization which are planar trigonal orbitals. The sp^1 is also another type of hybridization from one s and one p orbitals. We can consider a simple hydrocarbon, for instance ethylene, C_2H_4 and describe sp^2 hybrids. In ethylene each Carbon forms three σ bonds with sp^2 hybrids with the other carbon and two hydrogen. One more electron left over on each carbon atom orbits in the vertical plane as shown in Figure (1.2). These electrons are not independent of each other and form a looser bond known as a π bond. In ethylene double line between the two carbon atoms known as a double bond signifies a σ bond and a π bond. Similarly we can consider another simple hydrocarbon, for instance, acetylene C_2H_2 has two sp^1 hybrids on each carbon and form σ bonds that link it to the other carbon and one hydrogen. The two electrons left over on each carbon atom form two π bonds which together with the σ bond form triple bond between carbon atoms. The two electrons in the single π bond of ethylene are coupled, and results in the energy levels split. The lower energy state is called a bonding state and the higher one is an antibonding state. The lower energy state

is occupied and the higher one is empty under normal conditions. When there are more double bonds in a molecule each energy levels split further.

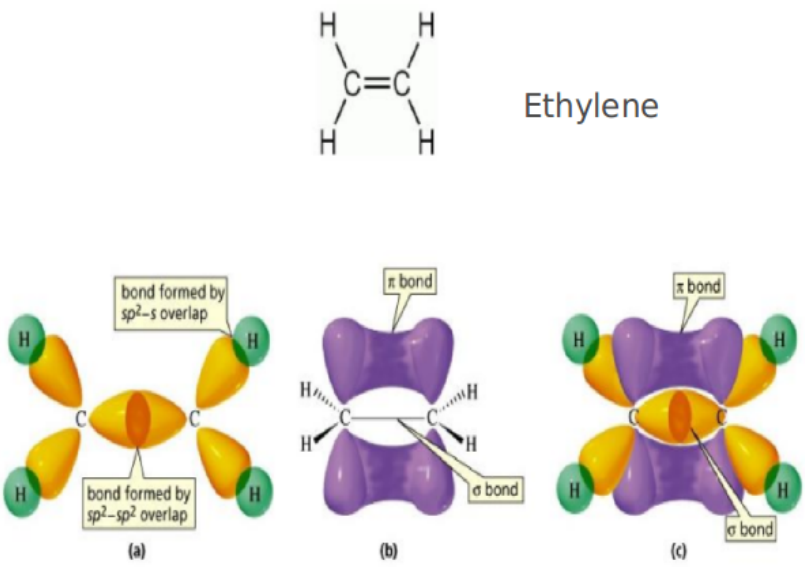

Figure 1.2: Example of the formation of σ and π bonds in the small organic molecule of Ethylene (Top). (a) The bonds formed for each carbon atom in the molecule. Each carbon atom shares sigma bond with each other and with its 2 neighboring hydrogen atoms. (b) The π bond forms double bonds between carbon atoms together with σ bond. (c) The total bonds in the molecule. [Pictures taken from Socratic.org.]

In electrically insulating polymers all the four valence electrons of the carbon atom form four sp^3 hybrids which form σ bonds with each of other four atoms in the neighbors. On the other hand, in unsaturated polymers the four outer electrons form three sp^2 hybrids which are involved in σ bonding, and one π electron which orbits perpendicular to the plane formed by σ bonds. The orbital of π electron is called p_z orbital since this orbit is in the vertical plane while the σ bonds are in the horizontal plane. This electron is not independent of another π electron and form a looser bond known as π bond but σ bonds are stable and determine the structural backbone of the molecule. The π bond is weaker than the σ bond because the overlap of the p_z wave functions of the adjacent carbon atoms is small. The two electrons in the single π bond of ethylene are coupled,

hence the energy levels split. The lower energy state is called a bonding state and the higher is an antibonding state. The lower energy state is occupied and the higher one is empty under normal conditions. When there are more double bonds in a molecule each energy levels split further. In benzene and pentacene there are three and five double bonds which will cause three-fold and five-fold splits.

In polyacetylene each carbon is σ bonded to only two neighboring carbons and one hydrogen atom leaving one unpaired π electron on each carbon atom. If the carbon-carbon bond lengths were equal, the chemical formula, $(-CH)_n$ with one unpaired electron per formula unit, would imply a metallic state. However, in real polyacetylene, the structure is dimerised as a result of the Peierls instability with two carbon atoms in the repeat unit, $(-CH = CH)_n$ as shown in Figure 1.1. In this structure, $(-CH =)_n$, single and double bonds alternate. Polymers with such structures are known as conjugated polymers. This means that the π bond between one of the two adjacent carbons add one single bond between one of two adjacent carbons alternately and realizes the formation of single and double bond-alternate structure known as conjugated polymers or oligomers as shown for some of them in Figure 1.1. Each energy level of π bond splits into that at π and π^* states and since there are many double bonds in conjugated polymers band structure consisting of bonding states or lower energy band and an antibonding states or higher energy band are formed. As each bond can hold two electrons per atom (spin up and spin down), each orbital in the π band is filled with two electrons of antiparallel spin and that of the π^* band is empty under normal conditions. The energy difference between the lowest unoccupied molecular orbital (LUMO) in the π^* band and the highest occupied molecular orbital (HOMO) in the π band is the π-π^* energy gap known as a band gap [21] usually denoted by (E_g). The π and π^* orbitals are referred as frontier orbitals that play a decisive role both in chemical activation and optoelectronic properties of conjugated polymers. The electrons can be excited from occupied orbitals to unoccupied orbitals with the absorption of energy equal to the energy difference between the two orbitals. The band gap energy

is the same as the minimum energy required to excite electrons from HOMO to LUMO. Consequently, since there are no partially filled bands, conjugated polymers are typically semiconductors. All conjugated polymeric materials have large conjugated units, i.e., regions with resonant single and double bonds, which determine their conduction and valence energy levels and thus their energy gaps.

Several conjugated polymers including the most studied one are insoluble or do not dissolve in common solvents. However, the addition of side chains to the main chain of the conjugated polymers induce the solubility and also ease the formation of chain packing in the solid films. Electronic excitation for a molecule that contains π-electron generally requires only a modest amount of energy, typically 1 to 3 eV. Thus the corresponding optical absorptions occur in the visible range and the band gap of conjugated polymers is within the semiconductor range of 1.5 to 3.5 eV [22] which covers the whole range from infrared to ultraviolet region. The thermal activation of charge carriers from HOMO to LUMO states is negligible and because of this a pure undoped organic film is insulator. If undoped, they have, therefore, essentially no free charge carriers and considered as a material of high-resistivity or of low conductivity ($\sigma \leq 10^{-8} Scm^{-1}$) at room temperature [23] except for trans-PA which has conductivity $\sigma \leq 10^{-5} Scm^{-1}$ [14, 24]. The high-resistivity one could possibly find applications particularly in electronics or optoelectronic provided that free charge carriers are introduced into it either from metal-conjugated polymer contacts, by doping, or by exciting electrons from HOMO to LUMO by optical absorption. A free charge carrier refers to an additional electron in an antibonding orbital or one that is removed from a bonding orbital. In general, polymeric material can have importance from the point of view of electrical conduction only if free charge carriers are introduced into it and thereby conductivity is enhanced. The mechanism by which the charge carriers, either holes or electrons, are added to the HOMO of the π band and the LUMO of π^* band, respectively, is known as doping. We will discuss the methods in which doping is accomplished in the next section.

A chain of conjugated polymers is held together by strong covalent bonds. On the other hand, the force that exists between molecular chains in a film is a week van der Waals attraction. Since the intermolecular van der Waals interaction is very weak, molecular crystals are usually soft and flexible. The flexibility character of the molecular chains of the film render it the structure of unstirred boiled spaghetti. Thin films of polymers are often formed by solution processing such as spin casting, which result in polycrystalline or amorphous solids with entangled long polymer chains. The entanglement among the chains increases the mechanical strength of the film. This property makes these films more robust than the crystalline films prepared from small molecules though their electrical properties are less compared to that of crystalline solids. In a solid the long polymer molecules are generally packed together non-uniformly and ends up in forming both crystalline and highly disordered amorphous domains. The amorphous regions are composed of coiled and tangled chains, whereas in crystalline regions linear polymer chains are oriented in a three dimensional matrix. The weak intermolecular van der Waals bonds give rise to a phonon related dynamical disorder even in perfect small molecule crystals. Consequently, this flexibility nature together with other chemical defects restrict the length of each chain of conjugated polymers in a film not to stretch indefinitely. Instead it makes twists or kinks that subdivide the polymer of the same physical chain into a number of conjugated segments and separate them. Also, these twists or kinks disrupt the π bonds and cause each segment to behave like a separate entity, and the molecular film to be considered as a collection of distinct molecular sites or chromophores. The mean length of these conjugation segments is known as a conjugation length. This means that the polymer chains can not be aligned over their wide length due to this disordered defect and as a result the localization length of a π-electron cloud is limited to a definite conjugation length. Random distribution of conjugation lengths in turn gives rise to a distribution of transition energies of the π-electrons. These conjugation length segments, bounded by an energy barrier created by the defects or kinks, have random distributions.

A charge carrier is then scattered with a mean free path that approaches the distance between adjacent sites. This means that besides other chemical effects the poor coupling between the molecules in the solid film leads to a strong localization of charge carriers on each conjugation length which may move coherently within the conjugation length, and conduction occurs via a sequence of charge transfer steps from one conjugation length to another similar to the hopping between defect states in inorganic semiconductors. As conjugation length is made longer, the electronic transition energies decrease.

A very simple model to verify this is to view a conjugated polymer chain as a sequence of finite conjugated boxes uncoupled electronically from one another and to consider only the unpaired π electrons of the carbon atoms in a one dimensional box. In such a model the polymer is characterized by a distribution of box lengths corresponding to conjugation lengths. If we neglect the interaction between charge carriers, we can approximately write the single particle energies of the electronic bands in a conjugated segment consisting of n monomers using H*ü*ckel theory as

$$\epsilon_n = 2\beta cos\frac{k\pi}{n+1}. \tag{1.1.1}$$

where k denotes the k-th level (or orbital) of the band, and β is the electronic transfer integral between two adjacent monomers. In the transport process we can assume that the hole (electron) charge carriers occupy the orbital with highest (lowest) energy, that is, the HOMO (LUMO) in each conjugated segment. Upon charge transfer between neighboring conjugated segments with different chain length, the energies of the donor and acceptor levels are therefore different. If the variation in chain lengths is random (within certain limits), the energies relevant for the transport process will also be random and related to the chain length in the following way:

$$\epsilon_{HOMO} = 2\beta cos\frac{\pi}{n+1}. \tag{1.1.2}$$

An electronic transfer integral between adjacent carbon sites in a conjugated system

is typically around 2.5 eV. Consequently, going from 20 to 40 monomers in the chain, the HOMO energy increases by 0.04 eV, which is a typical number for the spread in energies of the states involved in transport. The amorphous molecular film deposited by spin coating or evaporation has the surrounding polarization that varies spatially in a random fashion of the absolute values of the molecular energies. These energies are excited state energies [25] for both neutral and charged excited states and has a Gaussian distribution with a variance σ, a main parameter which designates the energetic disorder.

Therefore, the distribution of segment lengths results in the distribution of electron states, and the polymer chains are not aligned with each other over their whole length, but can align only in small crystal regions. The polymer chains may either extend through a number of crystallite regions or may be folded back on themselves within these regions. In either case, ordered crystallites are interconnected by amorphous regions. These different local arrangements modify the energies of the conjugated segments because of the variation of the electron polarizability and of local dipole interactions between neighboring chains [22]. This effect, combined with the distribution of segment lengths, broadens the electronic density of states by about 0.1-0.2 eV and results in localization of charge carriers [26], and because of this electronic conduction occurs by hopping of the carriers from one localized state to another. Thus to deal with the charge carriers transport in amorphous polymeric solids it is convenient to consider conjugated segments of the polymer chain as a randomly distributed chromophores and the interactions between them. The π electrons are delocalized over the individual conjugation length, but conductivity of the film largely depends on the transfer integral between neighboring conjugated segments that is strongly affected by the defects. Moreover, the numerous defects introduce a high density of trap states.

1.2 Doping of conjugated polymers

The term doping is used to refer a process of charge injection onto macromolecular chains. Or in a very general sense, any process that results in an addition of electrons in an antibonding orbitals or removal of electrons from a bonding orbital is said doping. It is a central process that can control the main electronic and optical properties of conjugated polymers over the full range from the insulator to metal since there are no free charge carriers on the molecular units of pristine organic solids under normal situation. There are different ways of accomplishing this process, and also corresponding important phenomena and applications. Some of these ways or mechanisms are: chemical doping, electrochemical doping, photo doping, and charge injection at a metal-conjugated polymer contact or interface.

Chemical doping of conjugated polymers is a process in which charge carriers are generated by an electron transfer from polymer chains to acceptor dopants which results in the formation of free holes or vice versa, that is electron transfer occurs from the donor dopant to the polymer chain in which free electrons are formed. The process also involves the associated insertion of counterions to maintain the over all charge neutrality, i.e., during the free hole formation (p-type doping) the polymer chain acts as a poly(cation) and during n-type doping the polymer chain acts as poly(anion). The doping can be carried out by exposure of the polymer to the vapor phase of an electron acceptor (such as iodine or AsF_5) or donor (such as the vapor phase of an alkali metal), by means of charge transfer in solution.

In the case of electrochemical doping, the polymer sample is a film deposited on one of electrodes of an electrochemical cell. Electrons are removed or added to the polymer electrochemically from the external circuits by controlling the electrical voltage between this electrode and the counter electrode; and therefore the doping level. Charge neutrality is maintained by ions that diffuse into (or out of) the polymer structure from the electrolyte to compensate the electronic charge; for example, Li metal can be used as another electrode with $Li^+ClO_4^-$ as electrolyte dissolved in a suitable solvent.

While increasing the density of charge carriers and thereby conductivity [27], however, both chemical and electrochemical doping are accompanied by an intercalation of anions or cations in between the polymer or oligomer chains [28–32]. These ions are too big to be inserted into the undoped polymer structure which is quite closely packed, and therefore structural changes are produced. The structural changes can include rotations or translations of the conjugated polymer chains, or both can be observed depending on the size of the intercalated ion. This effect weakens the interchain coupling. Also, these anions or cations create an electrical potential on the chains, which can shift and even modify the relative positions of the charge carrier levels. Essentially, the positions of the self-trapped carriers on the chains are determined by the position of the dopants.

In addition to that mentioned above the presence of counterions near the conjugated polymer chains can play a major role in various processes depending up on their arrangement with respect to the chains. In conjugated polymers since the covalent bonds form a one-dimensional structure, there are three possible cases. The first is the possibility for the dopants to form chains parallel to the polymer chain direction, or to form planes that separate planes of parallel polymer chains, or a third possibility is that a plane of mixed composition, consisting of alternating polymer chains and dopant linear stacks. In the third case the dopants distribution is so random that they can be strong source of disorder. In the first as well as the second cases the dopants separate the chains by layers and weaken the coupling between the chains of different layers that can lead to anisotropy in conductivity [28]. During doping, the amount of dopants in a sample increases progressively from zero to a maximum of one dopant for about two to three polymer repeat units. However, the ability to dope conjugated polymers or oligomers using especially chemical techniques is, in general, determined by a combination of the availability of its unoccupied space and the weak interchain forces that allow the diffusion of dopant ions between the chains.

For the resultant polymer dopant structure of case two, discussed above, iodine doped

with ordered pentacene film [27] is a good example provided that the doping level is not high [31, 32]; at the high doping level the dopants form planes between the layers and also form chains parallel to the chains of pentacene molecules. This means that at high level of doping the counterions are available in all directions between the chains of the host molecules. This has an effect of increasing the separations between the chains of the host molecules and decreasing the coupling between them and consequently degrades the conductivity. When the doping level has not reached the phase in which conductivity decreases (or when it is in the conductive phase) the iodine molecules are ionized to I_3^- anions with the total composition of $(PEN)I_{2.2}$. From this composition it is clear that the total number of iodine anions I_3^- (or anion chains) intercalated between the layers of pentacene molecules is less than the total number of pentacene molecules. Apparently, the number of pentacene molecules that are left uncharged is the same as the difference between the total numbers of pentacene molecules and anion chains. Thus, for equivalent or less doping level, the system achieves a thermodynamic equilibrium state with a certain distribution of holes over the total number of pentacene molecules and also a particular way of anions distribution.

Contrary to chemical and electrochemical doping, a charge carrier can be injected into the polymer film without introducing counterion into the film from metal-conjugated polymer contact and also by photo-absorption. Here electrons and holes can be injected from metallic contacts into the π^* and π bands of the polymer, respectively. This can be clearly explained in terms of injection in the polymer light-emitting diodes, thin-film transistors and solar cells.

The simplest conjugated polymer based light emitting-diode consists of a single polymer layer contacted by metal electrodes, one of which is transparent, on the top and bottom of the film. One electrode serves as an electron injecting contact and the other as a hole injecting contact. When a sufficient voltage bias is applied to the metal contacts, electrons and holes are injected into the LUMO of π^* and HOMO of the π bands of the

polymer, respectively. The injected electrons and holes, while drifting by the applied electric field in the opposite directions through the polymer, form both the singlet and triplet states of Frenkel excitons upon recombining on a conjugated segment of the polymer film. An exciton, a bound electron-hole pair, is said to be singlet if its spin is 0 and triplet if it is in a spin 1 state. Only the singlet state exciton decays by emitting light.

Conjugated polymer field-effect transistors are devices that consist of parallel plates of metal gate and conjugated polymer which are separated from each other by a thin sheet of dielectric material known as gate insulator. There are other two contacts between each of the two ends of polymer length and metal electrodes known as source and drain. When a bias is applied between the gate and source electrodes polarizing the later negatively, holes are injected into the polymer film from the source and gate contact. With an additional bias applied between the source and drain contacts a current flows laterally between these two contacts. The source to drain current is modulated by the gate voltage producing the field-effect transistors action.

The mechanism for the photovoltaic cell is the reverse of light-emitting diode. By photo absorption conjugated polymer locally losses electron and at nearby (it) gains hole or in other words electron-hole pairs are formed locally and also separated into free carriers depending upon the energy of excited electron. The process involves the generation of holes and electrons by a large optical absorption in the visible spectrum which are then followed by a transport of charges toward electrodes to produce a current.

Thus, as discussed above doping is a common feature of conjugated polymers and almost all its electronic applications need doped conjugated polymers. Now we consider the transport properties of the charge carriers across the solid conjugated polymer film.

1.3 Charge Transport

An easily polarizability property of an organic polymeric solid leads to a pronounced polaron character of mobile carriers with low mobility, and to a large binding energy of excitons. Thus it is necessary to briefly investigate the polaron properties and their consequences for a charge carrier transport in organic polymer solids. The term polaron known as a quasi particle is referred to a superposition of a moving charge carrier and a phonon cloud. The phonon cloud accounts for the distortion of the surrounding lattice (the coupling of a free charge carrier to the polarization of the lattice by the carrier) which travels with the charge carrier. This quasi particle is called a large polaron if the radius of the phonon cloud is larger than the lattice constant of a solid film. In contrast, when a charge carrier induces (polarizes) its environment and gets trapped by a potential well created by a strong lattice polarization (distortion) occurring within a unit cell, the carrier is confined to a volume of one unit cell or less, and the quasi particle is called a small polaron. The self trapped small polaron is distinguished from a mobile large polaron on the basis of the strength of the electron-lattice interaction which is described by a dimensionless parameter known as coupling constant. When the coupling constant is larger than five small polaron is observed. The large polaron moves much like a quasi free charge carrier described by the Boltzmann equation with scattering events, whereas the small polaron moves by hopping between neighboring ions. Polymeric organic semiconductors including the low molecular weight polymeric films are examples of materials with small polarons. The bandwidth of this material is narrow in which the conductivity is usually disturbed by phonon scattering, and hopping mechanisms may prevail even if the material has crystalline structure. The bandwidth of low molecular weight polymeric crystal is maximum at a temperature close to zero, and decreases with the increase of temperature. The electron phonon coupling increases with temperature which in turn increases the polaron mass that also has an influence on the conductivity.

In organic crystals the mobility of a charge carrier which is the basic parameter for transport is defined as $\mu = \frac{q}{m^*}\tau$ where m^* is the effective mass of a charge carrier q, and τ is a mean time between scattering events. In polymeric organic crystals the mobility at room temperature is in most cases less than $1cm^2/(Vs)$, which is very small compared to a value $10^3cm^2/(Vs)$ for inorganic semiconductors. A major reason for the low mobility is the poor structural perfection of polymeric organic crystals, which is the cause for the creation of trap levels and scattering centers. Other reasons are the low dielectric constant of polymeric materials which is the cause for the charge carrier in this material to behave as a polaron, and the weak intermolecular interactions in an organic polymeric crystals. This weak intermolecular van der Waals interaction leads to a localization of the HOMO and LUMO wave functions in each molecule. This means that the filled HOMO and the empty LUMO levels of each molecule are separated from those of neighboring molecules by a potential barrier. If the intermolecular barrier is low, the stronger coupling is related to a larger overlap of wave functions of adjacent molecules, and bands similar to those in inorganic semiconductors are formed. Higher potential barriers may still allow charge carrier conductivity by phonon assisted hopping which will be discussed further below.

The intermolecular barriers are expressed in terms of intermolecular transfer integrals. These quantities describe the electronic coupling between molecular orbitals of adjacent molecules (HOMOs and LUMOs) and depend sensitively on the spacing and relative orientations of the molecules. For acenes the typical values are in the range of some tens of meV [33]. In the regime of band conduction the bands are formed by linear combinations of the orbitals of each molecule, and the transfer integral V affects the effective mass of a mobile carrier moving in a given direction by $m^* = \frac{\hbar^2}{2|V|d^2}$ where $\hbar$ denotes the Planck constant, d is the distance between adjacent molecules in the considered direction. If the electron-phonon coupling is not weak enough to be neglected in the regime of hopping conduction the transfer integral is involved in the charge transfer rate w for a hopping transitions between adjacent molecules described by Marcus electron rate equation [34],

$$w = \frac{|V|^2}{\hbar^2}\sqrt{\frac{\pi}{\pi\lambda kT}}exp^{(-\frac{\lambda}{4kT})}, \tag{1.3.1}$$

where k is the Boltzmann constant, T is temperature, and λ is a reorganization energy which describes the vibrational relaxation which is proportional to the electron-phonon coupling strength. The reason for the existence of reorganization energy is a structural relaxation shown by organic molecules when a charge is introduced. As mentioned earlier in the above section the bands in organic crystals are narrow in the range of hundred meV due to a small amount of wave function overlap of π electrons. These two conditions, molecular or relaxation and narrow band widths impose limits for band like conduction in organic semiconductors.

In conjugated polymeric solids, as explained in the previous sections, there exists a structural disorder that gives rise to energetic disorder of charge carriers as well as localization of the states since many organic polymers cannot be grown as single crystals by evaporating or spin coating. Particularly, when the length of a polymer backbone chain increases the polymer chain structure is transformed from a highly ordered chain alignment to that consists of crystalline and amorphous regions. Even in perfect low molecular weight (small organic polymer molecule) crystals the weak intermolecular van der Waals bonds give rise to a phonon-related dynamical disorder which affects the mobility of charge carriers. Thus, the transport of charge carriers in organic molecular solids along a macroscopic distance involves different charge carrier transfer dynamics which depends on the structure of the material at different scales. To see these processes let us consider a solid polymer film which is the assembly of polymer chains and inject a charge carrier in to the film. At the beginning the charge carrier migrates inside a given chain, that is, at the intrachain level of certain conjugation length. When the interchain couplings are ignored, conduction in such a molecular chain is a one-dimensional process. In such a one-dimensional system as well as in two-dimensional systems any disorder irrespective of its magnitude will induce localization [35], which is known as Anderson localization at zero Kelvin of temperature.

This means that the charge carrier wave function is not delocalized over the total length of the chain; instead it is restricted to a given chain segment or length of $\lambda = \frac{1}{\alpha}$. In other words it means that the amplitude of the charge carrier wave function is large in a limited volume of localization radius $\lambda = \frac{1}{\alpha}$ (or in a limited length for a conduction in one-dimension) and decays rapidly outside this volume (or length for the one-dimensional case). When the chain length is much larger than the localization length, the charge carrier is not able to cross along the chain and thus the chain is an insulator at absolute zero temperature. But, when the temperature is larger than zero Kelvin, phonons are created and assist the charge carrier to move along the chain by hopping, despite the fact that scattering against these same phonons restrains the motion of the charge carrier.

On the other hand, when the interchain coupling is taken into account interchain transport can take place. In the case when the disorder energy is weak that exists mostly when the chains are parallel to each other, the interchain coupling, provided that it is large enough, introduces some three-dimensional charge carriers interaction features. These three dimensional features give the charge carrier an opportunity to use other paths, and overcome one-dimensional effects or one-dimensional localization which has an effect of reducing conductivity. Such a process can be envisaged only if the chains are parallel to each other so that the overlap integrals for the weak van-der-Waals interactions between neighboring polymer chains are large enough. This type of film is crystalline and high quality materials which is prepared at most care, and expensive in comparison to that of a large molecular weight polymer films which are easily manufactured. In a common conjugated polymer film there are no structural regularity and spatially extended electronic states or in other words there exists strong energetic and spatial disorders in a conjugated polymer film which have significant influence on the conductivity of charge carriers in all directions. Such systems are disordered organic semiconductors which include polymers and low molecular weight systems, and our main focus is on the conduction process of charge carriers in these systems not in the crystalline ones.

In all disordered solid media which also include conjugated polymers, all kinds of defects and disorders are present besides the localization effects inherent in one-dimensional systems. Because of this the charge carriers are located on localized states, or possibly on limited conducting areas, which can be chain segments or more extended conducting regions. These localized states are also called sites. Since localized states by themselves are like traps for charge carriers and behave as a resistance for the passage of current, the charge carriers conduction in a medium that contains localized states of whatever origin can only take place by means of transitions of charge carriers from occupied states to neighboring unoccupied states usually with the assistance of a phonon. The phonon is either absorbed or emitted so that the energy is conserved in the process of the charge carrier transition. This transfer of charge carriers between sites localized at different positions in space is commonly known as tunneling (hopping), and transport occurs via a sequence of charge carrier transfer steps from one conjugated unit identified as sites to another similar to the hopping of charge carriers between defect states in inorganic semiconductors.

The mechanism of hopping conduction was first proposed to explain the temperature dependence of the DC electrical conductivity in crystalline semiconductors which have been doped and compensated [36, 37]. In this model the conduction occurs by hopping of electrons between randomly situated localized donor states of time independent disordered energy landscape which are filled and empty because of the compensation by acceptors that also create a Coulomb potential which perturbs the donor energy levels. This model was later extended to the case of conduction in amorphous semiconductors of sufficiently large disorder potential which has all the states lying in the mobility gap. In highly disordered or amorphous inorganic semiconductors defects or deviations from ideal landscape give rise to a continuous tailing of energy states into the band gap. The deep states in the band gap occur less frequently because the centers which produce such states are less probable. However, when such deep states occur, each state or defect center

produces a localized level. The defect centers in the band gap closer to the band edges are shallower states, when close enough to the band edges their levels broaden into bands, and the resulting states are no longer localized. Overlapping levels and narrow bands all merge into the tailing states. Thus, when going from deep tail states to the band states a transition from localized to delocalized states occur at a critical energy called the mobility edge. Charge carriers which are thermally activated above the mobility edge contribute to charge transport, while charge carriers at lower energy are localized in defect states.

The basic difference between amorphous inorganic semiconductors and disordered organic semiconductors is the shape of the density of states (DOS). In a disordered inorganic semiconductor the DOS is found to have a mobility edge and a tail of localized states with an exponentially decreasing distribution extending into the band gap and described as $g(\varepsilon) = \frac{N}{\varepsilon_o} \exp\left(- \frac{\varepsilon}{\varepsilon o} \right)$ where N is the total concentration of localized states in the band tail, and ε_o is the energy scale of the DOS distribution. In contrast, the energies of charge carriers on localized states in disordered organic polymers have a Gaussian distribution [38] whose DOS has the form

$$\rho(\varepsilon) = \frac{N}{\sqrt{2\pi\sigma^2}} exp\left(-\frac{\varepsilon^2}{2\sigma^2} \right), \tag{1.3.2}$$

where N is the total number of states (concentrations), ε is the energy of a charge carrier on a site relative to the center of the DOS assumed to be zero in this case, and σ is the energy scale of the distribution that determines the amount of energy disorder whose values in most disordered organic materials is of the order of 0.1 eV [38]. The cause for the energetic disorder is believed to be the fluctuation in lattice polarization energies and the distribution of segment length in the π or σ bonded main chain polymers discussed in the previous section. The Gaussian shape of the DOS was assumed based on the Gaussian profile of the excitonic absorption band and by recognition that the polarization energy is determined by a large number of internal coordinates, each varying randomly by small amounts [38].

Our consideration of charge carrier transport is for the materials where the disorder aspect is dominant and the electron-phonon coupling is weak enough to render the polaronic effects in the conduction process, though sufficiently strong to guarantee coupling to the heat bath. For this mode of transport Miller and Abrahams rate equation [39] is preferred instead of Marcus expression given by Equation (1.3.1) to describe a sequence of each charge carrier transfer steps from one site to another. The Miller and Abrahams rate equation [39] for the transition rate ν_{ij} for hopping from a localized occupied site i to an unoccupied site j is expressed as

$$\nu_{ij} = \nu_0 exp(-2\alpha|\Delta\mathbf{R}_{ij}|) \begin{cases} exp\Big(-\frac{\varepsilon_j-\varepsilon_i}{k_BT}\Big) & \text{if } \varepsilon_j > \varepsilon_i, \\ 1 & \text{if } \varepsilon_j \leq \varepsilon_i. \end{cases} \tag{1.3.3}$$

where $|\Delta\mathbf{R}_{ij}| = R$ is the distance between the positions of a charge carrier before and after hopping. The coefficient ν_0 is an intrinsic rate, which can be regarded as an attempt frequency is determined by the tunneling (hopping) mechanism, is simply assumed to be of the order of phonon frequency $10^{13}s^{-1}$. α is the inverse localization length of charge carriers ($\alpha = \frac{1}{\lambda}$) or the wave function decay constant. The localization length is assumed to be the same for sites i and j. k_B is the Boltzmann constant, T is temperature, and ε_i and ε_j are the on site energies of a charge carrier when at sites i and j, respectively. These energies have a spectrum which has a Gaussian shape described by Equation (1.3.2). The term $exp(-2\alpha R)$ in Equation (1.3.3) is the overlap between the sites wave functions which decreases exponentially with the intersite distance R. The Boltzmann factor, $exp\Big(-\frac{\varepsilon_j-\varepsilon_i}{k_BT}\Big)$, shows an activated process or the probability of the existence of a phonon of energy equal to $\varepsilon_j - \varepsilon_i$ which is either absorbed or emitted in order to conserve energy in the hopping process. There is no other activation energy except the difference in charge carrier energies between different sites a carrier has to overcome in order to hop. The probability for hopping downward in energy is just $\nu_0 exp(-2\alpha R)$ by the principle of detailed balance with the premise that there are phonons that are always existing to absorb the energy difference between the final and initial states. In a disordered organic

molecules the intersite distance is subjected to also a variation of intersite electronic wave function overlap arising from both positional and orientational disorder of nonspherical molecules **??** known as off-diagonal disorder. The overlapp parameter $2\alpha a$ is subjected to distribution as well (off-diagonal disorder). In the analysis given in Reference [38], the off-diagonal disorder is also given by a Gaussian distribution to each site, with a certain variance.

1.3.1 Nearest neighbor hopping

Using the above rate equation it is possible to formulate the problem of the theoretical description of hopping conduction which is provided by transition events with the rates described by Equation (1.3.3) in the manifold of localized states with the DOS described by Equation (1.3.2). The Gaussian form of the DOS makes the problem complicated for the analytical approach to find the solutions of the hopping transport problems in disordered organic solids. The problem of finding analytical solutions (or finding transport parameter such as conductivity) becomes much more complicated in the case when the energy dependent and distance dependent terms in Equation (1.3.3) compete to determine the transport parameter particularly if the temperature has a value so that the thermal energy k_BT is about the same or less than the Gaussian width of the localized states. Because of this, most studies have been on the basis of computer simulations [38, 40–45].

However, the transport parameter such like conductivity that is provided by transition events with the rate described by Equation (1.3.3) in the manifold of localized states per unit volume N is derived analytically for high and low temperatures separately. For the high temperatures case an equation for the conductivity in the nearest neighbor hopping regime is derived on the basis of percolation theory [46]. Before applying the percolation method let us first see the theory described briefly in the next paragraph.

The percolation theory is one of the most important theoretical tools which is used to describe a charge carrier transport in a disordered system as described in detail elsewhere

[46]. It is modeled as a resistance network which link a randomly distributed sites (nodes) where each link between sites i and j assumed as a resistance R_{ij} which has a detrimental influence on the probability for the transition of a charge carrier across the link. These resistances are directly related to the transition rates given in Equation (1.3.3) for the case $\varepsilon_j \leq \varepsilon_i$. The resistance between two sites is considered to be equal with the distance between the sites as shown in Figure (1.3). According to percolation theory a pair of sites i and j are treated as connected if the distance between the sites, R_{ij}, is less than some threshold radius R_c. Pairs of nodes that fulfill this criterion, $R_{ij} \leq R_c$, form clusters. The size of these clusters will depend decisively on the magnitude of R_{ij}; if R_{ij} is large, the clusters are also large and the system may even be entirely connected. If R_{ij} is small, many clusters may only consist of two or three connected nodes, and large clusters are rather unlikely. Between these limits there exist one particular threshold radius $R = R_c$ at which at least one cluster exists that connects two opposite sides of the system.

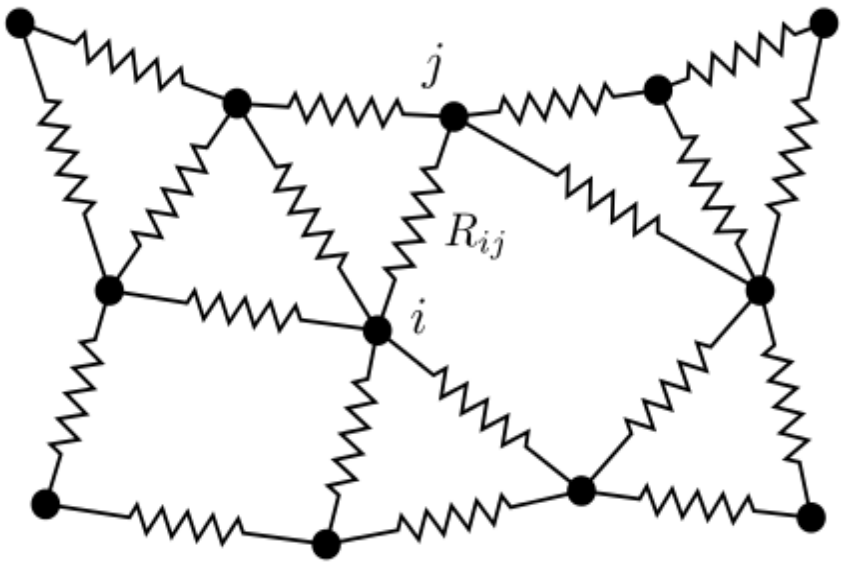

Figure 1.3: A random resistance network model of charge transport through a system.

If R is small, not many bonds will be formed in the system as shown in Figure (1.4a),

and the probability $P(R)$ for the transition of a charge carrier from one end to another becomes zero. As the magnitude of R increases, more and more bonds are formed in the system as shown in Figure (1.4b). In Figure (1.4c), R has become large enough to form a path that connect nodes through the system, and any node on this path could in principle be connected to an infinite amount of other nodes. This means that $P(R)$ is greater than zero and the value of R at which this occurs is called the percolation threshold, denoted by R_c.

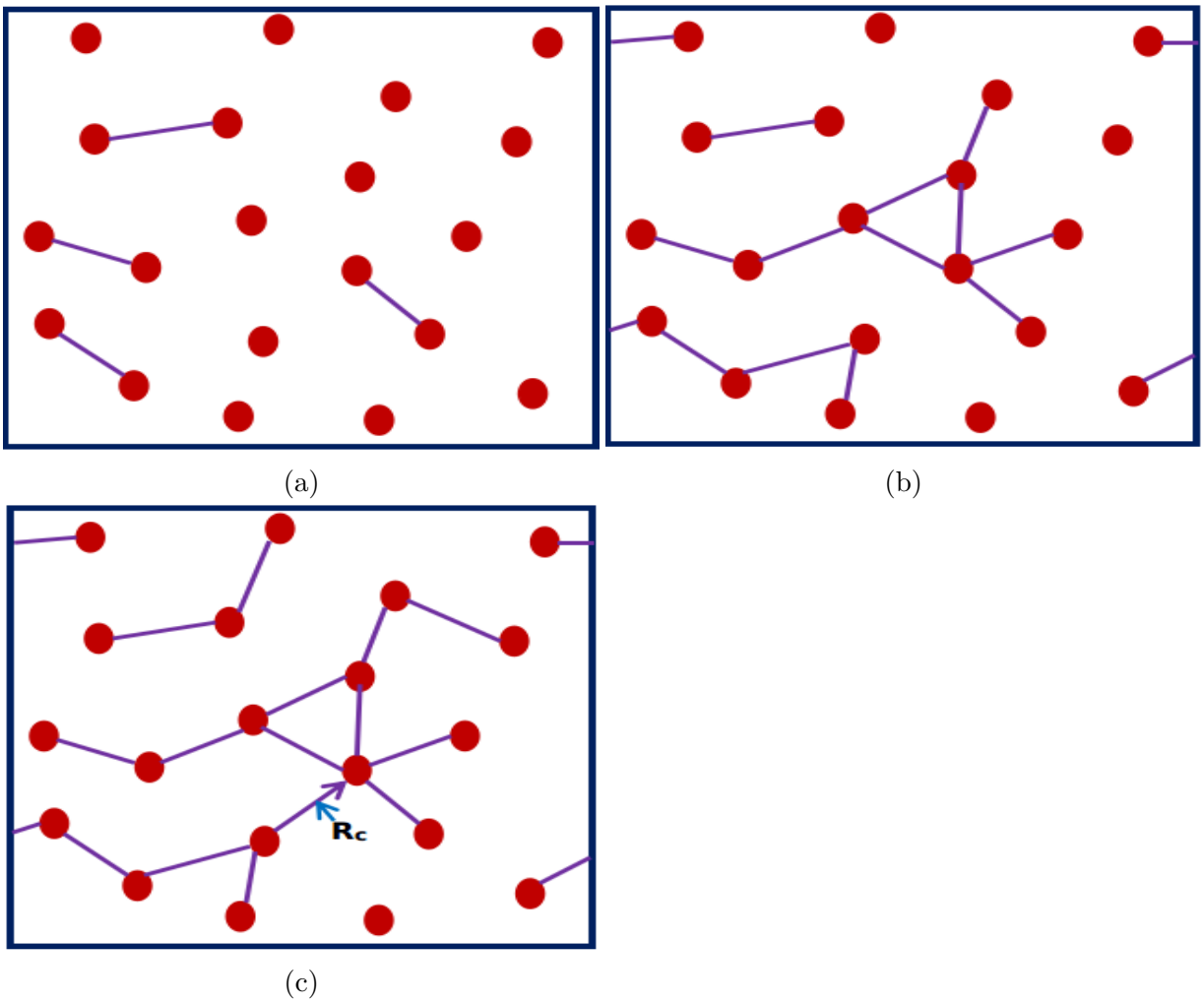

Figure 1.4: Percolation in a cluster of sites are shown as (a), (b), and (c) by increasing the percolation parameter R in the system , from a small value up to the percolation threshold R_c.

The value of R_c depends on the dimensions of a system, and in more complex criteria

for sites being connected, it also depends on several other parameters [47, 48]. In three dimensions, it is equivalent to finding a node j within a sphere of radius R around the node i. The percolation threshold, R_c, is the smallest radius possible that will create a long chain formed from connecting sites through the system, where every node is within a sphere of radius R_c around the previous node. The critical radius R_c can be expressed in the mean number of bonds per node,

$$\frac{4\pi N R_c^3}{3} = B_c \tag{1.3.4}$$

where $B_c = 2.7 \pm 0.1$ is the average number of neighboring sites available within the distance smaller than R_c.

The basis for applying percolation theory to analyze hopping transport is the concept of the resistance network used to derive the Miller–Abraham's rate equation [39]. In this approach, a charge carrier hopping possibility is assumed between each pair of sites (i, j) connected by a resistance R_{ij} of an electrical circuit. The resistance of the whole sample is equivalent to the network constructed from the elements R_{ij}. The value of R_{ij} is defined as [46, 49]

$$R_{ij} = \frac{k_B T}{e^2 \nu_{ij}} \tag{1.3.5}$$

where e is the elementary unit charge carrier, k_B is the Boltzmann constant, T is temperature, and ν_{ij} is the transition rate expressed in Equation (1.3.3) for the case $\varepsilon_j \leq \varepsilon_i$. Thus, we replace ν_{ij} in to Equation 1.3.5 by its value in Equation (1.3.3) and obtain

$$R_{ij} = R_o \exp\left(\frac{2R_c}{\alpha}\right) \tag{1.3.6}$$

where $R_o = \dfrac{k_B T}{e^2 \nu_o}$, the conductivity at the percolation threshold radius R_c. We know that conductivity is inverse of resistivity ρ which in turn is directly proportional to resistance.

In accordance with this we can write the conductivity as

$$\sigma = \sigma o \exp\left(-\frac{2R_c}{\alpha}\right), where \sigma o = \frac{1}{\rho_o}. \tag{1.3.7}$$

Substituting R_c in Equation (1.3.7) by the value we get for it from Equation (1.3.4) in terms of B_c and N, we will write the conductivity as

$$\begin{aligned} \sigma &= \sigma o \exp\left(-\frac{2}{\alpha}\left[\frac{3B_c}{4\pi N}\right]^{1/3}\right), R_c = \left[\frac{3B_c}{4\pi N}\right]^{1/3} \\ \sigma &= \sigma_o \exp\left(-\frac{\gamma}{\alpha N^{1/3}}\right) \end{aligned} \tag{1.3.8}$$

where the numerical constant $\gamma \approx 1.24 B_c^{1/3} \approx 1.73$ if B_c is taken to be 2.7. Due to the exponential dependence of the transition rates on the distances between the sites, the rates of electron transitions over distances $R < R_c$ are much larger than over distances R_c. Transitions over distances R_c are the slowest among those which are still necessary for the DC transport and hence such transitions determine the conductivity. This equation was obtained under the assumption that only spatial factors determine transition rates of electrons via localized states. This assumption is valid only at high temperatures.

1.3.2 Variable range hopping

If the temperature is not as high and the thermal energy $k_B T$ is comparable to or smaller than the energy spread of the localized states involved into the charge transport process, the problem of calculating the hopping conductivity becomes much more complicated. In such a case the interplay between the energy dependent and the distance dependent terms in Equation (1.3.3) determines the conductivity. In that case the hopping rate in Equation (1.3.3) describes variable range hopping and the destination site for each charge carrier is controlled by the optimum values of both energy difference and the distance between the final and initial positions. This means hopping may occur to a site at a larger distance if there are no closer sites with lower energy or to a closer distance with

a larger energy if there are no closer sites with lower energy as explained by Mott and shown in Figure (1.5).

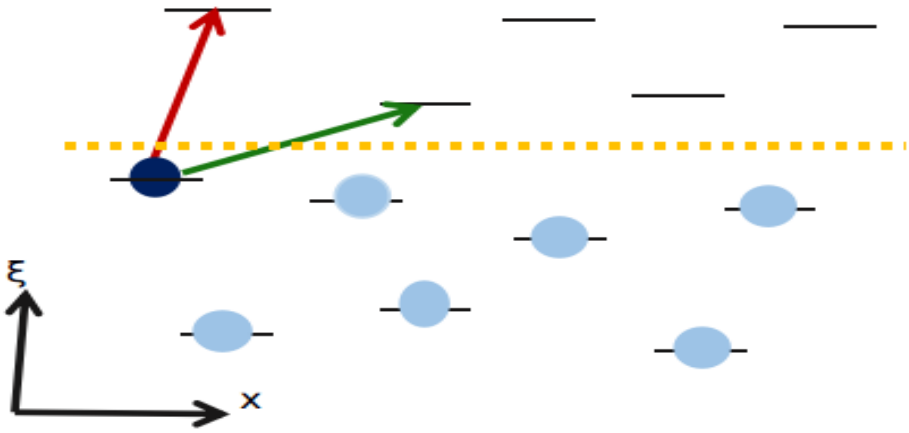

Figure 1.5: Motts variable range hopping model (VRH). A charge carrier might hop to either closer site at a higher energy (along red arrow) or to a farther site at a lower energy (along green arrow).

Employing this rate equation to amorphous semiconductors, and making use of the Einstein relation between mobility and diffusion coefficient, the temperature dependence of the hopping conductivity known as the variable-range hopping (VRH) model at low temperatures was first developed by Mott [36], which will be presented next.

Consider the usual expression for the conductivity σ,

$$\sigma = ne\mu, \tag{1.3.9}$$

where n is the charge carriers density, μ is the charge carrier mobility and e is the electronic charge. The charge carriers density is given by $n = k_B T N(\varepsilon)$ provided that the DOS $N(\varepsilon)$ at the Fermi level is assumed to be constant. The charge carrier mobility is obtained from the Einstein formula that shows its relation to the charge carrier diffusion coefficient D as $\mu = \frac{eD}{k_B T}$. The diffusion coefficient in turn is related to the hopping distance between initial

and final sites R and the temperature dependent hopping probability ν_{ij} as $D = \frac{1}{6}\nu_{ij}R^2$. Now we make use of these expressions in Equation (1.3.9) and obtain conductivity as

$$\sigma = \frac{R^2}{6}\nu_0 e^2 N(\varepsilon) exp\left(-2\alpha R - \frac{\varepsilon_j - \varepsilon_i}{k_B T}\right). \tag{1.3.10}$$

The argument made in this model is that at low temperatures where both the number and energy of phonons are small or $\frac{\varepsilon_j - \varepsilon_i}{k_B T} \gg 1$, hopping to nearest neighbors does not minimize $exp(-2\alpha R)$ term and is unfavorable since there are also on the average no small energy separations at the nearest neighbors. The hopping rate also vanishes for larger R because of the $exp(-2\alpha R)$ term although it is more favorable for the charge carriers to tunnel to more distant sites since energy separations between them has smaller value there is a higher probability that more distant sites will have smaller energy separations. Consequently, the hopping rate has a maximum somewhere in between the nearest neighbors sites and those at larger R. With this consideration Mott [36] considered the density of state $N(\varepsilon)$ as a constant and the same as that at the Fermi energy for a small energy range that encloses the Fermi energy at the middle as shown in Figure (1.6), and stated the optimization of the factor $\left(2\alpha R + \frac{\varepsilon_j - \varepsilon_i}{k_B T}\right)$ together with the condition for the existence of at least one state at a given spatial and energy separation,

$$\frac{4\pi}{3} N(\varepsilon)(\varepsilon_j - \varepsilon_i) R^3 = 1. \tag{1.3.11}$$

We substitute $(\varepsilon_j - \varepsilon_i)$ in the optimum factor $(\left(2\alpha R + \frac{\varepsilon_j - \varepsilon_i}{k_B T}\right))$ by its value in Equation (1.3.11) and then differentiate it with respect to R and obtain the optimum hopping distance R_{op} to be

$$R_{op} = \left(\frac{9}{8\pi\alpha N(\varepsilon) k_B T}\right)^{1/4}. \tag{1.3.12}$$

Substitution of R in Equation (1.3.11) by the expression for R_{op} in Equation (1.3.12) yields the optimized energy difference $(\varepsilon_j - \varepsilon_i)_{op}$; and if both of these optimized parameters are used in Equation (1.3.10) we get

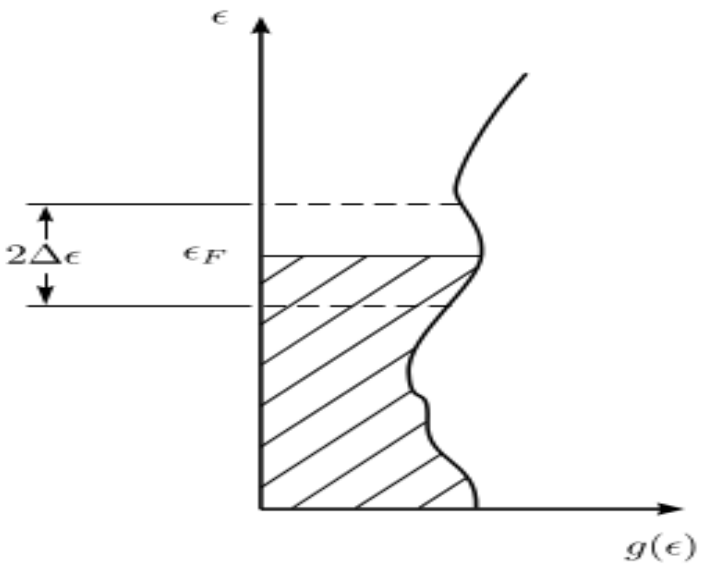

Figure 1.6: Effective region in the vicinity of the Fermi level, where the charge transport takes place at low temperatures.

$$\sigma = \sigma_0 exp\left(\frac{-T_0}{T}\right)^{1/4}, \tag{1.3.13}$$

where T is temperature, $\sigma_0 = \frac{e^2\nu_0}{4(2\pi^{1/2})}\left(\frac{N(\varepsilon)}{\alpha k_B T}\right)^{1/2}$ and $T_0 \approx 2\left(\frac{\alpha^3}{k_B N(\varepsilon)}\right)^{1/4}$. This equation is derived by considering three dimensional system and optimizing the hopping distance R accordingly. However, the optimization of R depends on the dimensionality of the system. Thus, we have to include the effect of dimensionality and consequently modify Equation (1.3.13) to the more general one that can be applied to one, two and three-dimensional systems as

$$\sigma = \sigma_0 exp\left(\frac{-T_0}{T}\right)^{\gamma}, \tag{1.3.14}$$

where T_0 is the characteristic temperature $T_0 \approx 2\left(\frac{\alpha^d}{k_B N(\varepsilon)}\right)^{\gamma}$, $\gamma = \frac{1}{d+1}$, and $d = 1, 2, 3$ is the dimensionality of the system.

This temperature dependence of the conductivity has been commonly observed in

several amorphous semiconductors. Also the temperature dependence of the conductivity observed in most conjugated polymers [50–53] has shown a behavior which has similarity with the Mott's VRH law. However, this theory of VRH model, derived for the case of constant DOS in the range for hopping conduction, is not capable of accounting for the commonly observed and almost established functional form of electric field dependence of the charge carrier mobility in disordered organic semiconductors whose DOS function is assumed to be Gaussian.

Because of the applications that conjugated polymers have in electronic devices [17,54] and since mobility is the base to determine the transport properties and thereby the efficiency (quality) of the active material used in the devices, a large number of works have been done on conjugated organic polymers to characterize the electric field dependence of the charge carriers mobility [55–57]. It has been shown that in several conjugated polymer films the mobility μ of charge carriers varies with electric field F over a wide range of the field in accordance with the Poole-Frenkel [58] law,

$$\mu = \mu_0 exp\left(\sqrt{\frac{F}{F_0}}\right), \tag{1.3.15}$$

where μ_0 and F_0 are material and temperature specific constants. The Poole-Frenkel law describes the lowering of a (Coulomb) barrier in the presence of an electric field. This type of equation for mobility was first observed by Gill in 1972 for poly-n-vinylcarbazole [55] as

$$\mu = \mu_0 exp\left[-\frac{(\Delta - \beta F^{1/2})}{k_B T_{eff}}\right], \tag{1.3.16}$$

where $\frac{1}{T_{eff}} = \frac{1}{T} - \frac{1}{T_0}$. In this expression μ_0 is the mobility in the absence of electric field, Δ is the activation energy also in the absence of electric field, and β and T_0 are parameters of the system. Thereafter, several other experimental studies on different disordered organic materials have shown up with similar results [38, 56, 57, 59].

Despite all the numerous consistent experimental results, a theory that accounts for

the elementary steps in the transport mechanism for the charge carriers of disordered conjugated polymers is still not unified. Mainly there are two transport models; the small polaron hopping model [60–62] and Gaussian Disorder Model (GDM) [38]. Both models, as explained above, describe the transport process in conjugated polymers as a hopping of carriers among localized sites which are identified with the donor or acceptor molecules or functionalities associated with polymer chain. But they differ on the physical process by which the hopping occurs. The small polaron hopping model is based on the formation of small polarons as a result of the change in molecular conformation following the removal or addition of an electron. It considers that the disorder energy is unimportant relative to the intra (inter) molecular deformation energy, and for the transfer of charge, activated transfer of deformation is required.

On the other hand, as described above, the GDM is stated based on disorder energy. It assumes that the coupling of the charge to intra (inter) molecule is weak and the activation energy arises from the static energetic disorder of the hopping sites. This is explained from the fact that conjugated polymers are lacking a long-range order, justified by the inhomogeneously broadened absorption spectra of Gaussian profile, thereby causing narrow transport bands of an ordered structure to split into Gaussian distributions localized density of states (DOS). This phenomenon is described as energetic or diagonal disorder whereas fluctuations of intersite distances which is also a common feature of this material is described as geometric or off-diagonal disorder.

The GDM model is the approach that B*ä*ssler and coworkers [38, 59] first used to establish a unified equation that can account for the charge transport in organic materials based on its degree of disorder. They made the assumption that the energies of the charge carriers on the hopping sites are uncorrelated and has a Gaussian distribution of width σ_D; and also described the off-diagonal disorder by a Gaussian distribution with the width Σ for each site. Here off-diagonal disorder represents the variation of the overlap

of the intersite wave functions that arise due to both positional and orientational disorder of nonspherical molecules. They tested their assumption numerically using kinetic Monte Carlo simulations method on the basis of an established Miller and Abrahams rate equation Equation (1.3.3). In short this model describes a solid conjugated polymer as a disordered system that consists of a number of localized charge carrier transporting units or chromophores identified as sites of a certain average lattice parameter, whose sites energies are uncorrelated and have a spectrum which is similar to a Gaussian distribution centered at zero with specific width σ; each chromophore or site is, centered at a point with a radius known as localization radius, in turn is subjected to the same type of distribution about the average position. With this scheme, B*ä*ssler *et al.* described the electric field F and temperature T dependence of the mobility with the next phenomenological equation

$$\mu = \mu_0 exp\left[-\left(\frac{2\sigma_D}{3k_BT}\right)^2\right]\begin{cases} exp\left\{C\left[\left(\frac{\sigma_D}{k_BT}\right)^2 - \Sigma^2\right]F^{1/2}\right\} & \text{if } \Sigma \geq 1.5, \\ exp\left\{C\left[\left(\frac{\sigma_D}{k_BT}\right)^2 - 2.25\right]F^{1/2}\right\} & \text{if } \Sigma < 1.5, \end{cases} \tag{1.3.17}$$

where μ_0 is the mobility in the limit $T \longrightarrow \infty$ and $F \longrightarrow 0$, and C is an empirical constant that depends on sites spacing usually called lattice parameter. This GDM based calculation shows the temperature dependence of mobility at zero electric field as $\mu \propto T^{-2}$, which is different from the Arrhenius behavior. Furthermore, the simulations based on GDM reproduced $\ln \mu \propto F^{1/2}$ law only in a narrow field range at a relatively high values of electric field $F \sim 10^8 Vm^{-1}$ [38], whereas experiments indicate that this behavior occurs over a much wider range of fields $10^6 - 10^8\ Vm^{-1}$ [55,63,64]. Nevertheless, this model has widely been used for the analysis of experimental data on transport in disordered organic semiconductors [65,66].

After the establishment of the equation on the basis of GDM there have been continuing efforts [41, 67–72] to amend the equation so that it can describe the $\ln \mu \propto F^{1/2}$ behavior over a much broader field range. The amendments have been made mostly on the

spatial correlations between the energies on different sites and the solutions were found using analytical as well as kinetic Monte Carlo simulation approaches. The first suggestion was forwarded by Gartstein and Conwell [68]. These authors considered the spatial correlations between the energies of neighboring sites and obtained Monte Carlo simulation results that describe μ versus F over a wide field range similar to that demonstrated experimentally by Gill in 1972 [55]. Using this idea, another research group [69] derived analytical expression for a one-dimensional transport considering long-range energy correlations due to charge-dipole interactions in the material, and also demonstrated that the results they obtained are in agreement with that observed in experiment. This idea, the presence of long-range energy correlations due to charge-dipole interactions in the material, was later extended to a three-dimensional motion. Here, the positional disorder that was considered in Reference [38] was neglected. Then, a phenomenological equation that shows an empirical relation between mobility and electric field was proposed by Novikov *et al.* [41] on the basis of Monte Carlo simulation results . The equation for this model, known as Correlated Gaussian Disorder Model (CDM), is given as

$$\mu_C = \mu_0 exp\left[-\left(\frac{3\sigma_C}{5k_BT}\right)^2 + 0.78\left(\sigma_C^{3/2} - 2\right)\left(\frac{ebE}{\sigma_C}\right)^{1/2}\right], \tag{1.3.18}$$

where b is the shortest distance between neighboring sites or lattice parameter of cells arranged on a cubic lattice. This equation has successfully shown the $\ln \mu \propto F^{1/2}$ behavior over the field range similar to that shown in experiment [55]. This equation can be applied only for polar materials since it was derived with a randomly oriented dipole moment at each lattice site with the unrealistically large concentration assumption [71]. However, the Poole-Frenkel behavior has been observed in several conjugated polymers including those which do not have permanent dipole moments [63]. This is, therefore, a signal to cast doubt on the theory that associates the charge-dipole interactions as the universal explanation for the $\ln \mu \propto F^{1/2}$ behavior [41].

In most of the previous works and in this work as well, the effect of charge carriers

density was not included in the analysis made to understand the dependence of charge carriers density on temperature and electric field. The effects of charge carriers density on hole mobility in solution-processable conjugated polymers developed for PLEDs and PFETs were reported for both organic field effect transistors [73, 74]. In 2003 Tanase and her coworkers [73] measured mobilities for solution processed amorphous conjugated polymers in organic field-effect transistors and organic light emitting diodes. They found that the hole mobility of the film used in PFETs was larger than that used in PLEDs by 3 orders of magnitude. The possible reasons suggested for the huge difference in mobility values obtained from diodes and FETs, based on a single semiconducting polymer, was the large difference in charge carriers densities in these devices. The charge carriers density for a field effect transistor varies mainly on the basis of gate voltage and that for diode varies with the voltage across the thickness. Accordingly, the density for PFETs is grater than $10^{16} cm^{-3}$ and that for PLEDs is less than $10^{16} cm^{-3}$. The combined plots of mobility versus charge carriers densities of the results from the diode and field-effect measurements show that the hole mobility is constant for charge carrier densities less than $10^{16} cm^{-3}$ and increases with a power law for densities greater than $10^{16} cm^{-3}$. Following this, another similar experiments were done in 2004 [74] to separate the effects of electric field and charge carriers density on mobility since both charge carriers and electric field vary with the potential difference across the thickness of PLEDs. It means that, experimentally in PLEDs, it is difficult to separate the effects of electric field and charge carriers on charge carriers mobility. However, analyzing the results of their measurements they suggested that at room temperature the charge carrier density dependence of mobility is dominant, but at low temperatures it is necessary to consider an electric field dependence of mobility. In this paper [74] the charge carrier density dependence of mobility, for the unified diode and field-effect measurements, was analyzed on the basis of the equation derived by Vissenberg and Matters for the high charge carriers density regime [75] plus the charge

carrier density independent contribution determined from the current voltage characteristics of hole only diodes at low voltages. In this equation, only the change carriers density dependent mobility is included, the field dependence of the mobility is disregarded, and the equation fails to reproduce the experimental current versus voltage characteristics at low temperatures and high voltages. Realizing the defect of this equation Pasveer and coworkers [42] formulated a unified theoretical description for charge carrier mobility that encloses the effects of temperature, charge carriers density, and electric field based on the basis of the numerical solution of the master equation representing charge carrier hopping in a lattice. Here, the charge carrier conduction is considered as a thermally assisted tunneling process with Miller-Abrahams rates Equation (1.3.3) in disordered conjugated The variation of hopping sites about the average separation or the positional disorder was neglected. The numerical results obtained were excellently fitted with the experimental current-voltage data of two semiconducting polymers. These results justify that the transport properties of charge carriers can be explained based on uncorrelated site energies GDM using Miller and Abrahams rate equation without considering the multi phonon hoping processes or polaronic effect. This formalism has been termed as extended Gaussian disorder model (EGDM) since the correlation of the site energies is not included.

In References [73, 74] the reason suggested for the large difference between the mobilities for the same active material in PLEDs and PFETs is connected with the charge carriers density difference. The claim that the mobility does not vary with charge carriers density for the lower density less than $10^{16} cm^{-3}$ was justified based on the constant hole mobility obtained experimentally [73] for conjugated organic polymer used in PLEDs. This is not valid when an electric field is kept constant at negligibly low value ($5 \times 10^4 V/cm$) and charge carriers density is varied in the range less than $10^{16} cm^{-3}$ at temperatures less than or equal to room temperature. This means that charge carriers dependence of mobility exists at lower densities as well. This will be demonstrated using

kinetic Monte Carlo simulation methods. Using the same method, we will also show parameters that determine the density dependence of mobility at constant low ($5\times10^4 V/cm$) electric field are both energy distribution width σ and temperature T. At lower values of $\hat{\sigma} = \frac{\sigma}{k_B T}$, where k_B is the Boltzmann constant, the charge carrier mobility does not vary with charge carriers density whether the density is high or low. But, at larger values of $\hat{\sigma}$, that corresponds to temperature values which is less than or equal to room temperature, the mobility variation with charge carriers density is verified.

The expressions for the electric field dependence of hopping mobility, formulated in References [38, 42] and described above, have been widely used to analyze experimental data. Despite the wide usage for the experimental data analysis, the capabilities of these formalisms to correctly express electric field dependence of hopping mobility were put under question in recent publications [44, 45, 76]. One of the reasons for the doubt is the absence of a localization radius in both expressions which was shown in these References using computer simulations and analytical calculations as the only spatial parameters responsible for the dependence of hopping mobility on the applied electric field in a system of random sites. The second point raised is, particularly on the formalism in Reference [42], the assumption of a regular cubic lattice (the exclusion of the spatial disorder) and the use of small (smaller than that in References [38, 65]) and constant localization radius that restricts the charge carriers hopping to almost nearest neighbors which leads to a weak electric field dependence mobilities. The dependence of charge carrier hopping mobility on temperature and electric field was expressed [**?**] introducing an effective temperature concept that contains the electric field. Furthermore, it was shown that both lattice parameters and localization radius are relevant for the electric field dependence of mobility on regularly spaced sites, whereas the localization radius is the only spatial parameter responsible for the field dependence of the mobility in a system of randomly distributed sites. Consequently, it was concluded that lattice models are not suitable for theoretical studies of the field dependent hopping mobility in spatially

disordered systems such as organic disordered semiconductors [45].

The results found on the basis of computer simulations for the charge carrier mobility as a function of electric field, temperature, charge carrier density, morphology, and spatial parameters in most of the previous works [41–43, 77] did not involve the variation of intersite electronic wave function overlap which is known as spatial disorder or off-diagonal disorder. There are also Monte Carlo simulation approaches [38, 44, 45, 67, 76] that involved spatial disorder. As we mentioned above the formalism described in Reference [38] the spatial disorder was mimicked by distributing the overlap parameter $2\alpha a$ separately for each site in a Gaussian manner with a variance Σ around the value $2\alpha a = 10$. The Gaussian distribution was suggested here based on the fact that the actual distribution of the overlap parameter for disordered organic polymer is not known explicitly. In References [44, 45, 76] they considered randomly distributed sites with a constant average intersite distance which is the same as the inverse of the cube root of sites density. Here, the distribution of the overlap parameter was enclosed in the distribution of transporting sites.

In this work, we devise a method like that mentioned in References [44, 45, 76] to include the spatial disorder and show a charge carrier mobility as a function of electric field, temperature, charge carrier density, morphology, and localization radius on the basis of kinetic Monte Carlo simulation methods. The model is devised in such a way that charge carrier is localized any where inside a sphere centered at regularity distributed sites. The radius of the sphere is related to the localization radius. This assumption is based on the fact that charge carriers, basically electrons, are localized in a certain region not strictly localized at one point. The size of the region is related to the width of the wave function of the charge carrier which in turn is related to the decay constant which is usually called inverse localization length or radius. In this model the charge carrier hopping takes place from any place inside of one sphere and lands at any place inside another sphere. It means that, for instance, the hopping distance from inside one sphere

to another nearest neighbor sphere can have a value between $(b-2r)$ to $(b+2r)$ provided that b is the distance between the centers of neighboring spheres and r is the radius of a sphere. With this model and considering weak electron-phonon coupling, we used uncorrelated Gaussian disorder model (GDM) and Miller and Abrahams rate equation for our kinetic Monte Carlo simulations. Some of the important properties that we show are the functionality of the mobility on charge carriers density, temperature, localization length and electric field along the length of the film. We will present the detail procedures of the calculations and results we obtain in the second and third parts of this thesis.

The purpose of this thesis is, in short, to get insight on the effects of experimentally treatable parameters such as temperature, the applied potential or electric field, and the charge carrier density on charge carriers mobility in conjugated organic polymers. Charge carriers in conjugated polymers arise from doping mechanism. This mechanism gave birth to electronic devices such as organic polymer based FETs and light emitting diodes. These interesting properties have attracted the attention of researchers and a lot of work has been done to precisely understand the transport properties of the charge carriers as a function of the experimentally controllable parameters mentioned above. However, the area is still active for research as the problem has not been fully settled because of the nonlinear variation of charge carriers density with doping as well as injection from metallic contacts and the disordered nature of the solid conjugated polymers. Results that modify the previous results are constantly showing up. For instance, the temperature dependence of the mobility has been shown previously [38, 78] to be described by the non-Arrhenius behavior relation. This result was modified by new recent experimental results [79] that have demonstrated this relation by an Arrhenius behavior for a high charge carrier density. According to this recent report the previous relation works only for the low charge carriers density case. In this thesis we will try to discuss the transport properties of charge carriers in the electroactive conjugated polymer film that can be used in PLEDs or PFETs. Specifically we will introduce the charge carriers, holes, into a conjugated polymeric thin

film from metallic contacts, and analyze numerically the charge carriers hopping mobility at different charge carriers density, temperatures, electric fields, localization radius and energy distribution width on the basis of the model we mentioned above.

The rest work presented in this thesis is organized as follows. In Chapter **??** we will briefly present the general idea of Monte Carlo simulation methods giving more focus on kinetic Monte Carlo the one that we use to solve our problems. Then we will introduce our model and present the detail procedure of our calculations. The results of our calculations will be presented and analyzed in Chapter 3. In the last chapter we will present a summary and conclusions of our work.

Chapter 2

Methodology

As mentioned in the previous chapter, the Gaussian disorder model (GDM) has become almost the most dominant theoretical approach for charge carrier transport in disordered organic semiconductors. In the GDM approach, to obtain the necessary data for the analysis of the system charge carrier mobility requires methods of calculation which is either analytical or numerical. So far, kinetic Monte Carlo simulation methods have been applied widely and shown useful numerical results. In the following sections of this chapter we will briefly describe the main methods of Monte Carlo simulation we employ for our study, and then introduce our model. We then describe the detail methods and procedures of our Monte Carlo simulation approach for our work.

2.1 Monte Carlo Simulation Methods

The approach that is viable to evaluate a multiple integral in dimensions higher than two is Monte Carlo method. The function is sampled at n points distributed randomly in the domain of integration, and then the mean of these function values is multiplied by the area or volume or similar other parameters of the domain to obtain an estimate for the integral. The error in this estimate goes to zero as $n^{-1/2}$. There are also certain types of problems which need an alternative powerful approach, known as stochastic simulation. Stochastic simulation methods try to mimic or replicate the behaviours of

a system by exploiting randomness to obtain a statistical sample of possible outcomes. Because of the randomness involved, simulation methods are also commonly known in some contexts as Monte Carlo methods. Such methods are useful for studying: nondeterministic (stochastic) processes, deterministic systems that are too complicated to model analytically, deterministic problems whose high dimensionality makes standard discretization infeasible. The two main requirements for using stochastic simulation methods are knowledge of relevant probability distribution and a supply of random numbers for making random choices.

This means that Monte Carlo (MC) method is a numerical method that uses random numbers to solve mathematical and physical problems, which are particularly not easy to model analytically, and also not suitable to probe experimentally. To describe the latter more we can take, for instance, the dependence of a hopping charge carrier mobility on charge carriers density and applied electric field in conjugated organic light emitting diodes can not be seen separately in experiment since both electric field and charge carriers density are formed by external potential difference across the contacts. Besides this there is a limitation in experiment, for example to measure very high temperature, is not easy. These problems do not exist in Monte Carlo simulation approach. In general, its main advantages are its basic simplicity and the possibility to use it for a range of problems. The term 'Monte Carlo' came from the city of Monte Carlo in the principality of Monaco in France, which is known for its gambling houses. Monte Carlo methods were developed in the 1940s by von Neumann, Ulam, Metropolis and others, who primarily motivated by problems in nuclear physics such as neutron diffusion, and presented the article with a title The Monte Carlo method" in 1949 [80]. However, the method was well known and used to solve problems in statistics before 1949. Since it requires a large number of calculations, practical usability is based on computers.

The computation algorithm is simple in the Monte Carlo calculations, and leads to the process of generating a random event. The process is repeated N times, each trial is

independent of the others, and the results of all trials are averaged together to provide an estimate of the quantity of interest. The same is true for doing a scientific experiment and is sometimes referred to as methods of stochastic, or statistical experiments or trials. The error compared to the estimated value is approximately equal to the square root of the number of trials, i.e.,

$$error \propto \sqrt{\left(\frac{1}{N}\right)}, \tag{2.1.1}$$

where N is the number of trials.

A typical example that can illustrate the use of the Monte Carlo method as a method of integration is shown by calculating the value of π. We can do this by finding the area of a circle of unit radius centered at the origin which is inscribed in a square as shown in Figure(2.1). On the other hand it is possible to generate a number of several trial shots in the square $OABC$. Each trial means choosing two independent random numbers from a uniform distribution $[0, 1)$. Each pair of numbers are used to designate the coordinates of a point either inside a quadrant or in a square outside the quadrant. By calculating the distance of the random point from the origin we can determine whether the point is landed in the quadrant or in the square outside the quadrant. It is in the quadrant if the distance is less than or equal to one and considered as if the hit is scored. and recorded as m. Otherwise, the trial shot lands in the square outside the quadrant. The total number of hits recorded is denoted by m out of the total shots denoted by N. The areas of the square and quadrant are r^2, and $\pi r^2/4$, respectively. So the probability of the hit within the quadrant (p_q) is the area of the quadrant (A_q) divided by the area of the square (A_{sq}), which is related to the number of hits recorded and the total number of shots as described below

$$p_q = A_q/A_{sq} = \pi r^2/4/r^2 = \frac{\pi}{4} = \frac{m}{N}, \tag{2.1.2}$$

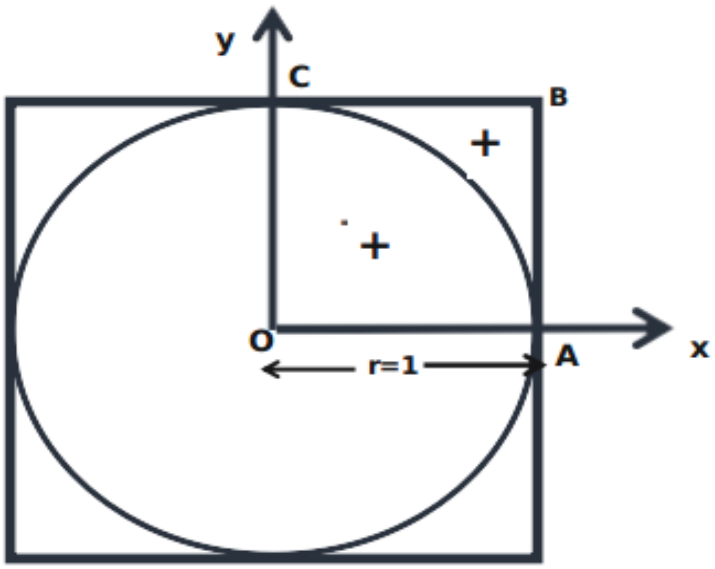

Figure 2.1: The geometry for the hit and miss integration to find the area of the circle.

which implies that

$$\pi = \frac{4m}{N}. \tag{2.1.3}$$

The main parameters needed for this method are N times pair of random numbers generated from a uniform distribution. This means that random numbers are the inputs for Monte Carlo simulations which are generated by simple programs, and discussed more in the next section. The accuracy of the estimate of π using hit and miss experiments depend on the number of trials as shown in Figure(2.2). As the plots in this figure show the value of π is approached with the increase of the number of trials designated by N.

Besides the examples mentioned above Monte Carlo simulation methods can be applied in different areas such like traffic, population growth, finance, genetics, chemistry, Materials Science, Statistical Physics, Bio-Physics. These methods have also been used to study the transport behaviours of charge carriers in disordered organic semiconducting polymer films [81–85]. We will also apply these methods to study the transport properties of the charge carriers in amorphous organic polymer films.

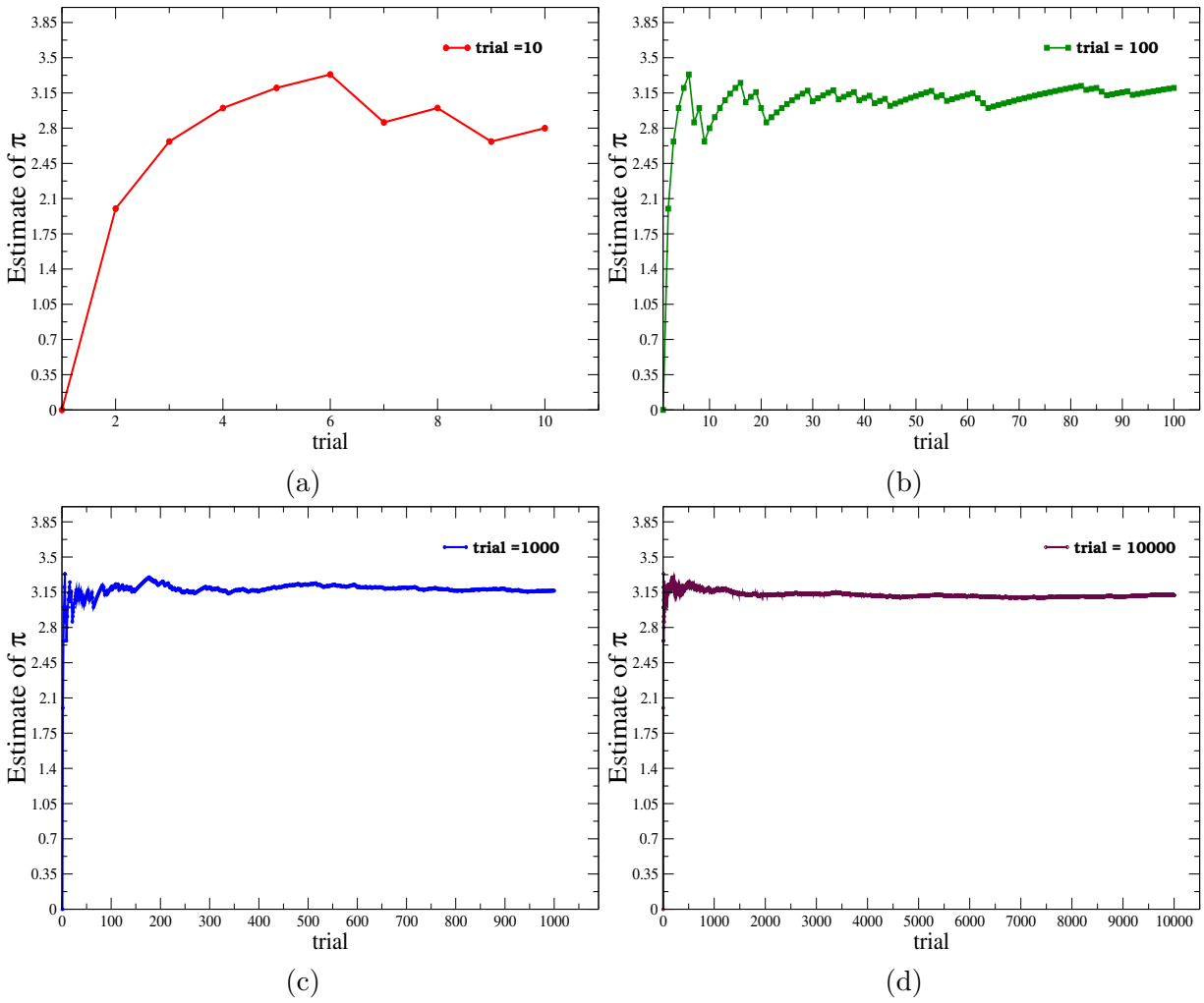

Figure 2.2: The estimate of π as a function of the number of MC trials by hit and miss of a circle of unit radius inscribed in a square for (a) N = 10, (b) N = 100 (c) N = 1000 (d) N = 10000.

2.2 Random Number Generation

As described in the above section every Monte Carlo simulation method is based on the production of independent random variables that are distributed according to a distribution function that is not necessarily explicitly known. This type of random variable production depends on the availability of an algorithm that provides sequences of numbers that are uniformly distributed on the interval [0, 1). The production of these numbers is known as random number generation. The program that produces these non overlapping

uniformly distributed sequences of random numbers is known as a pseudo-random number generators. The most important features of a desirable random number generator are that its sequence satisfies the known statistical tests for randomness, the probability distribution is uniform, the sequence has a long period, the method is efficient, the sequence is reproducible, and the algorithm is machine independent. Many random number generators supplied with computer systems are of the congruential type. In linear congruential method each term in the sequence can be found from the preceding one by the relation

$$X_{i+1} = (aX_i + c)(modM), i = 0, 1, ., ., m - 1 \tag{2.2.1}$$

where the initial value, X_0 is known as seed, and a, c, and M are nonnegative integers. Applying the modulo–m operator in Equation(2.2.1) means that $aX_i + c$ is divided by M, and the remainder is taken as the value of X_{i+1}. The random number U in the unit interval $0 \leq U < 1$ are given by

$$U_i = \frac{X_i}{M} \tag{2.2.2}$$

The sequence of numbers generated by Equation(2.2.1) repeat itself after at most m steps, yielding a period for the random number generator. The statistical properties of the random numbers in Equation (2.2.2) depends on the quality of random number generator which in turn depends on the choices of a and c, and in any case its period cannot exceed M.

In the special case when $c = 0$, Equation (2.2.1) simply reduces to

$$X_{i+1} = aX_i(modM), i = 0, 1, ., ., m - 1 \tag{2.2.3}$$

Equation (2.2.3) is a multiplicative congruential generator. It is readily seen that an arbitrary choice of X_0, a, c, and m will not lead to a pseudo-random sequence with good statistical properties. Number theory has been used to show that only a few combinations of these produce satisfactory results. In computer implementations, m is selected as a large prime number that can be accommodated by the computer word size. Among the

stochastic Monte Carlo simulation methods we will briefly present below the one that we have used for our work which is kinetic Monte Carlo method starting with Metropolis Monte Carlo method.

2.3 Metropolis Monte Carlo Method

One of the ways in which an arbitrary nonuniform probability distribution is generated and widely used was introduced by Metropolis, Rosenbluth, Rosenbluth, Teller and Teller and Teller in 1953. The Metropolis Monte Carlo method is a method that is used to find the averages of a function $g(x)$ like that shown in Equation(2.3.1) on the basis of an algorithm that rejects a certain possible sampling attempts

$$< g >= \int \frac{p(x)g(x)dx}{\int p(x)dx}, \tag{2.3.1}$$

where $p(x)$ is an arbitrary probability distribution that need not be normalized.

Metropolis method can be established in the context to estimate, for instance, one-dimensional definite integrals as explained elsewhere [86], or to construct a phase space trajectory in canonical ensemble as discussed in [87]. Let us say that we want to use importance sampling to generate random variables in accordance with an arbitrary probability density $p(x)$. The Metropolis method produces a set of random walk points x_i whose asymptotic probability distribution approaches $p(x)$ after a large number of steps. The random walk is defined by specifying a transition probability $W(x_i -> x_j)$ from one value x_i to another value x_j such that the distribution of points $x_0, x_1, x_2, ...$ converts to $p(x)$. To find an appropriate transition probability it is sufficient (but not necessary) to satisfy the condition of detailed balance or microscopic reversibility which is written as

$$p(x_i)W(x_i -> x_j) = p(x_j)W(x_j -> x_i). \tag{2.3.2}$$

The relation shown in Equation (**??**) does not specify the transition probabilities $W(x_i -> x_j)$ uniquely. A suitable scheme for constructing the distribution points in a canonical ensemble involves choosing a transition probability which satisfies Equation (2.3.2). The scheme for the choice of the transition probability $W(x_i -> x_j)$ that is consistent with the condition given in Equation (2.3.2) was first suggested by Metropolis *et al.* [88] in 1953 as

$$W(x_i -> x_j) = min[1, \frac{p(x_j)}{p(x_i)}]. \tag{2.3.3}$$

For a system in equilibrium at an absolute temperature T the canonical distribution $p(x)$ is described as

$$P(E) = \frac{\exp\left(-\frac{E}{k_B T}\right)}{Q}, \tag{2.3.4}$$

where E denotes the energy of the system at a particular state, k_B is Boltzmann constant and Q is the partition function of the system. Replacing $P(x)$s in Equation (2.3.3) by the values in Equation (2.3.4) will yield

$$\frac{P(E_j)}{P(E_i)} = \exp\left(-\frac{E_j - E_i}{k_B T}\right), \tag{2.3.5}$$

and Equation (2.3.3) becomes

$$W(E_i -> E_j) = min[1, \exp\left(-\frac{E_j - E_i}{k_B T}\right)]. \tag{2.3.6}$$

If the system is at a position x_i with energy E_i and we want to generate x_{i+1} in the nearest state with energy E_j, we can implement this choice of $W(x_i -> x_{i+1})$ by applying the Metropolis algorithm described below:

1. Choose a trial position $x_{trial} = x_i + \delta_i$, where δ_i is a random number in the interval $[-\delta, \delta]$. The energy of the system at a trial position is E_j.

2. Calculate $w = \frac{p(x_{trial})}{p(x_i)} = \exp\left(- \frac{E_j - E_i}{k_B T} \right)$.

3. If $w \geq 1$ or $E_j < E_i$, accept the change and let $x_{i+1} = x_{itrial}$.

4. If $w \leq 1$ or $E_j > E_i$, generate a random number r.

5. If $r \leq w$, accept the change and $x_{i+1} = x_{itrial}$.

6. If the trial change is not accepted, then let $x_{i+1} = x_i$.

These steps are repeated many times to sample many points of the random walk before the asymptotic probability distribution $p(x)$ is attained. With the known $p(x)$ it is possible to compute the average parameter of interest. We have seen that Metropolis Monte Carlo samples configuration space and generates configurations according to the desired statistical mechanics distribution. However, there is no time in Metropolis Monte Carlo, and the method cannot be used to study evolution of a system or kinetics. An alternative computational technique that can be used to study kinetics of slow processes is the kinetic Monte Carlo (kMC) method. This method will be discussed in the next section.

2.4 Kinetic Monte Carlo Method

The kinetic Monte Carlo (kMC) method is a variant of the Monte Carlo method intended to simulate the time evolution of a particular process of interest. It is a powerful technique that is used to extend the amount of time scale of simulations far beyond the vibrational time scale. The time scale between sequence of states is far beyond the vibrational time scale As compared to the Metropolis MC method, kMC method has different schemes for the generation of the next state. The main idea behind kMC is to use transition rates that depend on the energy barrier between the states with time increments formulated so that they relate to the microscopic kinetics of the system. In Metropolis MC method we decide whether to accept a move by considering the energy difference between the states. In

kMC methods we use rates that depend on the energy barrier between the states. Kinetic MC generates a sequence of configurations and times when the transitions between these configurations occur. This solves the master equation [89] in the sense that a certain configuration is obtained at time t with a probability $p_i(t)$ that is a solution of the master equation. The idea of kMC is not to compute probabilities $P_{ij}(t)$ explicitly, but to start with some particular configuration, a representative for the initial state of the experiment one wants to simulate, and then to make a sequence of other configurations with the correct probability. There are useful algorithms that yield a sequence of configurations.

2.4.1 In Frequent-Event Systems

An infrequent-event system is one in which the dynamics is characterized by occasional transitions from one state to another, with long periods of relative inactivity between these transitions. The infrequent event designation corresponds to a single energy basin, and the long time between transitions arises because the system must surmount an energy barrier to get out from one basin to another as shown in Figure (2.3). From Figure (2.3), one can recognize that at the bottom of the energy basin the force on every atom or particle of the system is zero (or the energy of the system is minimum). This defines a particular state i of the system and the geometry at the minimum can be considered as R_i. The system will vibrate about this minimum energy if the system is heated. As it vibrates, we still say it is in state i if it has not yet escaped over a barrier. Adjacent to the state i there are other potential basins, each separated from state i by an energy barrier. The important property of an infrequent-event system caught in a particular basin is that it stays there for a long time relative to the time of one vibrational period. Then, for each possible escape pathway to an adjacent basin, there is a rate constant k_{ij} that characterizes the probability, per unit time, that it escapes to the state j, and these rate constants are independent of what state preceded state i. Each rate constant k_{ij} is purely a property of the shape of the potential basin i, the shape of the ridge-top

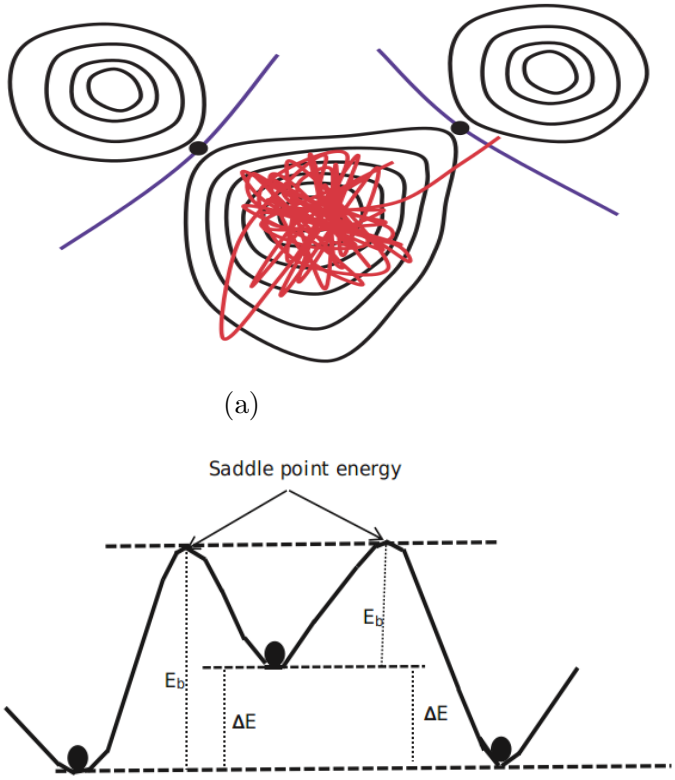

(a)

(b)

Figure 2.3: (a). The trajectory of potential energy surface for limited energy-barriers infrequent-event system. The lines and dots represents energy-barriers and saddle points, respectively. (b) The trajectory of a barrier energy from higher-energy state to lower-energy state. E_b and ΔE represents energy-barriers and the energy difference of the states, respectively.

connecting i and j and the shape of the potential basin j. Note that the state to state dynamics is a Markov walk, and the theory of the micro kinetic theory [90, 91] generally assumes that any such event occurs independently of all its predecessors. The transition out of state i depends on the set of rate constants $\{k_{ij}\}$ based on which one can design a simple stochastic procedure to propagate the system correctly from state to state. if we know these rate constants exactly for every state we enter, the probability that we see a given sequence of states and transition times in the kMC simulation can be determined.

On the other hand, the probability that the system is found in an initial state decreases if repulsive potential energy is added. It means that adding a bias potential to the actual

interaction potential leads to an increase of the probability of finding the system at a transition state [92]. This approach is more powerful if the bias potential is applied to increase the potential energy at the minima without altering the potential of unknown transition states so that the dynamics of the system can be simulated on the modified potential [93–98]. The most accurate and efficient formulation of such an approach is the hyperdynamics method developed by Voter [94, 95]. It is necessary to make certain that the bias potential vanishes at the transition state or saddle point. Voters bias potential is designed to perform this event if it exceeds the saddle point energy within the initial state energy basin. It is very important to provide the bias potential to greatly exceed the saddle point energy within the basin to get any significant acceleration of transitions in a system with many degrees of freedom.

2.4.2 The Rate Constant and First Order Processes

One of the fundamental ideas behind the entire kMC approach is that during its thermal vibrational motion in one of the potential energy surface basins the system losses the memory of its past history. Also one may assume that this loss of occurs continuously so that the system has the same probability of finding the escape path during each short increment of time it spends in the potential energy surface basin. This gives rise to a first order processes with exponential decay statistics that is analogous to nuclear decay. The probability that the system has not yet escaped from state i is given by

$$p_{survival}(t) = \exp(-k_{tot}t), \tag{2.4.1}$$

where k_{tot} is the total escape rate for escaping from the state. The probability that the system has escaped after a time t is

$$p(t) = 1 - \exp(-k_{tot}). \tag{2.4.2}$$

The probability distribution function per unit time for the first escape is

$$p(t) = k_{tot} \exp(-k_{tot}). \tag{2.4.3}$$

The average time for escape, τ, is can be found using the distribution function given by Equation (2.4.3) as

$$\begin{aligned} \tau &= k_{total} t[-\frac{1}{k_{tot}}] \exp(-k_{tot}t) \int_0^\infty - \int_0^\infty k_{total}(-1/k_{tot}) \exp(-k_{total}t) dt \\ \tau &= -t \exp(-k_{tot}t) \int_0^\infty + \int_0^\infty \exp(-k_{total}t) dt \\ \tau &= \tfrac{1}{k_{tot}}, \end{aligned} \tag{2.4.4}$$

where $k_{tot} = \sum_j k_{ij}$. The term on the right hand side represents the escape rate for each of the possible pathways from state i. Since escape can occur in one of several ways, we can make the same statement as above regarding these pathways, and the rate constant for each these pathways, k_{ij}, and the first-escape per unit time probability distribution for each path is

$$p_{ij} = k_{ij} \exp(-k_{ij}t), \tag{2.4.5}$$

although there is only one event to happen first for the system.

The Poisson distribution is centered around the average time for escape given by $\tau = \frac{1}{k_{tot}}$. When only considering this average time for escape, an executed jump from state i to state j would, therefore, simply advance the system clock by τ. Formally more correct is, however, to advance the system clock by an escape time that can be found properly from the distribution function $p(t)$. Generating an exponentially distributed random number, i.e., a time, say t_{draw}, drawn from the distribution $p(t) = k \exp(-kt)$, we draw a random number r from a uniform distribution on the interval (0,1), and then find the time t_{drawn} from the relation shown below

$$\int_0^{t_{draw}} k_{tot} \exp(-k_{tot}t) dt = r \exp(-k_{tot}t_{draw}) = 1 - rt_{draw} = -\frac{\ln(1-r)}{k_{tot}}.$$

Since $1 - r$ and r has similar uniform distribution on the range (0, 1), we prefer to write Equation (2.4.6) as

$$t_{draw} = -\frac{\ln(r)}{k_{tot}}. \tag{2.4.6}$$

This escape time only depends on the total rate constant and independent of the actual time taken for the pathway that the system follow to take out the system out of the current state i. This pathway, however, needs to be identified, to determine the possible neighboring state j to which the the system has to move. Therefore j is the starting point for the next kMC step, i.e., the next kMC step decides the escape from this particular state j. in the next section we will briefly see how the pathway that will take the system from state i to state j is chosen.

2.4.3 Normally distributed random variables

Generation of standard normal random variables from normal distribution is possible by inverting the distribution function together with uniformly distributed random numbers between 0 and 1. But, since the integral of this distribution function is not evaluated like exponential function the required random numbers are generated based on different methods. Among these methods we will present below the Box Muller method. The normal distribution function is

$$\rho(x) = \frac{1}{\sqrt{2\pi}} \exp(-\frac{x^2}{2}) \tag{2.4.7}$$

$$P(x < x) = \frac{1}{\sqrt{2\pi}} \int_{-\infty}^{x} \exp(-\frac{x'^2}{2}) dx' \tag{2.4.8}$$

To come to the method (the Box Muller method) we first show that $\frac{1}{\sqrt{2\pi}} \int_{-\infty}^{\infty} \exp(-\frac{x^2}{2}) dx = \sqrt{2\pi}$.

To prove this, consider

$$\left(\int_{-\infty}^{\infty} dx \exp(-\frac{x^2}{2}) dx \right)^2 = \int_{-\infty}^{\infty} \int_{-\infty}^{\infty} dx dy \exp\left(-\frac{x^2+y^2}{2} \right) \tag{2.4.9}$$

To evaluate this integral, we do change of variable

$$\begin{aligned} x &= r\cos\theta \\ y &= r\sin\theta \end{aligned} \tag{2.4.10}$$

where r and θ are polar coordinates random variables (r, θ) defined by $0 \leq \theta \leq 2\pi$. θ is uniformly distributed in the interval $[0, 2\pi]$ and may be sampled using $\theta = 2\pi u_1$, where $u_1 \in [0, 1]$.

$$\begin{aligned} x^2 + y^2 &= r^2 \\ \tan^{-1}\left(\frac{y}{x}\right) &= \theta \\ \int_{-\infty}^{\infty} \int_{-\infty}^{\infty} dx dy \exp\left(-\frac{x^2+y^2}{2} \right) &= \int_0^{2\pi} \int_0^{\infty} \exp\left(-\frac{r^2}{2} \right) \left| \frac{\partial(x,y)}{\partial(r,\theta)} \right| dr d\theta \\ \left| \frac{\partial(x,y)}{\partial(r,\theta)} \right| = \begin{vmatrix} \frac{\partial(x)}{\partial(r)} & \frac{\partial(x)}{\partial(\theta)} \\ \frac{\partial(y)}{\partial(r)} & \frac{\partial(y)}{\partial(\theta)} \end{vmatrix} &= \begin{vmatrix} \cos\theta & -r\sin\theta \\ \sin\theta & r\cos\theta \end{vmatrix} = r\cos^2\theta + r\sin^2\theta = r \end{aligned}$$

Thus

$$\int_0^{\infty} dr \exp\left(-\frac{r^2}{2} \right) r \int_0^{2\pi} d\theta = 2\pi \int_0^{\infty} r dr \exp\left(-\frac{r^2}{2} \right) \tag{2.4.11}$$

To solve this integral, we again use the change of variable method. Let $s = r^2/2$ and $ds = rdr$ Thus

$$2\pi \int_0^{\infty} r dr \exp\left(-\frac{r^2}{2} \right) = 2\pi \int_0^{\infty} ds \exp(-s) = 2\pi \Big[-\exp(-s) \Big]_0^{\infty} = 2\pi[-0+1] = 2\pi \tag{2.4.12}$$

$$\left(\int_{-\infty}^{\infty} dx \exp(-\frac{x^2}{2}) \right)^2 = 2\pi \quad or$$

$$\int_{-\infty}^{\infty} dx \exp(-\frac{x^2}{2}) = \sqrt{2\pi} \quad or$$

$$\frac{1}{2\pi} \int_{-\infty}^{\infty} \int_{-\infty}^{\infty} dxdy \exp\left(-\frac{x^2+y^2}{2}) \right) = 1 \tag{2.4.13}$$

New function can be define as

$$U(r) = \frac{1}{2\pi} \int_{x^2+y^2 \leq r^2} dxdy \exp\left(-\frac{x^2+y^2}{2}) \right) \tag{2.4.14}$$

This integral interval is $x^2 + y^2 \leq R^2$ we calculated this integral as

$$\begin{aligned} U(r) &= \frac{1}{2\pi} \int_0^{2\pi} d\theta \int_0^r r^{'} dr^{'} \exp\left(-\frac{r^{'2}}{2} \right) \\ U(r) &= \frac{1}{2\pi} \times (2\pi) \int_0^{\frac{r^2}{2}} dr \exp(-r) = 1 - \exp\left(-\frac{r^2}{2} \right) \\ U(r) &= 1 - \exp\left(-\frac{r^2}{2} \right) \end{aligned} \tag{2.4.15}$$

$U(r)$ is nondecreasing function satisfied as

$$\lim_{r \to 0} U(r) = 0 \tag{2.4.16}$$

$$\lim_{r \to \infty} U(r) = 1 \tag{2.4.17}$$

This means that $U(r)$ is a random number distributed in between $[0, 1]$. Let us call it U_2. Hence the above equation becomes

$$U_2 = 1 - \exp\left(-\frac{r^2}{2} \right) \tag{2.4.18}$$

$$\begin{aligned} \exp\left(-\frac{r^2}{2} \right) &= 1 - U_2 \\ -\frac{r^2}{2} &= \ln(1 - U_2) \\ r &= \sqrt{-2\ln(1 - U_2)} \end{aligned} \tag{2.4.19}$$

$$
\begin{aligned}
x &= r\cos\theta \\
y &= r\sin\theta \\
x &= \sqrt{-2\ln(1-U_2)}\cos(2\pi U_1) \qquad (2.4.20)\\
x &= \sqrt{-2\ln(1-U_2)}\sin(2\pi U_1) \qquad (2.4.21)
\end{aligned}
$$

Generating, stochastic variable $x \sim N(\mu, \sigma^2)$, with the mean μ and the variance σ^2, is given as

$$
\begin{aligned}
x &= \mu + \sqrt{-2\ln(1-U_2)}\cos(2\pi U_1) \qquad (2.4.22)\\
x &= \mu + \sqrt{-2\ln(1-U_2)}\sin(2\pi U_1) \qquad (2.4.23)
\end{aligned}
$$

2.4.4 The kinetic Monte Carlo procedure

There are Stochastic algorithms that will propagate a system from state to state correctly. The first one is less efficient and not widely used though valid. To describe it let us assume that all the rate constants are known for each state. Our system is in state i, and we have a set of pathways and associated rate constants $\{k_{ij}\}$. The probability distribution for each of these pathways is $p_{ij} = k_{ij}\exp(-k_{ij}t)$. Using the relation $t = -\frac{\ln(r)}{k}$ we can draw an exponentially distributed time t_j from the distribution for each pathway j. The actual escape can only take place along one of these pathways. Thus we find the pathway j_{min} which has the lowest value of t_j, and advance our overall system clock by t_{jmin}. We then move the system to a new state, and begin again from this new state. But, this is less than ideally efficient because we draw a random number for each possible escape path.

The second algorithm that can propagate the system from one state to another performs the job only with two random numbers is more efficient and used commonly. The procedure starts by determining (choosing viable) all N possible processes, a number of escape pathways, out of the present system configuration, say i state. Limiting a number of pathways to a finite value N corresponds with limiting the maximum distance (or the

maximum number of pathways for each particle) to which each particle in the system can move from one place to another within the time $t = -\frac{\ln(r)}{k}$. The corresponding N different rate constants are then assumed to yield the total rate constants $k_{tot} = \sum_{p=1}^{N} k_p$. Then we find a process which fulfills the condition

$$\frac{\sum_{p=0}^{q-1} k_p}{k_{tot}} \leq r < \frac{\sum_{p=1}^{q} k_p}{k_{tot}}, \tag{2.4.24}$$

where we have defined $\frac{k_0}{k_{tot}} = 0$, and r is a random number drawn from a uniform distribution on the range (0, 1). An expression in Equation (2.4.24) means that k_p element is added until it reaches a step where $r < \frac{\sum_{p=1}^{q} k_p}{k_{tot}}$ is satisfied, which signifies the selected pathway. The maximum value of q is N at which $\frac{\sum_{p=1}^{q} k_p}{k_{tot}}$ becomes 1. This procedure gives a probability of choosing a particular pathway that is proportional to the rate constant for that pathway. To advance the system clock we draw a random time from the exponential distribution for the rate constant k_{tot} or $\{t = -\frac{\ln(\omega)}{k_{tot}}\}$, where ω is another random number drawn from a uniform distribution on the range (0, 1) different from that mentioned above as r. Note that this time has nothing to do with which event or pathway is chosen. The transition time for the system from one state to another depends only on the total escape rate. Once the system is in the new state, the list of pathways and rates is updated, and the procedure is repeated.

2.5 The model

The system we study is a model of a conjugated polymer film similar to that shown in Figure ((2.4)).

The film can be used as an active material in electronic devices such as field-effect transistors or light emitting diodes or photo voltaic cells. The geometry of this material can be considered as a three dimensional rectangular box of sides L_x, L_y, and L_z. An electric field is established by applying a voltage across the material between two metallic electrodes contacts. The charge carriers are injected from the electrode contacts to the

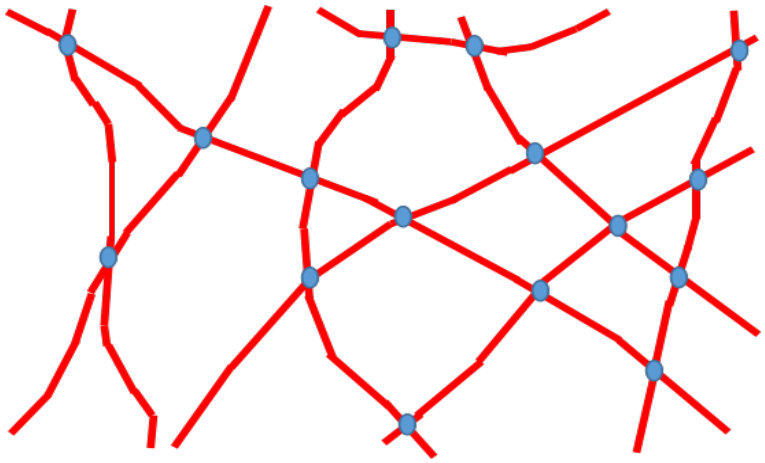

Figure 2.4: Structure of thin film built from conjugated polymer chains

polymer film and the electric field forces the charge carriers to move along a direction from one contact (source) to another contact (drain). The net direction of motion of the charge carriers and electric field are the same if the charge carriers are holes, and in the opposite direction if the charge carriers are electrons. In the case of polymer light emitting diodes both electric field and the density of the charge carriers depend on the electric potential difference between the electrodes. But, in polymer field effect transistors the charge carriers density depend on the gate voltage whereas the electric field along the channel length is formed by the electric potential difference between the source and drain electrodes. In real experiment since the values for these voltages and the corresponding devices geometry are known the range in which the charge carriers density varies for each of these devices can be determined. Based on these facts the density of charge carriers is identified to be varying in the range from $10^{14} cm^{-3}$ to $10^{16} cm^{-3}$ for PLEDs and from $10^{17} cm^{-3}$ to $10^{19} cm^{-3}$ in PFETs [73, 74]. In line with this we assume similar devices and introduce a certain number of charge carriers to our polymer film in such a way that the charge carriers density variation looks like that described above for both low and high charge carriers densities. We do not investigate the charge carriers density variation with

the parameters that have effects on it and also not need those parameter in our calculations as our focus, is not on that, on the effects of charge carrier density on mobility. The direction of the source-drain electric field, F_{SD}, is taken to be along the x-axis, which also becomes the direction along which the mobility is calculated. The magnitude of the electric field we use across the film is approximated on the basis of the operating values of the potential difference between the electrodes in a specific arrangement of a device. The width of the conducting channel is in the y-direction, and the z-axis points in a direction perpendicular to y-axis and also to the channel length in the the polymer film.

The model system is a super cell of a hypothetical simple cubic lattice with lattice parameter b in which each sub unit of a polymer chain is represented by a lattice point. These lattice points, known as states or sites, are localized on different molecules or conjugated polymer units (or segments). The segment length which is assumed as a lattice site has intrachain conjugation length of typically about 6-7 nm and interchain packing distance of roughly 0.3-0.4 nm. This means that the distance from a site on one chain to any one of its neighboring sites on the same chain is different from that on another nearby lying chain(s), and obviously the hopping process in a three-dimensional conjugated polymer system is anisotropic. In general it is not easy to identify the microscopic parameters of a polymer film and use them precisely as the film is the aggregate of patternless and intermingled chains. Because of this, we also approximate the hopping problem, as it is done elsewhere [38, 41, 42, 71], by the average of both intrachain and interchain hopping process. The lattice parameter, b, is also considered as an effective result of an average of interchain and intrachain lattice spacings. A disordered system is formed with $L_x \times L_y \times L_z$ lattice sites distributed randomly in a cubic super cell of side L_x in the $x-$, $y-$, and $z-$ directions, respectively, and periodic boundary conditions are applied in all directions. The average intersite distance is $b = N^{-1/3}$, where N is the concentration of randomly distributed localized sites or states. The estimated value of the parameter N for organic conjugated polymer is between $N \approx 10^{20} cm^{-3}$ and $N \approx 10^{21} cm^{-3}$ [99]. The sites through

which a charge carrier hopping takes place reside inside a sphere centered at regularly placed points like that shown in Figure (2.5) for sites distributed in two dimensions.

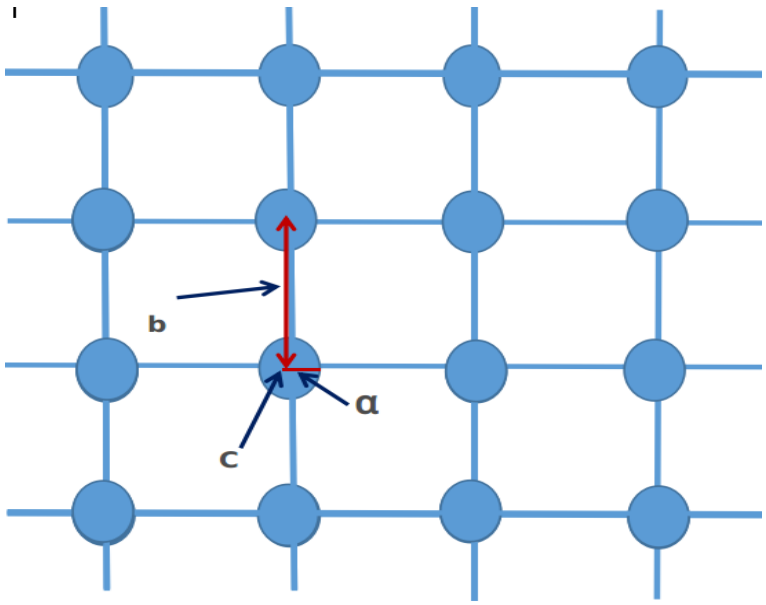

Figure 2.5: Regularly spaced spheres of radius r, distance between centers of neighboring spheres b, and localization length α.

The distance between the nearest neighbouring spheres centers is the same as the lattice parameter mentioned above as b. But, the distance between the nearest neighboring sites can be between $b-2r$ and $b+2r$, where r is the radius of each sphere which is related to the localization radius of a charge carrier wave function. This means that a charge carrier is placed randomly at any point inside a sphere and the minimum hopping distance is also a random variable that varies between $b-2r$ to $b+2r$. In the case when the spatial disorder is not considered r is taken to be zero and the sites are distributed uniformly on a regularly distributed grids in a cubic box of side L_x like that shown in Figure ((2.6)). We mimic that the system is energetically disordered by assigning energies drawn from the Gaussian distribution given in Equation (1.3.2) at the randomly distributed hopping sites.

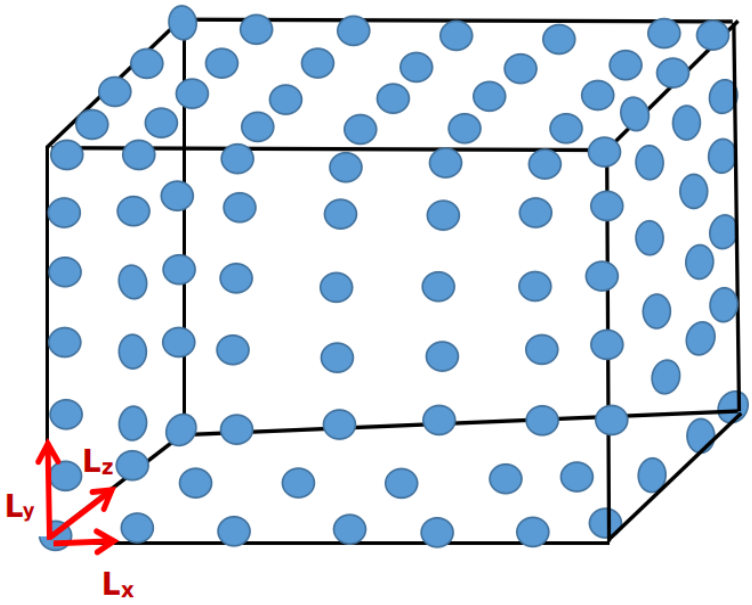

Figure 2.6: Three dimensional cubic super cell of lattice with sides L_x, L_y, and, L_z.

2.6 Simulation Details

As we described in the above section we establish $L_x \times L_y \times L_z$ charge carriers hopping sites in three dimensions. The average number of sites along each dimension is assumed to be the same and the average distance between the nearest neighboring sites or the the lattice spacing is unit length, and the average number of sites per unit volume is $N = 10^{21} cm^{-3}$. To these sites a certain number N_h of charge carriers are introduced and randomly placed on different sites. The electric field along the x-axis due to the source-drain bias V_{SD} is assumed by the average value from the relation $E_{SD} = \frac{V_{SD}}{L}$, where L is the length between source and drain. This assumption is made based on the fact that this field is almost constant in the majority of the region where charge carriers move as verified recently in Reference [57]. Therefore, we can calculate the electric potential energy due to the source-drain bias field for a charge carrier at each regularly spaced site from the following relation

$$U_{SD}(x, y, z) = F_{SD}eb(x - L_x) = \frac{V_{SD}}{L_x}b(x - L_x), \tag{2.6.1}$$

where the minimum is fixed at the right edge of the polymer film or at $x = L_x b$ in this case. Note that $x = 0$ and $x = L_x b$ coincides with the left and right edges of the polymer film, respectively.

In consistence with the Gaussian disorder model (GDM) all sites to which a hop of a charge carrier is possible are assigned random energies sampled from a zero-centered Gaussian distribution function given in Equation (1.3.2). The random energy at a site means the energy of a charge carrier when it resides in that site. Likewise in Reference [38] these energies are assumed to be uncorrelated, and ε is the energy of a charge carrier at a site and σ is the standard deviation that determines the amount of energy disorder in the film. Mapping this distribution to that of a uniformly distributed random numbers between 0 and 1 it is possible to solve for the disorder energy for a charge carrier at each site in terms of the random numbers and a material specific Gaussian width σ from Equation (2.4.23).

The results presented in the next chapter are obtained with the standard deviation in the Gaussian distribution of on-site energies of σ between 0.06 eV to 0.14 eV, which is specified for different disordered organic polymers as explained elsewhere [42, 73, 100]. The hopping rate across the sites from an occupied site, say i, to an empty site, say j, which are separated from each other by a distance R_{ij} is assumed to be governed by Miller and Abrahams formalism [39] which is similar to that given by Equation (1.3.3). This equation helps us to determine the transition probability for a system of charge carriers from one configuration to another (we will present the detail in the next section).

The change in energy for a charge carrier when at different hopping sites i and j is described as

$$U(\mathbf{R}_j) - U(\mathbf{R}_i) = [\varepsilon(\mathbf{R}_j) + U_{SD}(\mathbf{R}_j)] - [\varepsilon(\mathbf{R}_i) + U_{SD}(\mathbf{R}_i)], \tag{2.6.2}$$

where U_{SD} is the potential energy contributions from the source-drain field, $\mathbf{F}_{SD}$. We have neglected the effect of electrostatic potential energy due to Coulomb interaction after independently verifying its negligible effects on the dynamics of charge carriers in the low density. We have neglected the effects of of electrostatic potential energy due to Coulomb interaction with the intuition that the average distance between charge carriers is larger than 21 lattice parameter for a lower density less than or equal to $10^{16} cm^{-3}$ and the static electric fields due to charge carriers hardly affect the transport properties of the charge carriers in the sample lattice. The reason for this claim comes from the fact that the contribution of these charges on the difference between the energies at the neighboring hopping sites which also determine the small walking step and thereby drift speed is relatively negligible. In addition to this, we also assume that double occupancy of the same site does not occur as it is not energetically favorable for the level of the carriers density we are now dealing with and weak electron phonon coupling. Here, the rectangular coordinates of all the sites are known in the code during the three dimensional sites formation. And the charge carriers are also identified with the names from 1 to N_h given to them when they are first introduced to the sites. Therefore, the coordinates of each charge carrier are known at every moment in the code, and the magnitude of the distance between any two sites $\mathbf{R}_{ij}$ can be easily calculated numerically from the relation

$$R_{ij} = \sqrt{(x_i - x_j)^2 + (y_i - y_j)^2 + (z_i - z_j)^2}. \tag{2.6.3}$$

2.7 Simulation Procedures

In our simulation we start the procedures by forming a three dimensional lattice of $L_x \times L_y \times L_z$ regularly spaced points or locations of the centers of spheres with the same radius r. Then unoccupied hopping sites of charge carriers are randomly formed inside each sphere. In the second procedure we calculate the on-site disorder energies $\varepsilon(x, y, z)$

for each site from Equations (2.6.2 and 2.4.23), and $U_{SD}(x, y, z)$ from Equation(2.6.1). In the third step we introduce N_h number of charge carriers to the system by randomly placing them on the unoccupied sites formed in the first procedure. N_h is chosen in order that the charge carriers density varies in the range for that of OLEDs or OFETs. For values of gate voltage V_g in the operation range of OFETs; between -10 V, -30 V, we use number of charge carriers corresponding to charge carriers densities between $10^{17}cm^{-3}$ and $5 \times 10^{8}cm^{-3}$. Similarly for values of source-drain voltage V_{SD} in the operation range of OLEDs, between 1 V to 3 V, the we use number of charge carriers which correspond to densities between $10^{14}cm^{-3}$ $10^{17}cm^{-3}$. In the fourth procedure, the exact three dimensional charge carriers distribution governed by the effective energy introduced above is realized. Initially, the charge carriers are distributed randomly throughout the total volume of the film. An equilibrium state of charge carriers distribution is assumed to be achieved in a certain number of MC time steps (MCTSs). That is, we pick the first particle and check if its neighboring sites are empty or occupied. If there is no empty site we assign zero for its probability of hopping, and go to the second particle. But, if there is (are) neighboring unoccupied site(s), we calculate the total energy difference of the particle between the neighboring empty sites and initial site from Equation(2.6.2). Then we solve for the transition rate using Equation (1.3.3) excluding ν_0 for each possible hopping site. We repeat this procedure for all charge carriers, and divide each transition to the total transition rates to find the probability of hopping for each possible path as shown by Equation (2.4.24). The sum of the probabilities for all possible paths is normalized to one, and the transition from one configuration to another takes place by one of the N_h charge carrier along one path. This means that we use the probability length for each path and realize a transition of a system of charge carriers from one configuration to another by moving one of the charge carriers based on a stochastic approach.

The probability that a charge carrier hops from an occupied site i to an unoccupied site j can be written from the rate equation, Equation(**??**), as

$$P_{ij} = \frac{\nu_{ij}}{\sum_{j=1}^{N_h} \sum_{i=1}^{l} \nu_{ij}}, \tag{2.7.1}$$

where the values of ν_{ij} are obtained from Equation (**??**) where i counts the possible nearest neighboring sites for each charge carriers from one to, say l, and j counts the number of charge carriers from one to the last, say N_h. Equation (2.7.1) ensures that a detailed balance condition is satisfied in the steady state condition. Obviously $\sum_{i=1}^{N_h} \sum_{j=1}^{l} P_{ij} = 1$ and, therefore, these probabilities generate a sequence of length intervals between 0 and 1. To decide for a particular hop we generate a random number r from a uniform distribution also in the interval between 0 and 1, which points at a particular interval and consequently at a particular destination site to which one of the the charge carriers jumps with the scheme given below which similar to that given by Equation (2.4.24)

$$\sum_{i=0}^{N_h-1} \sum_{j=0}^{l-1} P_{ij} \leq r < \sum_{i=1}^{N_h} \sum_{j=1}^{l} P_{ij}, \tag{2.7.2}$$

where we have defined ($P_{00} = 0$). We have restricted the possible destination sites j in Equation (2.7.1) to the 26 nearest neighbor sites in an average volume of $3 \times 3 \times 3$ lattice sites. Even if more number of possible destinations are involved, a vast majority of the hopping events occur to the nearest neighbor sites, and the effect of this restriction is negligible. This step is repeated for a certain number of MCTSs until we record enough data. One MCTS corresponds to moving one charge carrier after choosing from all charge carriers according to the procedure described above. Using Equation (2.4.4) and that expressed for conjugated polymers in References [38, 101] the mean dwelling time τ of a charge carrier at site i which is equivalent to the mean time for the transition that occurs between the states identified by the procedure described above is given as

$$\tau = \frac{1}{\sum_j \nu_{ij}}. \tag{2.7.3}$$

$$\tau = \frac{1}{\sum_{j=1}^{N_p}\sum_{i=1}^{26}\nu_{ij}} \tag{2.7.4}$$

The actual hopping time τ_h is distributed about the mean time τ, where the minimum and maximum limits approach zero and infinity, respectively. This distribution can be expressed by an exponential probability distributions of the type $\frac{1}{\tau}\exp\left(-\frac{\tau_h}{\tau}\right)$ as explained in the previous section. To find the actual hopping time τ_h, consider

$$p(\tau_h) = \int_0^{\tau_h} \frac{1}{\tau} exp\left(-\frac{t}{\tau}\right) dt. \tag{2.7.5}$$

Since τ_h is in the interval $[0, \infty)$, $p(\tau_h) = 0$ if $\tau_h = 0$ and 1 if $\tau_h = \infty$, or in general it has a value between 0 and 1. Consequently, a random number r taken from a uniform distribution between 0 and 1 can be mapped to it. Hence, we evaluate the integral in Equation(2.7.5) and then solve for τ_h in terms of r and τ as

$$\tau_h = -\tau log(1 - r). \tag{2.7.6}$$

This approach, which introduces a stochastic behavior in both the transition path [from Equation (2.7.1)] and the time needed for the transition, ensures that the mean transition time (between two configurations or states) is simply the mean of the inverse transition rates between these two states.

We let the system pass through $(m-1) \times 10^n$ MCTS to ensure that the system has reached a steady state distribution. It should be noted that different generations of the on-site energies from the GDM results in small but nevertheless notable differences in the simulation results. The results are therefore averaged over 15 different generations of energy distributions.

The fifth and final simulation procedure involves recording of the displacement of the charge carriers along the length in the direction of $\mathbf{F}_{SD}$ together with the time taken for this displacement to occur. The recording is performed for last 1×10^n MCTSs. The

displacement of the charge carriers along the length in the direction of $\mathbf{F}_{SD}$ as a function of time gives the velocity, and the mobility of the charge carriers is obtained from the ratio of the velocity and source-drain bias electric field. This means that we obtain detailed information regarding the transport properties of charge carriers. Finally, simulation data are collected as a function of the charge carrier concentration, source-drain voltage, F_{SD}, and temperature, T for different localization radius.

Chapter 3

Results and Discussion

The main focus of this work is on the transport properties of charge carriers in organic disordered semiconducting conjugated polymers. This means that the dependence of the main transport coefficient, mobility, on different parameters that characterize the materials as well as externally applied parameters are investigated based on the results found from kinetic Monte Carlo simulation approaches. One of the parameters that determine the magnitude of the charge carrier mobility is the energy disorder strength or energy scale, commonly expressed by the standard deviation σ of the energies distribution. In most of our simulations, as done elsewhere [38,42], the energies of a charge carrier that originate from an electric field and temperature are expressed in terms of this disorder energy. The localization length of a charge carrier wave function is another parameter that has effects on a charge carrier mobility. This parameter is expressed in terms of a lattice parameter called lattice sites spacing. The lattice sites spacing, denoted by b as mentioned above, shows the average distance between the centers of nearest neighbouring spheres as we explained in Chapter **??** Section2.6. In addition to these two parameters mobility depends also on charge carriers density ρ and sites concentrations N (or number of states per cm^3). For a cubic sample of volume $200nm \times 200nm \times 200nm = 8 \times 10^6 nm^3$, 8×10^6 sites are introduced so that there is on average $N = 10^{21} cm^{-3}$ states or one site per nm^3. The lattice spacing is related to the site concentrations as $b = N^{-1/3}$. In the calculation we fix the total number of sites and vary the density of charge carriers

ρ by varying the number of charge carriers which are introduced to the sample. The main transport parameter, mobility, is expressed mostly in terms of lattice parameter b, disorder parameter σ, unit charge on electron e, and phonon frequency ν_0 (or in units of $\frac{b^2\nu_0 e}{\sigma}$). When these parameters are known explicitly, mobility is also expressed explicitly. The range of electric field magnitudes used for our calculations is chosen to highlight regimes of different transport behaviour. Most experimental data [**?**, **?**, 42, 55, 63, 73, 74] fall, however, into the regime which is below what is referred to as low field strengths (or less than or equal to $1 \times 10^5 Vcm^{-cm}$). The numerical results we obtained using kMC simulations are presented and analyzed in the following sections.

3.1 The effects of disorder energy, charge carriers density, and electric field on mobility

In this section we will present our simulation results which describe the transport properties of a charge carrier mobility. Mainly the charge carrier mobility as a function of charge carriers density, applied electric field, and temperature of the materials. Finally, We will discuss the effect of energy disorder parameters on the charge carrier mobility at lower charge carriers density for organic semiconducting films when used in light emitting diodes, and also give analysis on the possible values for the localization length of the wave function for a charge carrier at hopping sites comparing our simulation results for the charge carrier with the experimentally found ones.

We first present the results we obtained for a charge carrier mobility as a function an external applied electric field for different charge carriers density and energy disorder, and compare with those reported experimentally and theoretically using kMC simulation methods. Let us start with the results obtained for a charge carrier mobility variation with electric field for $r = 0$ or regular grids for different values of $\hat{\sigma} = \frac{\sigma}{k_B T}$ and also two different values of localization length. The mobilities are plotted (on a logarithmic scale)

as a function of electric field in units of $\frac{\sigma}{ea}$ for disorder energy parameter $\hat{\sigma} = \frac{\sigma}{k_B T}$ in the range from 1 to 6 as shown in Figure (3.1) localization length $\alpha = 0.1band0.2b$ for the same charge carriers density.

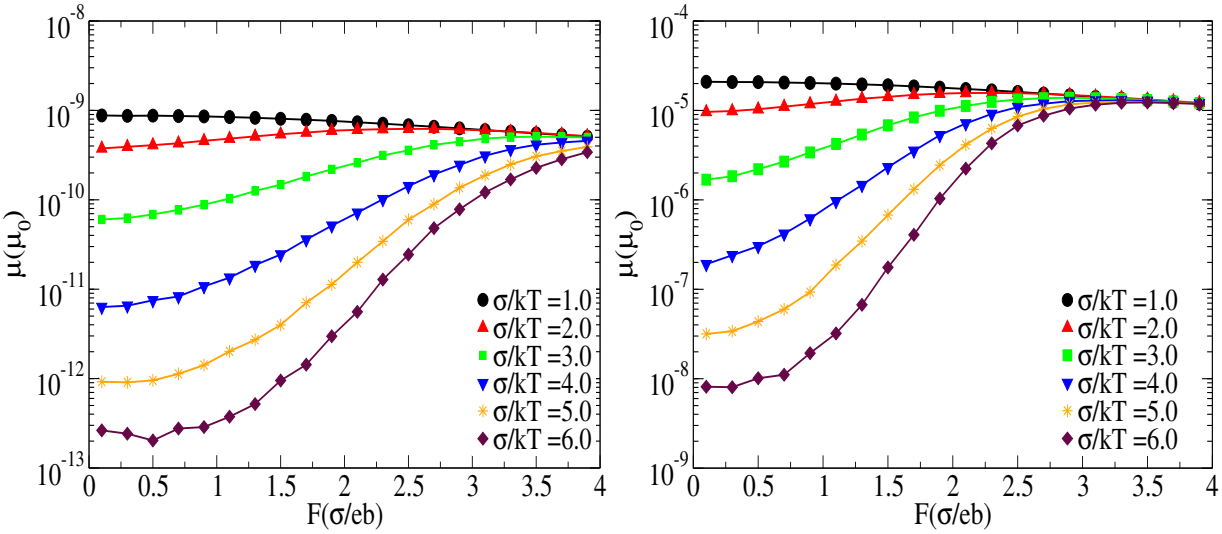

Figure 3.1: Charge carrier mobility (μ) versus electric field (F) for different values of disorder $\hat{\sigma}$ and localization length α. (a) $\alpha = 0.1b$, (b) $\alpha = 0.2b$, where b is lattice spacing and $\mu_0 = \frac{b^2 \nu_0 e}{\sigma}$

.

The plots in both Figures (3.1) (a and b) show that the charge carrier mobility in the lower electric field region decreases with the increase of the disorder parameter $\hat{\sigma}$ as verified and justified in the previous reports [38, 42, 55]. As the plots for the higher disorder energy parameter $\hat{\sigma}$ show, the mobility increases with the increase of electric field until a saturation value is attained corresponding to each $\hat{\sigma}$. The saturated mobility values for different $\hat{\sigma}$ are nearly the same and reached at nearly the same electric fields provided that the localization length α is the same. The reason for the occurrence of the saturation value is due to the fact that the electric field that appears in Equation (1.3.3) reduces the barrier height for an energetic uphill jumps from transport energy level in the field direction and thereby enhances the mobility in the hopping conduction of charge carriers as described in Reference [58]. On the other hand, drift mobility is calculated

from $\mu = v/F$ relation which leads to mobility reduction with the increase of electric, where v is a drift velocity of charge carrier due to the applied electric field F. This means that increasing the electric field is more effective in reducing the activation barrier, though reduces also the mobility, until the electric potential energy difference between two sites separated by lattice spacing b due to applied electric field, eFb, approaches (but doesn't surpass) the energy scale (or disordered energy σ). If eFb is greater than σ an excess energy from eFb above σ which is the same as $eFb - \sigma$ does not have any contribution to speed up hopping conduction but reduces mobility since it appears in the mobility calculation, $\mu = v/F$. The reference energy value we took here, the energy scale σ, to justify the statement that electric field raises mobility until eFb reaches σ may not be exact and needs experimental verification though it makes sense and seems reasonable. Due to this reason the effect of electric field in increasing the charge carrier mobility is more significant for the larger disorder energy scale (or σ) of a material. Similarly temperature plays a crucial role in reducing the difference between the energies at the transport level and that of the hopping particle at the equilibrium level. Most of the curves in Figures (3.1) (a and b) show an overall similar behaviour except that there is an increase of mobility with the increase of localization length. We also observe that the mobility saturates at lower electric field in the case of larger localization length. This indicates that a charge carrier conduction increases with the localization length and the effect of electric field on mobility decreases with the increase of localization length. This means that when α increases the charge carriers hopping distance may not be limited to only that between nearest neighbours, it may include also the distances larger than that between nearest neighbours. The charge carrier hopping rarely occurs when the localization length is small (or the state is strongly localized) at relatively high disorder energy parameter $\hat{\sigma}$ in a lower electric field region.

Our next simulation results are for charge carrier mobility variation with electric field for $r = 0$ or regular grids for different values of $\hat{\sigma} = \frac{\sigma}{k_B T}$ and also for four different

charge carriers density and the same localization length. The mobilities are plotted (on a logarithmic scale) as a function of electric field in units of $\frac{\sigma}{ea}$ for different values of $\hat{\sigma} = \frac{\sigma}{k_B T}$ in the range from 1 to 6 as shown in Figure (3.2) and for the same value of localization length $\alpha = 0.1b$.

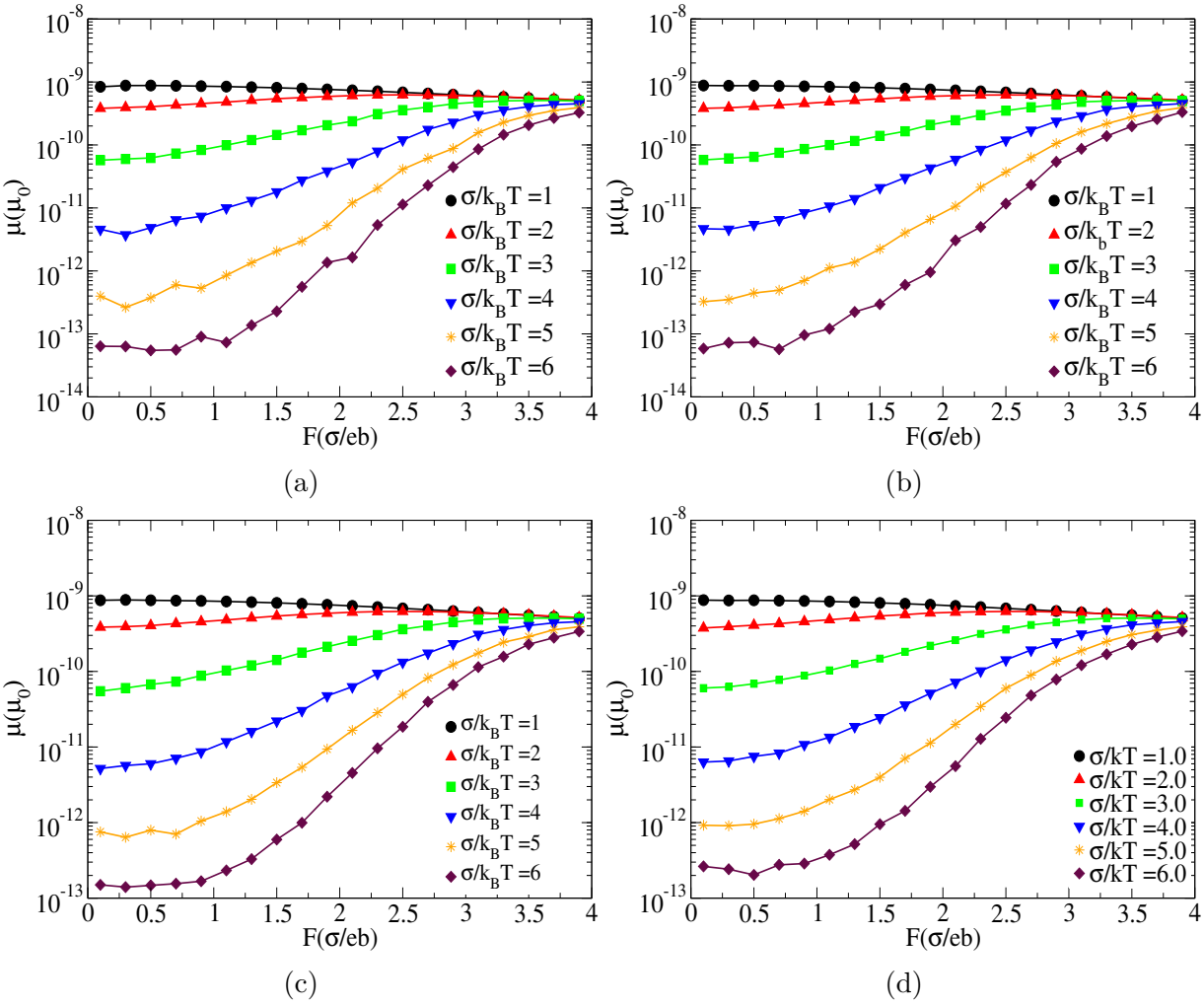

Figure 3.2: Simulation results of charge carrier mobility (μ) versus electric field (F) for different values of disorder $\hat{\sigma}$ and charge carriers density with localization length $\alpha = 0.1b$ (a) $\rho = 1 \times 10^{15} cm^{-3}$, (b) $\rho = 1.5 \times 10^{15} cm^{-3}$, (c) $\rho = 5 \times 10^{15} cm^{-3}$ and (d) $\rho = 1 \times 10^{16} cm^{-3}$, where b is lattice spacing and $\mu_0 = \frac{b^2 \nu_0 e}{\sigma}$

The plots in Figures (3.2) (a to d) show the change of mobility with the electric field in a similar way regardless of charge carriers density variation. Like that shown in Figure (3.1) the mobility of a charge carrier increases with the increase of electric field until

saturation value is attained when the disorder energy parameter, $\hat{\sigma} is greater tan$ 2. The increment becomes more pronounced when $\hat{\sigma}$ increases which is in line with the suggestion made above, that says, the effect of electric field on the activation barrier between localized hopping sites increases with the increase of the barrier as discussed above. We also observe slight increment of mobilities with charge carriers density though the density is low (in the range of the density for light emitting diodes [73, 74]) for disorder energy parameter, $\hat{\sigma}$ is greater than 2. As we see in the plots when the disorder parameter $\hat{\sigma}$ decreases the variation of mobility with charge carriers density decreases until the disorder parameter $\hat{\sigma} = 3$ where mobilities for different change carriers densities are nearly the same at each electric field value as shown by the curves in Figures (3.2) (a to d). Our results for $\hat{\sigma} = 3$ is similar to that shown experimentally in References [73, 74]. Our results for larger values of $\hat{\sigma}$ is similar in agreement with that shown in Reference [42] though there are slight variations with that shown in [74]. To understand the reason for the slight variations with the experimental ones we have separated σ and temperature and calculated mobility versus charge carriers density; we will discuss more on this below. As suggested in the previous studies the reason for the increment of mobility is due to the fact that the number of deep states, in the Gaussian density of states, that are filled with charge carriers increase with the increase of charge carriers density. As a consequence the higher the charge carriers density the more states with near lying energies (little difference in energies) become available for the charge carrier.

The curves in Figure (3.3) show simulation results of charge carrier mobility versus electric field for $r = 0$ or regular grids for different values of $\hat{\sigma} = \frac{\sigma}{k_B T}$ and also for four different charge carriers density and the same localization length. The results here are for similar parameters used in Figure (3.2) except the localization length α. The mobilities are plotted (on a logarithmic scale) as a function of electric field in units of $\frac{\sigma}{ea}$ for different values of $\hat{\sigma} = \frac{\sigma}{k_B T}$ in the range 1 to 6 and for the same value of localization length $\alpha = 0.2b$. The lots in Figures ((3.3) and (3.3)) show that a charge carrier mobility increases with

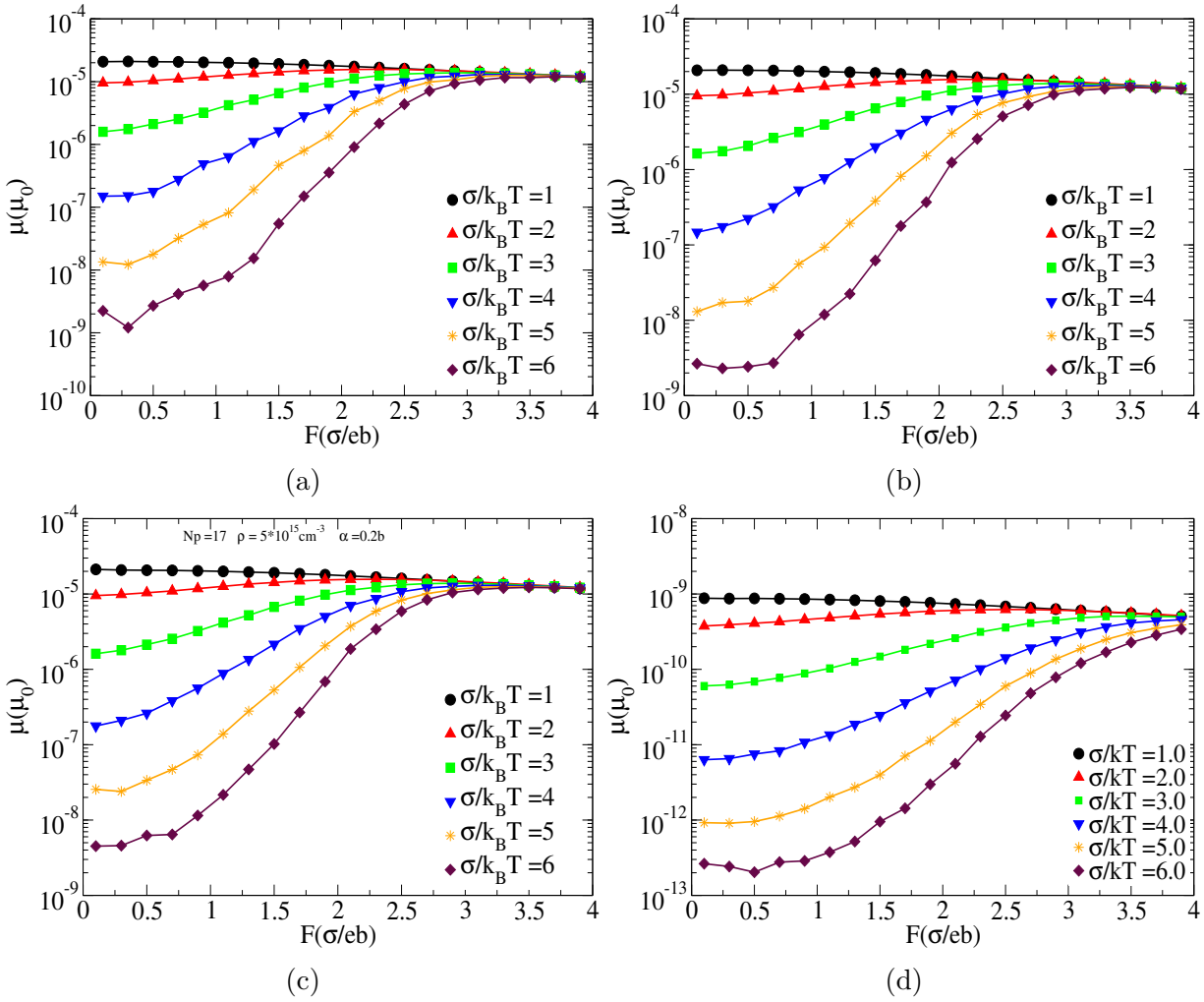

Figure 3.3: Simulation results of charge carrier mobility (μ) versus electric field (F) for different values of disorder $\hat{\sigma}$ and charge carriers density with localization length $\alpha = 0.2b$ (a) $\rho = 1 \times 10^{15} cm^{-3}$, (b) $\rho = 1.5 \times 10^{15} cm^{-3}$, (c) $\rho = 5 \times 10^{15} cm^{-3}$ and (d) $\rho = 1 \times 10^{16} cm^{-3}$, where b is lattice spacing and $\mu_0 = \frac{b^2 \nu_0 e}{\sigma}$

an applied electric field until the saturation value is attained for pronounced disorder parameter $\hat{sigma}$ for both values of localization length. The difference is that apart from the shift (increase) in values with the localization length the mobility increases faster and saturates at lower electric field in the case of larger localization length. This shows the direct relationship between hopping conduction and localization length. It means that when the localization increases the wave functions overlap between localized states increases which in turn makes the hopping conduction of charge carriers easier, and also

limits (to a small range) the reducing effect of the electric field on the activation barrier between hopping sites.

In Figure (3.4) we have shown simulation results of a charge carrier mobility as a function of charge carriers density for different values of energy disorder parameter $\hat{\sigma}$ at external applied electric field $F = 0.1 \times \frac{\sigma}{eb}$.

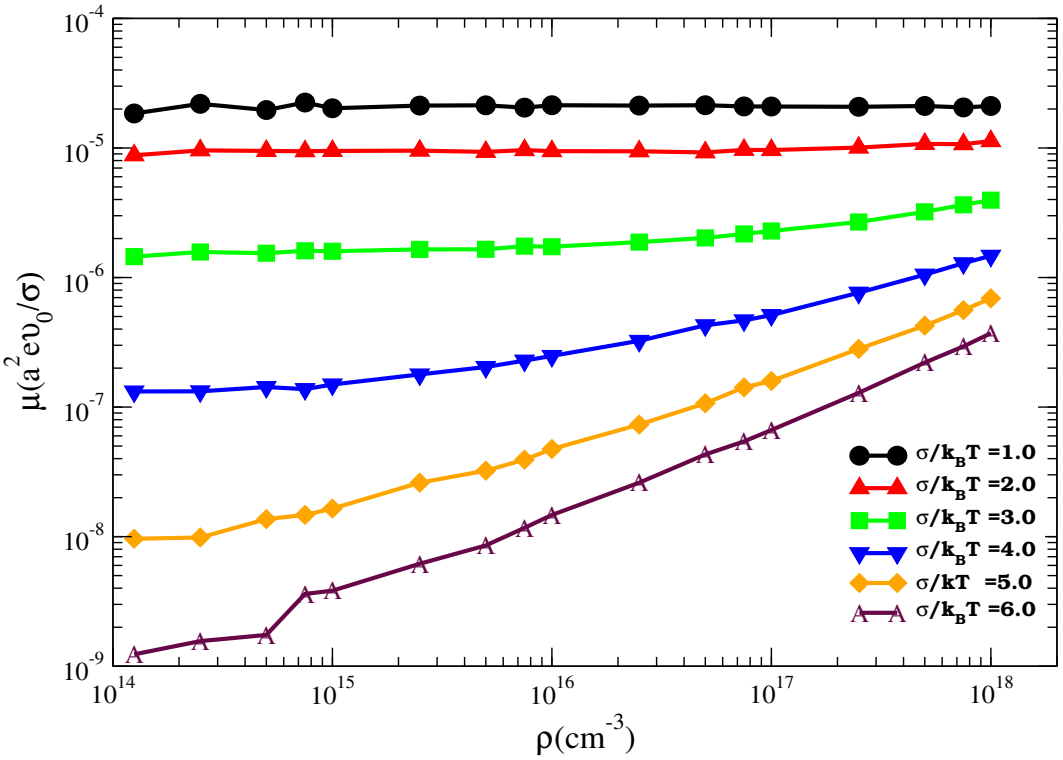

Figure 3.4: Simulation results of a charge carrier mobility versus charge carriers density in a disorder organic material with a Gaussian DOSs for different energetic disorders parameter $\hat{\sigma}$ in the range from 1 to 6. Both mobilities and charge carriers densities are plotted (on a logarithmic scale) in units of $\mu_0 = \frac{b^2 \nu_0 e}{\sigma}$ and cm^{-3}, respectively localization length $\alpha = 0.1b$.

The curves in Figure (3.4) show that the charge carrier mobility increases with the increase of charge carriers density for both the lower and higher charge carriers densities if the energetic disorder parameter $\hat{\sigma}$ is greater than 3 in agreement with that reported in [42]. For the disorder parameter $\hat{\sigma} = 3$ the mobility is nearly constant if the charge carriers density change is in the lower density range, but there is a slight increment of mobility with

the increase of density for the higher density region. This result is in a good agreement with the experimental results demonstrated in References [73, 74]. But, our results of a charge carrier mobility versus charge carriers density in the the low density region for pronounced energetic disorder parameter are at variance with the general conclusion made in this reference; i.e, the charge carrier mobility does not change with the charge carriers mobility. We investigate this more by separating the energetic disorder scale σ from thermal energy k_BT. Like that shown experimentally [74] we have calculated a charge carrier mobility as a function of charge carriers density for different temperatures used in experiment fixing σ at single value. The simulation results for a charge carrier mobility versus charge carriers density for fixed electric fields at $F = 0.05 \times \frac{\sigma}{eb}$ and $F = 0.1 \times \frac{\sigma}{eb}$ for $r = 0$ or regular grids are presented in Figures ((3.5) and (3.6)). The mobilities as well as the densities are plotted (on a logarithmic scale) in units of $\frac{\sigma}{ea}$ and cm^{-3} for three different values of localization length $\alpha = 0.1b, 0.2band0.3b$.

As we observe in Figures ((3.5) and (3.6)), the charge carrier mobility does not vary with the charge carrier density in the range between $10^{14} - 10^{16}\ cm^{-3}$ when temperature is $T = 293K$ for all the panels. However, at the lower temperatures the charge carrier mobility increases with the increase of charge carriers density except at a relatively large localization length $\alpha = 0.3b$ displayed in Figures ((3.5) and (3.6))(c). In these panels the mobility is independent of charge carriers density in the lower density region less than $10^{15}\ cm^{-3}$ except that there is a slight rise of mobility with charge carriers density when the temperature is $T = 235K$ as one can observe in Figure ((3.6))(c). But, for all the temperatures chosen here our results show the increase of a charge carrier mobility with the increase of charge carriers density when the density is above $10^{16}\ cm^{-3}$. As discussed above the effect of density on mobility is more where the disorder energy is more. Our results shown here reflect this fact. It means that when temperature increases the energy difference between hopping sites at the transport level decreases and the effect of charge carriers density on mobility is compromised with that of temperature, electric field and

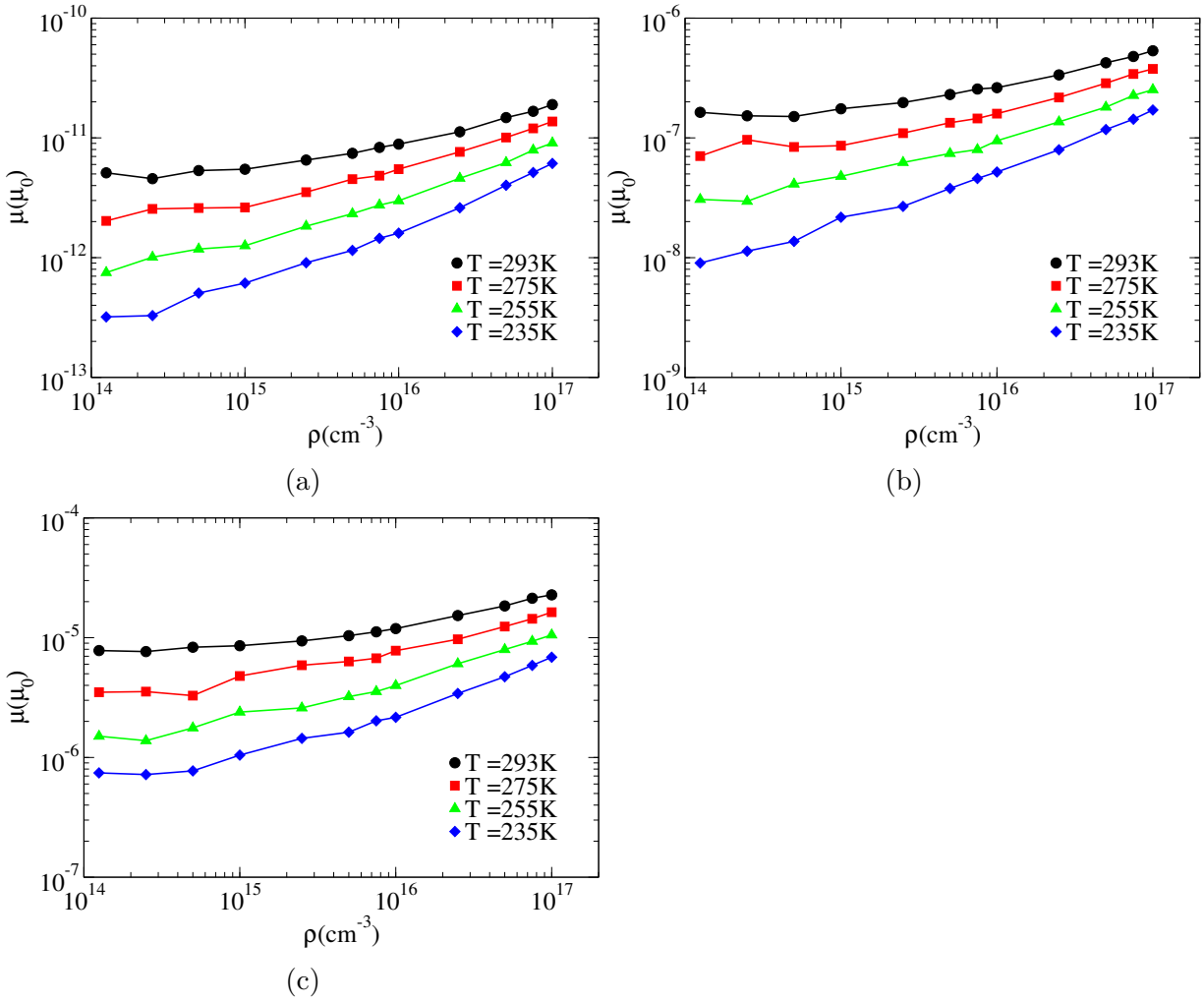

Figure 3.5: Charge carrier mobility as a function of charge carrier density at different temperatures (T) and localization length (α) for the same electric field $F = 0.1 \times \frac{\sigma}{eb}$ for (a) $\alpha = 0.1b$, (b) $\alpha = 0.2b$ and (c) $\alpha = 0.3b$

localization length (or wave function overlap).

Figure (3.7) show simulation results of a charge carrier mobility as a function of energetic disorder parameter $\hat{\sigma}$ for different charge carriers density.

In Figure (3.7) we observe that a charge carrier mobility decreases when the energy disorder parameter $\hat{\sigma}$ of the material increases. The change shown is similar in all charge carriers densities when the parameter value $\hat{\sigma}$ is in the range between 1 to 3. However, for the disorder parameter $\hat{\sigma}$ greater than 3 the mobility change with $\hat{\sigma}$ are different for different densities. The mobility decreases fast with the increase of $\hat{\sigma}$ in the case of lower

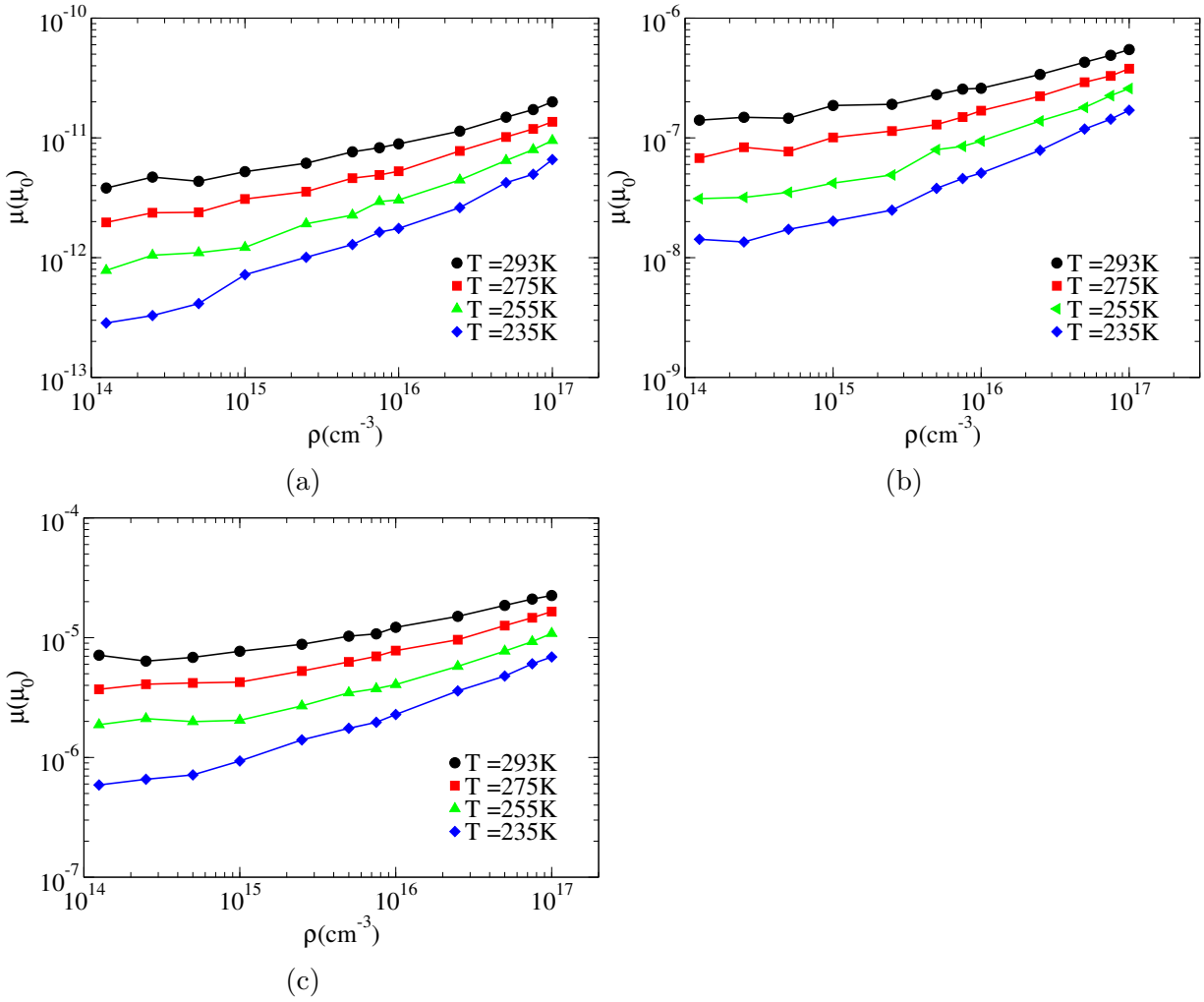

Figure 3.6: Simulation results of charge carrier mobility (μ) as a function of charge carrier density at different temperature T and localization length α for the same electric field $F = 0.05 \times \frac{\sigma}{eb}$ (a) $\alpha = 0.1b$, (b) $\alpha = 0.2b$ and (c) $\alpha = 0.3b$.

charge carrier densities than the higher ones. Over a typical temperature range, in the low energy disorder parameter regime, the mobility of the material shows a band-like transport and demonstrates the hopping transport for moderate disorder strengths. As the curvature of the charge carrier mobility decreases in a more disordered regime, the hopping transport displays a transition from a non–Arrhenius to Arrhenius temperature dependence [104].

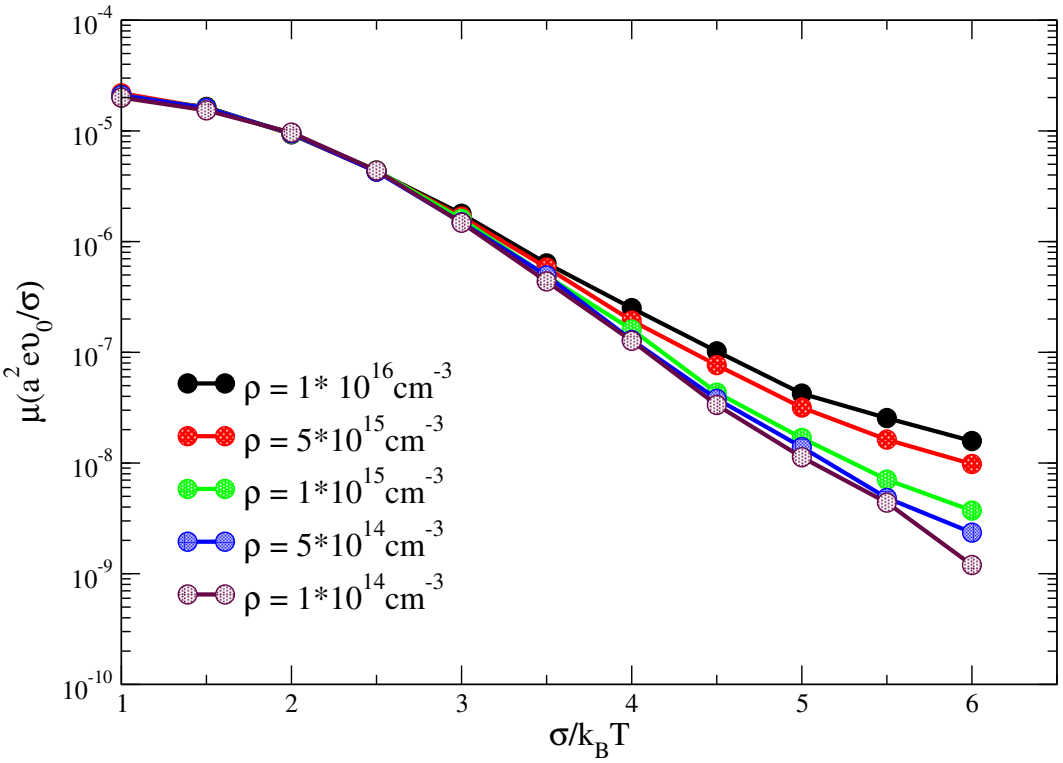

Figure 3.7: Mobility versus disorder parameter $\hat{\sigma}$ in the range from 1 to 6 for different charge carriers densities $1 \times 10^{14} cm^{-3}$, $5 \times 10^{14} cm^{-3}$, $1 \times 10^{15} cm^{-3}$, $5 \times 10^{15} cm^{-3}$, and $1 \times 10^{16} cm^{-3}$ at the same electric field $F = 10^4 V/cm$

3.1.1 The Effect of Lattice Site Spacing for Localization Length in Spatial Disorder of Lattice Sites for $\mu(F)$

To study the effect of lattice site spacing in spatial disorder of lattice sites for the electric field dependent carrier mobility $\mu(F)$ as a function of electric field F in organic disordered semiconductors (ODSs), we performed computer simulation of carrier mobility for hopping within a system of randomly distributed sites with lattice site spacing, and regular grid lattice sites; the parameters of the simulation is the same in both cases.

For our calculation, we used the room temperature which will give $k_B T = 0.025$ eV for the disorder parameter $\hat{\sigma} = 3$ and $\hat{\sigma} = 4$. This means that $\sigma = 0.075$ eV and 0.1 eV, respectively. The value of σ for disordered organic semiconductor is in between 0.05 eV

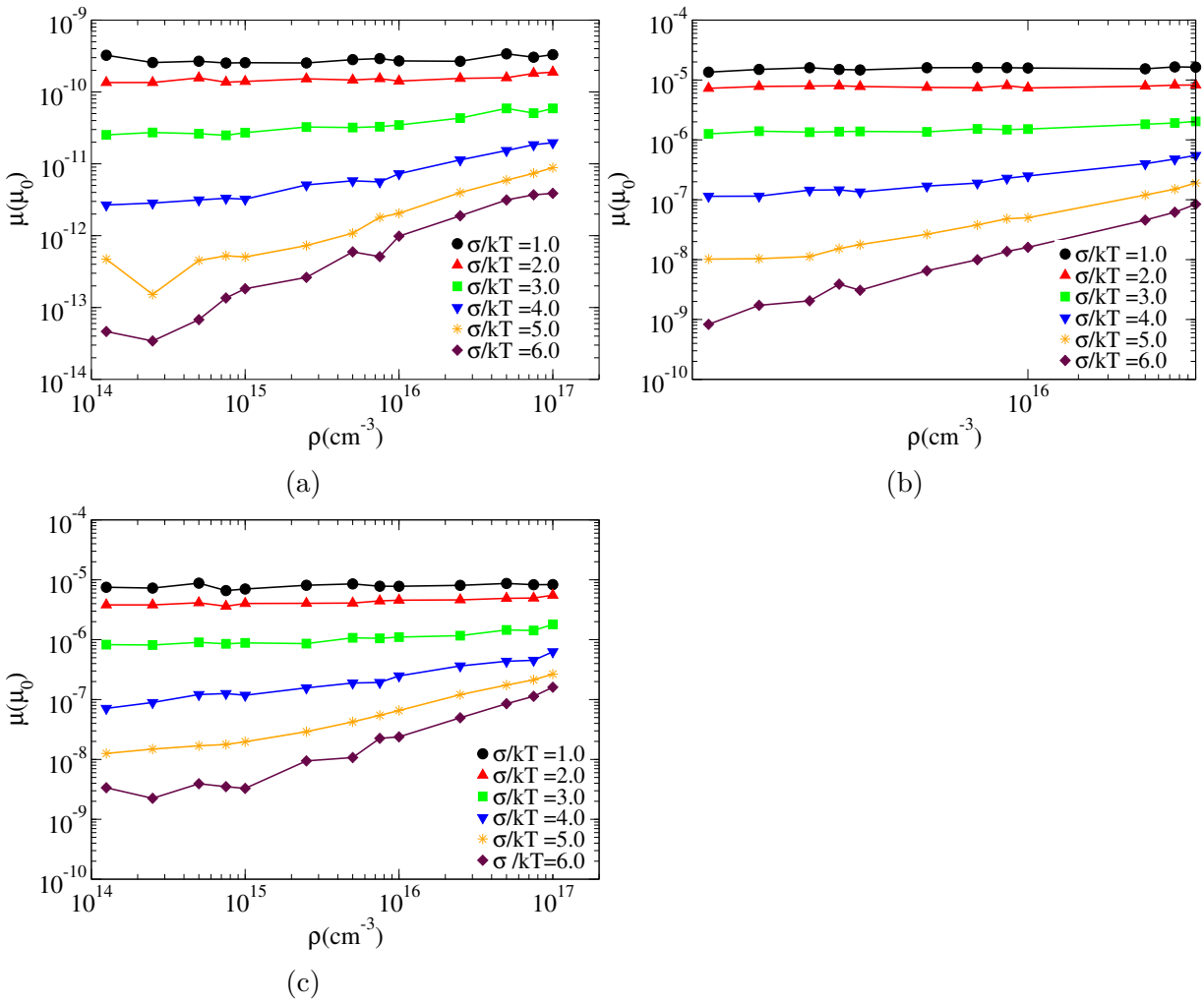

Figure 3.8: Simulation results of charge carrier mobility (μ) as a function of charge carrier density for the spatial disordered of lattice sites with different values of σ/k_BT, lattice site spacing of r and localization length (α). (a) $r = 0.1,\ \alpha = 0.1b$ and (b) $r = 0.1,\ \alpha = 0.2b$ and (c) $r = 0.2,\ \alpha = 0.2b$

to 0.14 eV [38, 105, 106].

Our simulation results are plotted in Fig.(3.9), for the value of $\alpha = 0.1b$, whereas in Fig.(3.10), and (3.11) for different values of α/b with different lattice site spacing parameter for realistic disorder parameters of $\hat{\sigma} = 3$ and $\hat{\sigma} = 4$. In our results of Fig. (3.9), (3.10), and (3.11), the data shown in black colors are for regular grid sites. The lattice sites are randomly distributed in a cubic box. The average distance between the nearest neighbours (or the average lattice parameter) is b. This means that the minimum

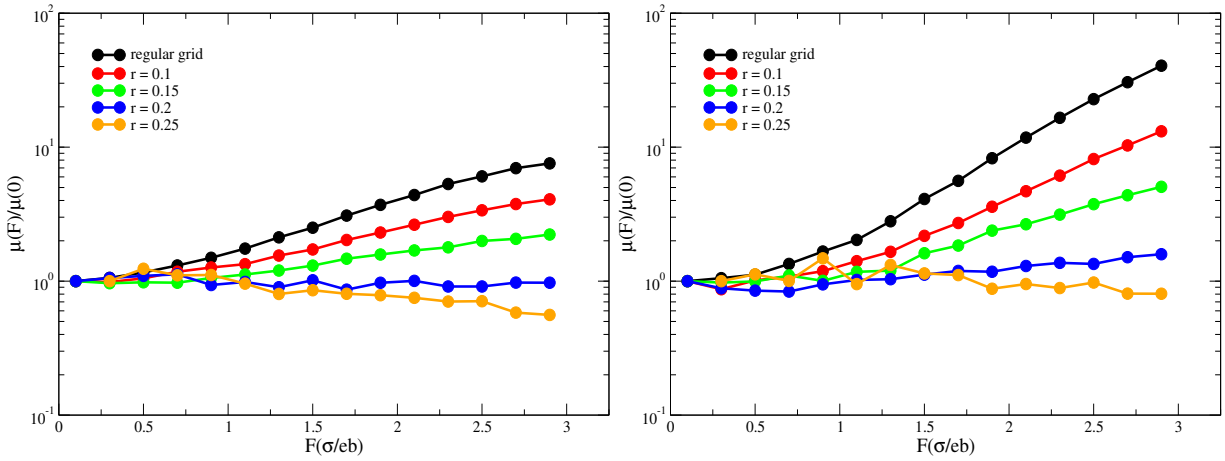

Figure 3.9: Simulation results of charge carrier mobility (μ) as a function of the electric field (F) for the comparison between regular grid lattice and spatial disordered lattice sites with different values of lattice site spacing of r. (a) $\sigma/k_BT = 3$ and (b) $\sigma/k_BT = 4$ with the ratio for both figures are $\alpha = 0.1b$.

distance that one charge carrier hops from site i to j is $|\vec{r_j} - \vec{r_i}| = b - 2r$, where r is lattice site spacing parameter which like a localization radius,and the maximum distance that the charge carrier hops between the nearest neighbouring site is $|\vec{r_j} - \vec{r_i}| = b + 2r$. In this case $r = 0.1$, 0.15, 0.2, and 0.25 a charge carrier may not be localized at a single point. It can be any where in a circle of radius r centered at site $\vec{r_i}$ until it hops to a point anywhere inside another circle of radius r centered at a site $\vec{r_j}$.

Figs.(3.9a) and (3.9b) show for $\hat{\sigma} = 3$ and $\hat{\sigma} = 4$, respectively, with the ratio of $\alpha = 0.1b$ for cubic lattice sites and with different lattice site spacing of r distributed in space randomly. In Fig.(3.9) we observe that the electric field dependence of carrier mobility $\mu(F)$ for $r = 0.1$ and 0.15 increases with the electric field for the ratio of $\alpha = 0.1b$. Whereas in Fig.(3.9a) for $\hat{\sigma} = 3$, and $r = 0.2$ the charge carrier mobility does not vary with an electric field, however for $r = 0.25$ mobility decreases with an electric field. Therefore, the value of $r = 0.25$ is compatible with the works of J. O. Oelerich and his group [44, 45] which present the electric field dependence of carrier mobility $\mu(F)$ in the spatially disordered system that decreases with an increase of an electric field for the same

material parameters. In Fig. (3.9b) for $\hat{\sigma} = 4$, and for the values of lattice site spacing equals $r = 0.2$ and 0.25 the charge carrier mobility does not vary with an electric field for the same parameter in a given electric field range. On the result of Fig.(3.9b) for the values of lattice site s pacing $r = 0.2$ and 0.25 has coincided with the simulation results obtained by J. O. Oelerich and his group [44, 45]. They stated that at $\hat{\sigma} = 4$ the carrier mobility in the spatial disorder lattice site is almost independent with an electric field for the same material parameter in the same range of electric fields.

As we observed the simulation result in Fig.(3.9) for the spatial disorder lattice site at the ratio of $\alpha = 0.1b$, and for lattice site spacing of $r > 0.15$ the charge carrier mobilities are decrease or does not vary with the electric field in the same range. As a result, we realize that it is not agreed with experimental measurements, which shows that substantial increases in the carrier mobility $\mu(F)$ with the electric field in ODSs [55, 108–110]. However, the charge carrier mobility $\mu(F)$ in cubic lattice sites and with lattice site spacing of $r = 0.1$ and 0.15 increases with the electric field in the same range which is a match to the works of the simulation result of Paseveer et.al [42] and the experimental result [55, 108–110]. The reason for the variance in the random lattice site spacing of our simulation data for $r > 0.15$ with the work of Paseveer et.al [42] is the way to choice the value of r with the ratio of $\alpha = 0.1b$ in the simulation. If the value of $r \leq \alpha$ the charge carrier found inside circle with localization radius α, otherwise is not found inside circle. In the work of J. O. Oelerich and his group [44, 45] shows the difference between regular array lattice site and special random lattice site of the parameter $\alpha = 0.1b$ for simulation of the disordered organic semiconducting material. They state that the electric field dependence of charge carrier mobility in the case of regular array does drastically differ from special random lattice site. Since the electric field dependence of charge carrier mobility increases with electric field on the regular array of lattice site whereas in special random lattice site decreases with electric field for the same material parameter. They suggest that this is due to the unreasonable choice of the

parameter $\alpha = 0.1b$ for their simulation work. In contrast to this work, our s simulation results reveal that it is not only for unreasonable choice of the parameter $\alpha = 0.1b$, but also the way to choice the lattice site spacing r. We have to choice the parameter of α/b by comparing the lattice site spacing r, since if the ratio of $\alpha/b < r$ the charge carrier mobility decreases with electric field whereas for the ratio of $\alpha/b \geq r$ the charge carrier mobility increases with electric field in the special random lattice site.

In Figs.(3.10) and (3.11), we display our simulation results for different values of α/b for parameters $\hat{\sigma} = 3$ and $\hat{\sigma} = 4$, respectively. In our simulation data, we represent the black color for a regularly array lattice sites. Our simulation results at a ratio of $\alpha = 0.2b$ agreed with the simulation work of Bassler and his research group [38,40] for the reduced GDM without non–diagonal disorders. The simulation data shown in Fig.(3.10), and (3.11) for different localization length and lattice site spacing of r red, green, blue, and Orange of 0.1, 0.15, 0.2, and 0.25, respectively, were obtained for a system of sites distributed in space randomly for the same concentration of sites N.

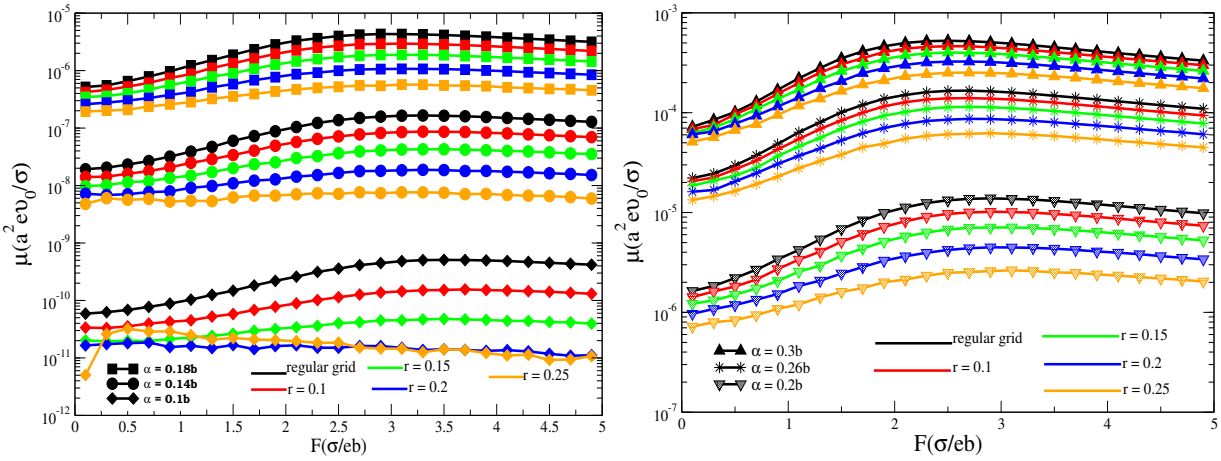

(a) (b)

Figure 3.10: Comparison of charge carrier mobility (μ) as a function of the electric field (F) for $\sigma/k_BT = 3$ between regular grid lattice and spatial disordered lattice sites with different values of α/b and lattice site spacing r.

Figs.(3.10) and (3.11) show that for $\alpha = 0.1b$ and $\alpha = 0.14b$ the charge carrier mobility $\mu(F)$ increases with an electric field for the spatial disorder of lattice sites for lattice site

spacing of $r = 0.1$ and 0.15. However, in Fig.(3.10) for $\hat{\sigma} = 3$ for lattice site spacing of $r = 0.2$ and 0.25 the charge carrier mobility $\mu(F)$ decreases with the electric field for the same material parameters. Fig. (3.11) for $\hat{\sigma} = 4$, we observe that at $\alpha = 0.1b$, the charge carrier mobility $\mu(F)$ does not vary with electric field, whereas at $\alpha = 0.14b$ increases with the electric field for the same parameters. Fig.(3.10), and (3.11), show that in the spatial disorder of lattice sites of the charge carrier mobility $\mu(F)$ decreases with the electric field at higher values of lattice site spacing of r at a lower ratio of α/b, whereas for lower values of lattice site spacing r at a lower ratio of α/b the charge carrier mobility $\mu(F)$ increases with the electric field. For the simulation results of a very small ratio of α/b and not too small $\hat{\sigma}$, the charge carrier mobility in the spatial disorder of lattice site decrease with increasing an electric field [44], even this decreases starts at a low electric field. Thus far the charge carrier mobility decreases with the electric field has been explained theoretically only for high values of electric field [112–115]. J.O. Oelerich and his co–workers [44, 45] considers only the effect of the ratio of α/b on charge carrier mobility with the disorder of the material , but to observe the effect of the ratio of α/b on charge carrier mobility we must construct the special random system with matching lattice site spacing r to the localization length α.

Fig.(3.12), we display our simulation results for different values of lattice site spacing r at the ratio of $\alpha = 0.1b$ and disorder parameters of $\hat{\sigma} = 3$ and $\hat{\sigma} = 4$, respectively. In this simulation data, we use the lattice site spacing $r \leq 2\alpha$ not greater than 2α. As a result, we observe that the field dependence of the charge carrier mobility $\mu(F)$ for $r \leq 2\alpha$ does not vary with an electric field at lower electric field range, whereas at higher electric field $\mu(F)$ increases with electric field. In Fig.(3.12a) for $\hat{\sigma} = 3$, show that the electric field dependence of the charge carrier mobility does vary with different values of lattice site spacing r for the same parameter in a given electric field range. However, in Fig.(3.12b) for $\hat{\sigma} = 4$, the electric field dependence of charge carrier mobility for different values of lattice site spacing r does not vary at lower electric field but it increases as the

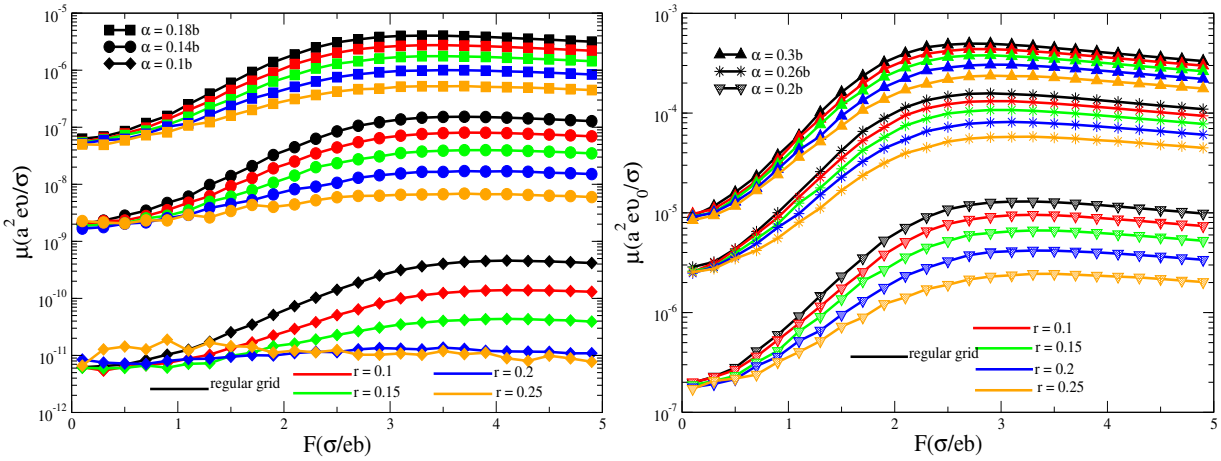

(a) (b)

Figure 3.11: Comparison of charge carrier mobility (μ) as a function of the electric field (F) for $\sigma/k_BT = 4$ between regular grid lattice and spatial disordered lattice sites with different values of α/b and lattice site spacing r.

value of the electric field increases. In Fig. (3.9b) for $\hat{\sigma} = 4$ at $r = 0.2$ and $r = 0.25$, the charge carrier mobility does not vary with electric field, which is similar to Fig.(3.12) at lower values of the electric field for $r \leq 2\alpha$. According to our simulation result for the values of $r = 0.2$ and $r = 0.25$ has been coincided with the work of J.O. Oelerich and his co–workers [44, 45]. They stated that at $\hat{\sigma} = 4$ the electric field dependence of the charge carrier mobility in the spatial disorder lattice site is almost independent with an electric field for the same material parameter in the same range of electric field. However, Passeveer et. al, [42] show the simulation on the lattice site at $\hat{\sigma} = 4$ and they have stated that the electric field dependence of charge carrier mobility increases with electric field. Therefore, in Fig.(3.12b) for $\hat{\sigma} = 4$ the electric field dependence of charge carrier mobility increase with electric field at higher values of electric field which has agreed with Passeveer et. al, [42].

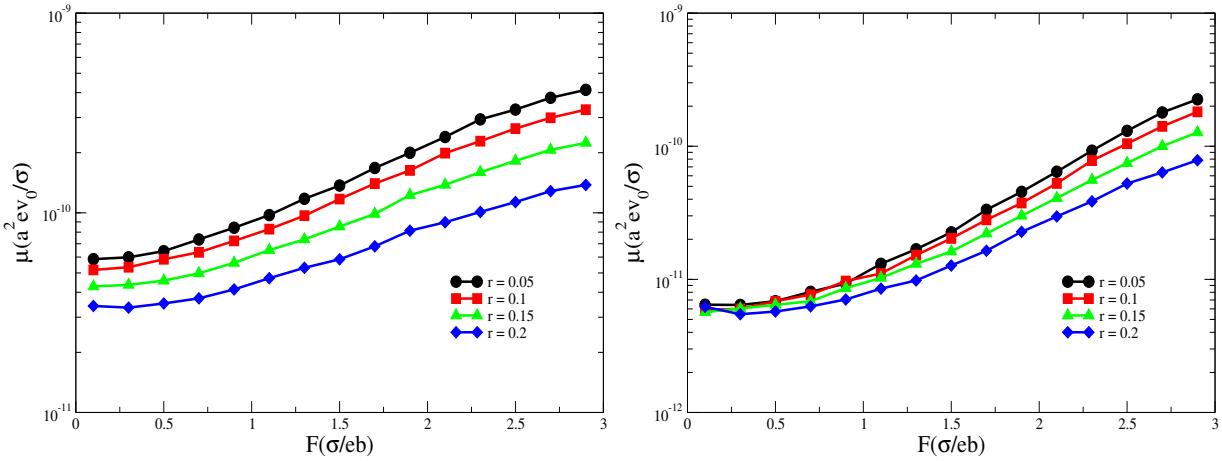

Figure 3.12: Simulation results of charge carrier mobility (μ) as a function of the electric field (F) in spatial disordered lattice sites with different values of lattice site spacing of r. (a) $\sigma/k_BT = 3$ and (b) $\sigma/k_BT = 4$ with the ratio for both figures are $\alpha = 0.1b$.

3.1.2 The Effect of Lattice Site Spacing r on Mobility in Spatial Disorder of Lattice Site

Fig.(3.13) the charge carrier mobilities are show as a function of electric field in unit $\sigma/e\alpha$ for different localization length and lattice site spacing r. We use the ratio α/b of $0.18 \leq \alpha/b \leq 0.3$ and different value of lattice site spacing r equals to 0.1, 0.15, 0.2, and 0.25. Our simulation results display for $r = 0.25$ and $r = 0.2$ in Figs. (3.13a) and (3.13b),respectively, which reveal that the charge carrier mobility converge onto a single curve. However, for $r = 0.15$ and $r = 0.1$ display on Figs. (3.13c) and (3.13d), respectively, the charge carrier mobility differ from each other for different values of the parameter α/b. Therefore, we observe from those curves, they differ from each other by lattice site spacing r for different localization length.

According to our simulation data, we show that the charge carrier mobility increases with electric field as the value of lattice site spacing r match to the ratio of α/b. However, as the value of lattice site spacing r larger than the ratio of α/b the charge carrier mobility

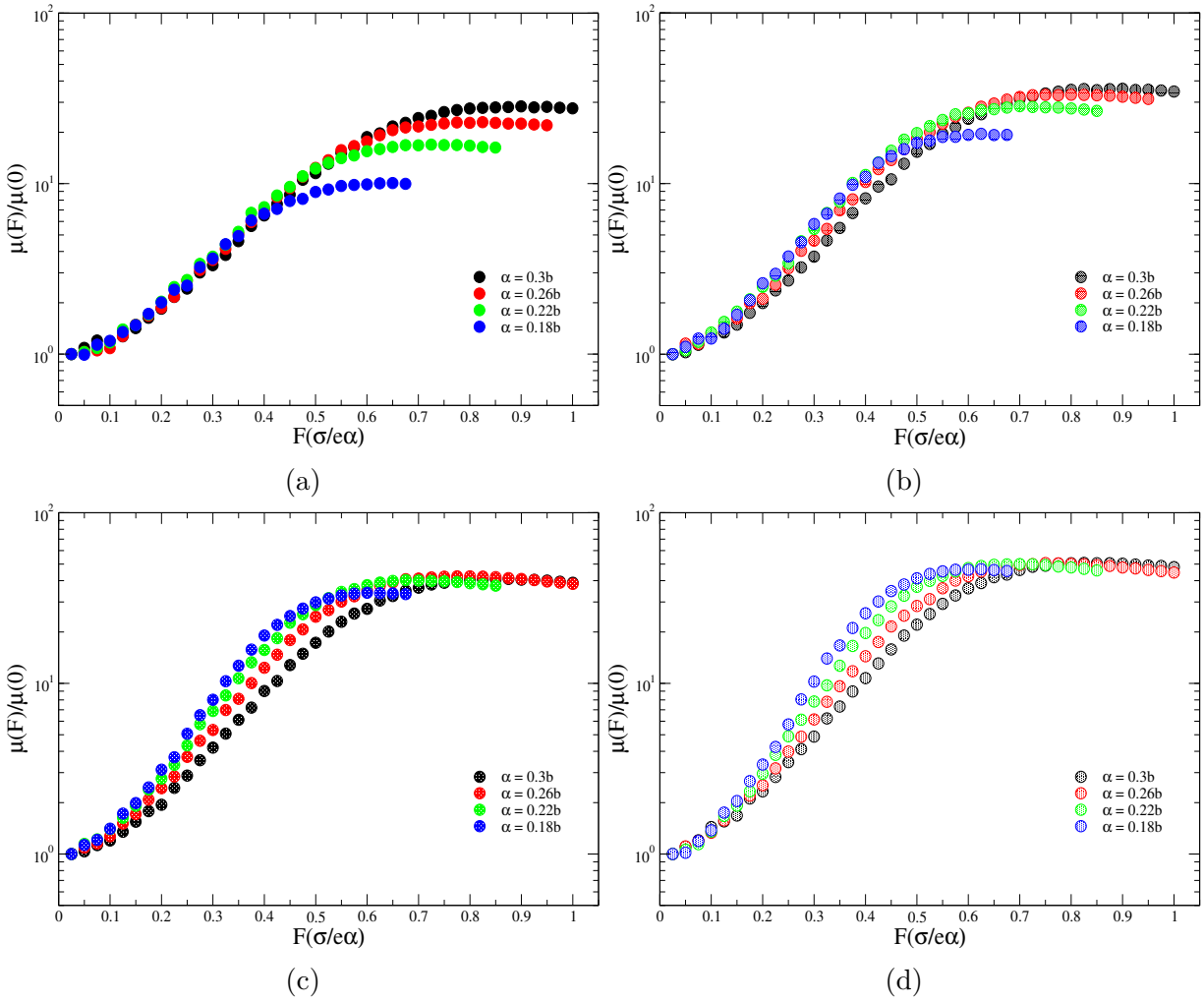

Figure 3.13: Simulation results of charge carrier mobility (μ) as a function of the electric field (F) for spatial disordered lattice sites with different values of α/b and lattice site spacing r. (a) $r = 0.25$, (b) $r = 0.2$, (c) $r = 0.15$ (d) $r = 0.1$, and the disorder parameter for all figures are $\sigma/k_BT = 4$.

does not vary with electric field. Therefore, the localization length and lattice site parameters are the decisive length scale for the field dependence of charge carrier mobility, as we choice proper lattice site spacing r to the localization length. However, as the lattice site spacing of r larger than the ratio of α/b then the localization length is the only decisive length scale for the electric field dependence of the charge carrier mobility. which is a good agreement with the simulation results of J.O. Oelerich and his co–workers [44, 45]. They prove that the localization length α and not the intersite distance b is the decisive

length scale for the electric field dependence of charge carrier mobility with the electric field.

3.1.3 The Influence of Disorder Parameter ($\hat{\sigma}$) the Mobility in Spatial Disorder of Lattice Sites with Lattice Site Spacing r

In Figs.(3.14) and (3.15) , we display our simulation results for different values of disorders ($\hat{\sigma}$) and lattice site spacing r for parameters of $\alpha = 0.1b$ and $\alpha = 0.2b$, respectively. According to the simulation data of Figs.(3.14a) and (3.14b) for $\alpha = 0.1b$ and ($\hat{\sigma}$) = 2, 3, 4, 5, and 6 show that the electric field dependence of charge carrier mobility $\mu(F)$ increases with electric field for the lattice site spacing $r = 0.1$ and $r = 0.15$, which is a good agreement with the work of Pasever et.al [42]. He state that the charge carrier mobility increases with electric field. However, In Fig.(3.14c) for the lattice site spacing $r = 0.2$, the electric field dependence of charge carrier mobility has different properties with the disorder parameters. Therefore, the electric field dependence of charge carrier mobility decreases at $\hat{\sigma} = 2$, does not vary at $\hat{\sigma} = 3$, and increases at $\hat{\sigma} = 4$, 5, and 6 with electric field. Fig.(3.14d) for the lattice site spacing $r = 0.25$, the electric field dependence of charge carrier mobility decreases with electric field for the disorder of $\hat{\sigma} = 2$, and 3, whereas for the disorder of $\hat{\sigma} = 4$, 5, and 6 does not vary with electric field. In general, we observe that in Fig. (3.14), if the lattice site spacing r increases with disorder parameter $\hat{\sigma}$ then the electric field dependence of charge carrier mobility does different property with electric field.

In Fig. (3.15) the electric field dependence of charge carrier mobilities are show as a function of electric field in unit of σ/eb for different values of lattice spacing $r = 0.1$, 0.15, 0.2, and 0.25, and disorder parameters of $\hat{\sigma} = 2$, 3, 4, 5, and 6. Our simulation data for $\alpha = 0.2b$ reveal that the electric field dependence of charge carrier mobility increases with

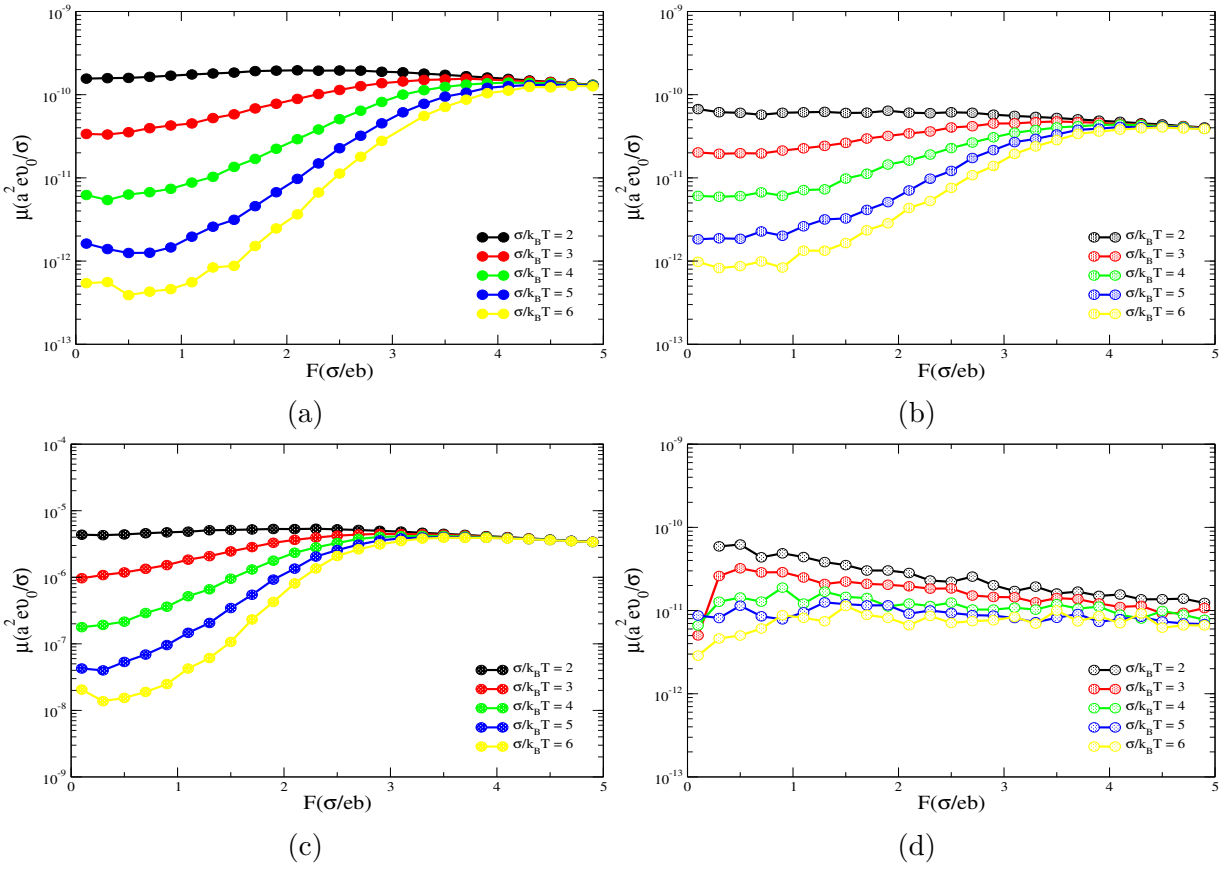

Figure 3.14: Simulation results of charge carrier mobility (μ) as a function of the electric field (F) for spatial disordered lattice sites with different values of σ/k_BT and lattice site spacing r. (a) $r = 0.1$, (b) $r = 0.15$, (c) $r = 0.2$ (d) $r = 0.25$, and the ratio for all figures are $\alpha = 0.1b$.

an electric field for lattice site spacing r and disorders of the material, which is a good agreement with the result of Basseler and his co–workers [38]. Therefore, we observe that as the values of lattice site spacing r is compatible with the ratio of α/b then the electric field dependence of charge carrier mobility increases with the electric field.

In Fig.(3.16) at $\alpha = 0.1b$ show that the effect of different disorder parameter and lattice site spacing of $r \leq 2\alpha$ on the electric field dependence of charge carrier mobility. In Fig.((3.16a) -(3.16d)) uses the disorder parameters of $\hat{\sigma} = 3$, 4, 5, and 6, respectively, to show the influence of electric field on the charge carrier mobility. As we see in Fig.(3.16a) for $\hat{\sigma} = 3$ the electric field dependence of charge carrier mobility has a variation at lower values of electric field for the lattice site spacing $r = 0.05$, 0.1, 0.15, and 0.2 with electric

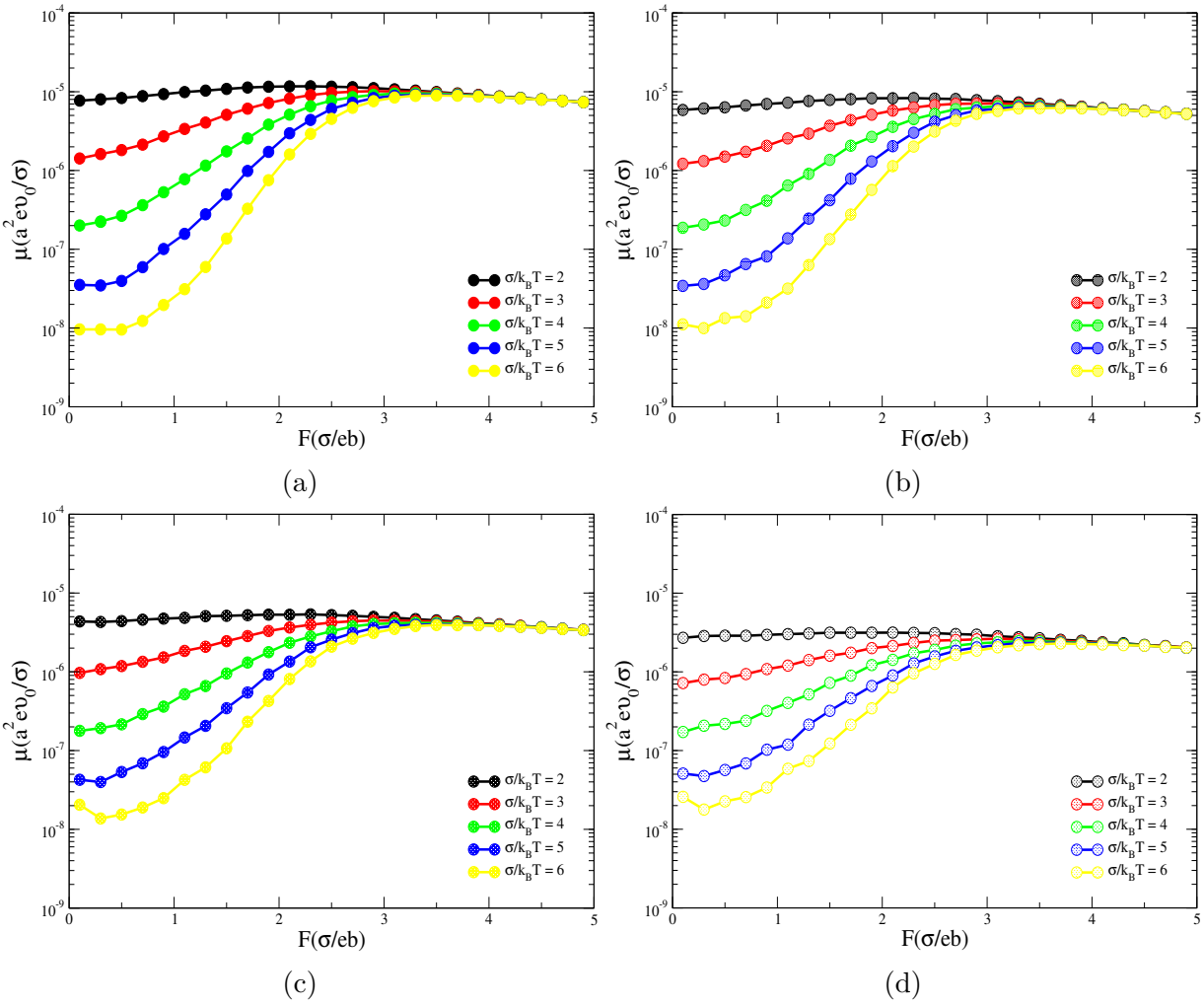

Figure 3.15: Simulation results of charge carrier mobility (μ) as a function of the electric field (F) for spatial disordered lattice sites with different values of σ/k_BT and lattice site spacing r. (a) $r = 0.1$, (b) $r = 0.15$, (c) $r = 0.2$ (d) $r = 0.25$, and the ratio for all figures are $\alpha = 0.2b$.

field. However, in Fig.((3.16b) -(3.16d)) for $\hat{\sigma} = 4$, 5 and 6, the electric field dependence of charge carrier mobility does not vary at lower value of electric field for the lattice site spacing of $r = 0.05$, 0.1, 0.15, and 0.2 with electric field. For larger values of electric field in Fig. (3.16) for the disorder parameters of $\hat{\sigma} = 3$, 4, 5, and 6 the electric field dependence of charge carrier mobility increases with electric field for the lattice site spacing of $r \leq 2\alpha$. According to our simulation results, we see that the influence of electric field on the charge carrier mobility observed at larger values of electric field whereas at lower values of electric

field does not vary with electric field.

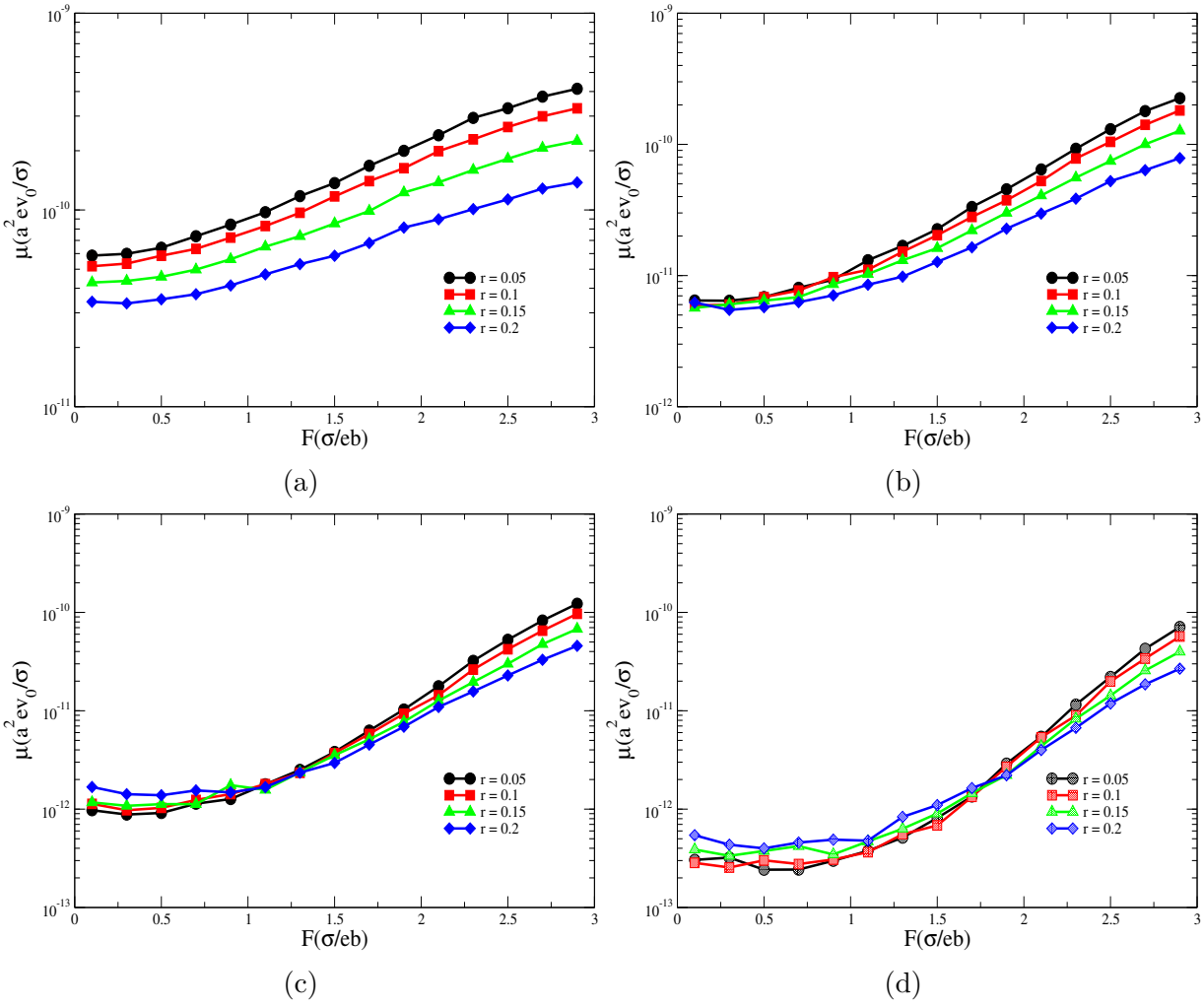

Figure 3.16: Simulation results of charge carrier mobility (μ) as a function of the electric field (F) for spatial disordered lattice sites with lattice site spacing r and different values of σ/k_BT. (a) $\sigma/k_BT = 3$, (b) $\sigma/k_BT = 4$, (c) $\sigma/k_BT = 5$ (d) $\sigma/k_BT = 6$, and the ratio for all figures are $\alpha = 0.1b$.

Chapter 4

Summary and Conclusions

In this chapter, we summarize and give a brief conclusion of the dissertation. In this thesis, we describe the properties of charge transport in disordered organic semiconductors using Monte Carlo simulation techniques based on the Gaussian disorder model.

A polymer is a material made up of macromolecules, which is composed of many repeating units of monomers and connected by covalent bonds. The carbon atom is used as a backbone for the polymer chain. Polymers are classified as synthetic and natural polymers. Organic semiconductors are carbon-based molecular materials held together by van der Waals forces. Organic materials have been used to conduct electricity, the ability to absorb light, and emit light with a material structure. Because of their strength, lightweight, mechanical flexibility, simple chemical modification, and low-cost processability at low temperatures than inorganic counterparts. Organic disordered semiconductors (ODSs) are also classified as conjugated polymers, molecularly doped polymers, and low-molecular weight organic glasses. Conjugated polymers are organic molecules that are designated by a backbone chain of alternating double and single bonds. They possess conjugated π–electrons that can be easily delocalized rather than being part of one valence bond. Conjugated polymers are the most important type of organic semiconductors used to fabricate for different types of optoelectronic devices due to their optical, electrical, and mechanical properties, such as organic light-emitting diodes (OLEDs), Organic field-effect transistors (OFETs), and organic solar cells (OSCs).

Charge transport in disordered organic semiconductors consists of a sequence of incoherent tunneling transitions between occupied to unoccupied localized states, known as hopping. The hopping transport of the charge carrier described by the Miller-Abrahams rate equation and the variable range hopping mode was described by Neville Francis Mott to study charge transport in a disordered material. They state that charge carriers either hop over a small distance with the high energy of activation or hop over an extended distance with low energy of activation. It has applied for a theoretical and numerical problem within the field of disordered semiconductors material. Gaussian disorder model(GDM) has been recommended by Bassler and co–workers to study charge transport in disordered organic semiconductors. The density of states (DOS) is taken as a form of Gaussian shape. They have used a Monte Carlo simulations approach to describe a charge carrier transport in amorphous organic materials based on GDM under an applied electric field. They have considered as an array of structureless points like hopping sites with cubic symmetry. Its energies have featured a Gaussian-type density of energetically uncorrelated states distribution with variance σ. Pasveer also studied the dependence of the charge-carrier mobility on temperature, charge carrier density, and electric field by numerically solving the master equation that gives a relationship between the occupation probabilities of all sites on a lattice. Since a fraction of the sites already occupied, charge transport is considered as a thermally assisted tunneling process with MillerAbrahams rate equation. They also use a Gaussian density of states with a width of σ, and a pair of like charges on a given site is prevented by Coulomb repulsion of each other. The basic parameter in charge transport is mobility, which depends on charge carrier density, electric field, and temperature.

In this thesis, we have used a Monte Carlo simulation using the Gaussian disorder model(GDM) to determine the charge transport properties in disordered organic semiconducting materials. Our material is modeled as a three dimensional cubic of super-cells whose lattice sides are L_x, L_y, and L_z, with lattice parameter b. In our system, we have

used regular grid lattice and spatial disordered lattice sites with lattice site spacing of r in a supper cell. After the construction of the lattice sites, we randomly distributed charge carriers on the lattice sites and Gaussian energy assigned to each lattice site. We also applied an external electric field along the positive x-axis. We use Miller-Abraham's rate equation to calculate the possible hops of all charge carriers from the occupied site i to an empty j, in which each charge carrier has a probability of transitions to the nearest neighboring site. After we perform hopping of the charge carrier, then we computed the hopping time of the charge carrier. In the final steps of our simulation, we have calculated the mobility of charge carriers.

We have studied the effect of charge carrier mobility as a function of charge carrier density in the range between $10^{14} - 10^{16}\ cm^{-3}$ by varying charge carrier density and disorders of organic semiconducting materials. Our simulation results have shown that the charge carrier mobility versus charge carrier density at lower charge carrier density and disorder is constant. However, at higher disordered and lower charge carrier density, the charge carrier mobility increases with charge carrier density. As a result, we concluded that the effect of the disorder parameter on the charge carrier mobility is more pronounced than the charge carrier density at lower charge carrier density.

We also performed a Monte Carlo simulation for the charge carrier mobility by varying the electric field, localization length, spatial random site distance, and temperature of the material to study a charge carrier mobility as a function of the electric field for the case of the regular grid and spatial disordered lattice site with different lattice site spacing parameter r and the ratio of localization length to the lattice parameter. According to our simulation results, We show that a charge carrier mobility increases with an electric field for the case of the regular grid and spatial disorder lattice site of lower or equal values of lattice site spacing r to the ratio of α/b. However, at higher values of lattice site spacing r to the ratio of α/b, the electric field dependence of charge carrier mobility for spatial disordered lattice sites differs from that of the regular grid case. Therefore, We

have to choose the parameter of α/b by comparing the lattice site spacing r if the ratio of $r > \alpha/b$, then the charge carrier mobility decreases with the electric field, whereas for the ratio of $r \leq \alpha/b$ the charge carrier mobility increases with the electric field in the spatial disordered lattice site. Finally, we conclude that both a localization length and lattice parameter are relevant for the electric field variation of charge carrier mobility in both the regular grid and spatial disordered lattice sites at lower or equal values of lattice site spacing r to the ratio of α/b cases. However, at higher values of the lattice site spacing r relative to the ratio of α/b, the only parameter responsible for the electric field dependence of charge carrier mobility is the localization length of disordered organic semiconducting materials.

DECLARATION

I hereby declare that this Ph.D. dissertation is my original work and has not been presented for a degree in any other university. All sources of material used for the Ph.D. dissertation have been duly acknowledged.

Name:**Seyfan Kelil**

Signature:– – – – – – – – – – – –

Place and time of submission: Addis Ababa University, June 2021

This Ph.D. dissertation has been submitted for examination with my approval as University advisor.

Name:**Dr. Lemi Demmeyu**

Signature:– – – – – – – – – ––

Bibliography

[1] A. J. Heeger. *Rev. Mod. Phys.*, 73:681, 2001.

[2] Paul C Painter and Michael M Coleman. *Fundamentals of polymer science: an introductory text*. Technomic, 1997.

[3] Norman Gerard McCrum, CP Buckley, Clive B Bucknall, Clive B Bucknall, and CB Bucknall. *Principles of polymer engineering*. Oxford University Press, USA, 1997.

[4] DD Eley. Phthalocyanines as semiconductors. *Nature*, 162(4125):819–819, 1948.

[5] Parfitt Eley. Perry and taysum. *Trans. Faraday Soc*, 49:79, 1953.

[6] H Mette and H Pick. Electric conductivity of anthracene monocrystals. *Z. Physik*, 134:566, 1953.

[7] Hideo Akamatu, Hiroo Inokuchi, and Yoshio Matsunaga. Electrical conductivity of the perylene–bromine complex. *Nature*, 173(4395):168–169, 1954.

[8] Oliver H LeBlanc Jr. Hole and electron drift mobilities in anthracene. *The Journal of Chemical Physics*, 33(2):626–626, 1960.

[9] Martin Pope, HP Kallmann, and PJ Magnante. Electroluminescence in organic crystals. *The Journal of Chemical Physics*, 38(8):2042–2043, 1963.

[10] Helmut Hoegl. On photoelectric effects in polymers and their sensitization by dopants1. *The Journal of Physical Chemistry*, 69(3):755–766, 1965.

[11] Chwan K Chiang, CR Fincher Jr, Yung W Park, Alan J Heeger, Hideki Shirakawa, Edwin J Louis, Shek C Gau, and Alan G MacDiarmid. Electrical conductivity in doped polyacetylene. *Physical review letters*, 39(17):1098, 1977.

[12] A. G. MacDiarmid and A. J. Heeger. *Synth. Met.*, 1:101, 1980.

[13] Alan J Heeger, ALAN G MacDiarmid, and Hideki Shirakawa. The nobel prize in chemistry, 2000: conductive polymers. *Stockholm, Sweden: Royal Swedish Academy of Sciences*, pages 1–16, 2000.

[14] A. J. Heeger, S. Kivelsun, J. R. Schrieffer, and W. P. Su. *Rev. Mod. Phys.*, 60:781, 1988.

[15] C. W. Tang and S. A. Van Slyke. *Appl. Phys. Lett.*, 51:913, 1987.

[16] C. W. Tang and S. A. Van Slyke. *Appl. Phys. Lett.*, 65:3610, 1989.

[17] J. H. Burroughes, D. D. C. Bradely, A. R. Brown, R. H. Friend, P. L. Burn, and A. B. Holmes. *Nature (London)*, 347:539, 1990.

[18] PM Borsenberger and DS Weiss. Organic photoreceptors for xerography. marcel dekker inc. 1998.

[19] Jean-Pierre Fabrges, editor. *Organic Conductors: Fundamentals and Applications.* Applied Physics; 4. Marcel Dekker, Inc., New York, 1994.

[20] S. F. Nelson, Y-Y. Lin, D. J. Gundlach, and T. N. Jackson. *Appl. Phys. Lett.*, 72:1854, 1998.

[21] Shigeki Kato. Perspective on a molecular orbital theory of reactivity in aromatic hydrocarbons. In *Theoretical Chemistry Accounts*, pages 219–220. Springer, 2000.

[22] I. H. Campbell and D. L. Smith. *Solid State Physics*, volume 55, chapter Physics of Organic Electronic Devices, pages 1–117. Academic Press, Los Alamos, New Mexico, 2001.

[23] A. Assadi, C. Svensson, M. Willander, and O. Inganäs. *Appl. Phys. Lett.*, 53:195, 1988.

[24] C. K. Chiang, C. R. Fincher, Y. W. Park, A. J. Heeger, H. Shirakawa, E. J. Louis, S.C. Gau, and A. G. MacDiarmid. *Phys. Rev. Lett.*, 39:1098, 1977.

[25] Kador L. Stochastic theory of inhomogeneous spectroscopic line-shapes reinvestigated. *J. Chem. Phys.*, 95:5574, 1991.

[26] A. B. Walker, A. Kambili, and S. J. Martin. *J. Phys.*, 14:9825, 2002.

[27] T. Minakata, H. Imai, and M. Ozaki. *J. Appl. Phys.*, 72:4178, 1992.

[28] T. Minakata, I. Nagoya, and M. Ozaki. *J. Appl. Phys.*, 69:7354, 1991.

[29] T. Mianakata, H. Imai, and M. Ozaki. *J. Appl. Phys.*, 72:5220, 1992.

[30] T. Mori and S. Ikehata. *Solid State Commun.*, 101:213, 1997.

[31] M. Cazayous, A. Sacuto, G. Horowitz, P. Lang, A. Zimmers, and R. P. S. M. Lobo. *Phys. Rev. B*, 70:81309, 2004.

[32] T. Ito, T. Mitani, T. Takenobu, and Y. Iwasa. *J. of Physics and Chemistry of Solids*, 65:609, 2004.

[33] Y. C. Cheng, R. Y. Silbey, D. A. da Silva Filho, J. P. Calbert, J. Cornil, J-P. Calbert, and J-L Brédas. *J. Chem. Phys*, 118:3764, 2003.

[34] R. A. Marcus. *Rev. Mod. Phys.*, 65:599, 1993.

[35] P. W. Anderson. *Phys. Rev.*, 109:1492, 1958.

[36] N. F. Mott and E. A. Davis. *Electronic Processes in Noncrystalline Solids*. Clarendon Press, Oxford, second edition edition, 1979.

[37] E. M. Conwell. *Phys. Rev.*, 103:51, 1956.

[38] H. Bässler. *Phys. Stat. Sol.(b)*, 175:15, 1993.

[39] A. Miller and E. Abrahams. *Phys. Rev.*, 120:745, 1960.

[40] PM Borsenberger, L Pautmeier, and H Bässler. Charge transport in disordered molecular solids. *The Journal of chemical physics*, 94(8):5447–5454, 1991.

[41] S. V. Novikov, D. H. Dunlap, V. M. Kenkre, P. E. Parris, and A. V. Vannikov. *Phys. Rev. Lett.*, 81:4472, 1998.

[42] W. F. Pasveer, J. Cottaar, C. Tanase, R. Coehoorn, P. A. Bobbert, P. W. M. Blom, D. M. de Leeuw, and M. A. J. Michels. *Phys. Rev. Lett.*, 94:206601, 2005.

[43] J. Zhou, Y. C. Zhou, J. M. Zhao, C. Q. Wu, X. M. Ding, and X. Y. Hou. *Phys. Rev. B*, 75:153201, 2007.

[44] Jan Oliver Oelerich, AV Nenashev, AV Dvurechenskii, F Gebhard, and SD Baranovskii. Field dependence of hopping mobility: Lattice models against spatial disorder. *Physical Review B*, 96(19):195208, 2017.

[45] AV Nenashev, JO Oelerich, AV Dvurechenskii, F Gebhard, and SD Baranovskii. Fundamental characteristic length scale for the field dependence of hopping charge transport in disordered organic semiconductors. *Physical Review B*, 96(3):035204, 2017.

[46] BI Shklovskii and AL Efros. Electronic properties of doped semiconductors, springer, new york 1984.

[47] Jan Oliver Oelerich. On the validity of the einstein relation for disordered systems. 2010.

[48] SD Baranovskii, IP Zvyagin, H Cordes, S Yamasaki, and P Thomas. Percolation approach to hopping transport in organic disordered solids. *physica status solidi (b)*, 230(1):281–288, 2002.

[49] Vinay Ambegaokar, BI Halperin, and JS Langer. Hopping conductivity in disordered systems. *Physical review B*, 4(8):2612, 1971.

[50] H. C. F. Martens, I. N. Hulea, I. Romijn, H. B. Brom, W. F. Pasveer, and M. A. J. Michels. *Phys. Rev. B*, 67:121203, 2003.

[51] S. Ukai, H. Ito, and S i. Kuroda. *J. J. Appl. Phys.*, 43:366, 2004.

[52] S. Ukai, H. Ito, K. Marumoto, and S i Kuroda. *J. Phys. Soc. Jpn.*, 74:3314, 2005.

[53] A. S. Dhoot, G. M. Wang, D. Moses, and A. J. Heeger. *Phys. Rev. Lett.*, 96:246403, 2006.

[54] C. D. Dimitrakopoulos and P. R. L. Malenfant. *Adv. Mater.*, 14:99, 2002.

[55] W. D. Gill. *J. Appl. Phys.*, 43:5033, 1972.

[56] L. B. Schein, A. Rosenberg, and S. L. Rice. *J. Appl. Phys.*, 60:4287, 1986.

[57] B. H. Hamadani, C. A. Richter, D. J. Gundlach, R. J. Kline, I. McCulloch, and M. Heeneey. *J. Appl. Phys.*, 102:044503, 2007.

[58] J. Frenkel. *Phys. Rev.*, 54:647, 1938.

[59] L. Partmeier, R. Richert, and H. Bässler. *Synth. Met.*, 37:271, 1990.

[60] J. X. Mack, L. B. Schein, and A. Peled. *Phys. Rev. B*, 39:7500, 1989.

[61] L. B. Schein, D. Dalatz, and J. C. Scott. *Phys. Rev. Lett.*, 65:472, 1990.

[62] J. Cornil, D. Beljonne, J-P. Calbert, and J-L Brédas. *Adv. Mater.*, 13:1053, 2001.

[63] P. W. M. Blom, M. J. M. de Jong, and M. G. van Munster. *Phys. Rev. B*, 55:R656, 1997.

[64] H. C. F. Martens, H. B. Brom, and P. W. M. Blom. *Phys. Rev. B*, 60:R8489, 1999.

[65] H. C. F. Martens, P. W. M. Blom, and H. F. M. Schoo. *Phys. Rev. B*, 61:7489, 2000.

[66] A. J. Mozer, N. S. Sariciftci, A. Pivrikas, R. Österbacka, G. Juška, L. Brassat, and H. Bässler. *Phys. Rev. B*, 71:035214, 2005.

[67] Yu. N. Gartestein and E. M. Conwell. *J. Chem. Phys.*, 100:9175, 1994.

[68] Yu. N. Gartestein and E. M. Conwell. *Chem. Phys. Lett.*, 245:351, 1995.

[69] D. H. Dunlap, P. E. Parris, and V. M. Kenkre. *Phys. Rev. Lett.*, 77:542, 1996.

[70] P. E. Parris. *J. Chem. Phys.*, 108:218, 1998.

[71] S. V. Rakhmanova and E. M. Conwell. *Appl. Phys. Lett.*, 76:3822, 2000.

[72] P. E. Parris, V. M. Kenkre, and D. H. Dunlap. *Phys. Rev. Lett.*, 87:126601, 2001.

[73] C. Tanase, E. J. Meijer, P. W. M. Blom, and D. M. de Leeuw. *Phys. Rev. Lett.*, 91:216601, 2003.

[74] C. Tanase, P. W. M. Blom, and D. M. de Leeuw. *Phys. Rev. B*, 70:193202, 2004.

[75] M. C. J. M. Vissenberg and M. Matters. *Phys. Rev. B*, 57:12964, 1998.

[76] S. D. Baranovskii. *Phys. Stat. Sol.(a)*, 215:1700676, 2018.

[77] L. Demeyu, S. Stafström, and M. Bekele. *Phys. Rev. B*, 76:155202, 2007.

[78] P. M. Borsenberger, L. Pautmeier, R. Richert, and H. Bässler. *J. Chem. Phys.*, 94:5447, 1991.

[79] N. I. Craciun, J. Wildeman, and P. W. M. Blom. *Phys. Rev. Lett.*, 100:056601, 2008.

[80] Nicholas Metropolis and Stanislaw Ulam. The monte carlo method. *Journal of the American statistical association*, 44(247):335–341, 1949.

[81] Heinz Bässler. Charge transport in disordered organic photoconductors a monte carlo simulation study. *physica status solidi (b)*, 175(1):15–56, 1993.

[82] M Silver, KS Dy, and IL Huang. Monte carlo calculation of the transient photocurrent in low-carrier-mobility materials. *Physical Review Letters*, 27(1):21, 1971.

[83] G Schönherr, H Bässler, and M Silver. Dispersive hopping transport via sites having a gaussian distribution of energies. *Philosophical Magazine B*, 44(1):47–61, 1981.

[84] Ranko Richert, L Pautmeier, and H Bässler. Diffusion and drift of charge carriers in a random potential: Deviation from einsteins law. *Physical review letters*, 63(5):547, 1989.

[85] L Pautmeier, R Ichert, and H Bässler. Anomalous time-independent diffusion of charge carriers in a random potential under a bias field. *Philosophical Magazine B*, 63(3):587–601, 1991.

[86] H. Gould and J. Tobochnik. *An Introduction to Computer Simulation Methods*, chapter Numerical Integration and Monte Carlo Methods, pages 364–367. Addison-Wesley Publishing Company, Inc., second edition edition, 1996.

[87] M. P. Allen and D. J. Tildesley. *Computer Simulation of Liquids*. Oxford University Press, Inc., New York, 1987.

[88] Nicholas Metropolis, Arianna W Rosenbluth, Marshall N Rosenbluth, Augusta H Teller, and Edward Teller. Equation of state calculations by fast computing machines. *The journal of chemical physics*, 21(6):1087–1092, 1953.

[89] K. A. Fichthorn and W. H. Weinberg. *J. Chem. Phys.*, 95:1090, 1991.

[90] CW Gardiner. Handbook of stochastic methods for physics, chemistry and the natural sciences. 2004.

[91] M Boudart. From the century of the rate equation to the century of the rate constants: a revolution in catalytic kinetics and assisted catalyst design. *Catalysis letters*, 65(1-3):1–3, 2000.

[92] Erik K Grimmelmann, John C Tully, and Eugene Helfand. Molecular dynamics of infrequent events: thermal desorption of xenon from a platinum surface. *The Journal of Chemical Physics*, 74(9):5300–5310, 1981.

[93] Helmut Grubmüller. Predicting slow structural transitions in macromolecular systems: Conformational flooding. *Physical Review E*, 52(3):2893, 1995.

[94] Arthur. F Voter. A method for accelerating the molecular dynamics simulation of infrequent events. *The Journal of chemical physics*, 106(11):4665–4677, 1997.

[95] Arthur F Voter. Hyperdynamics: Accelerated molecular dynamics of infrequent events. *Physical Review Letters*, 78(20):3908, 1997.

[96] MM Steiner, P-A Genilloud, and JW Wilkins. Simple bias potential for boosting molecular dynamics with the hyperdynamics scheme. *Physical Review B*, 57(17):10236, 1998.

[97] S Pal and KA Fichthorn. Accelerated molecular dynamics of infrequent events. *Chemical Engineering Journal*, 74(1-2):77–83, 1999.

[98] Jee-Ching Wang, Somnath Pal, and Kristen A Fichthorn. Accelerated molecular dynamics of rare events using the local boost method. *Physical Review B*, 63(8):085403, 2001.

[99] S. D. Baranovskii. *Phys. Stat. Sol.(b)*, 251:487, 2014.

[100] A. Melianas and M. Kemerink. *Adv. Mater.*, 10:1806004, 2019.

[101] G. Schönherr, H. Bässler, and M. Silver. *Phys. Stat. Sol.(b)*, 44:47, 1981.

[102] C Tanase, EJ Meijer, PWM Blom, and DM De Leeuw. Unification of the hole transport in polymeric field-effect transistors and light-emitting diodes. *Physical review letters*, 91(21):216601, 2003.

[103] C Tanase, PWM Blom, and DM De Leeuw. Origin of the enhanced space-charge-limited current in poly (p-phenylene vinylene). *Physical Review B*, 70(19):193202, 2004.

[104] Feng Xu, Dong Qiu, and Dadong Yan. Disorder-tuned charge transport in organic semiconductors. *Applied Physics Letters*, 102(8):39, 2013.

[105] Simon Züfle, Nico Christ, Siegfried W Kettlitz, Sebastian Valouch, and Uli Lemmer. Influence of temperature-dependent mobilities on the nanosecond response of organic solar cells and photodetectors. *Applied Physics Letters*, 97(6):178, 2010.

[106] S Yogev, E Halpern, R Matsubara, M Nakamura, and Y Rosenwaks. Direct measurement of density of states in pentacene thin film transistors. *Physical Review B*, 84(16):165124, 2011.

[107] WD Gill. Drift mobilities in amorphous charge-transfer complexes of trinitrofluorenone and poly-n-vinylcarbazole. *Journal of Applied Physics*, 43(12):5033–5040, 1972.

[108] LB Schein, A Peled, and D Glatz. The electric field dependence of the mobility in molecularly doped polymers. *Journal of Applied Physics*, 66(2):686–692, 1989.

[109] Akiko Hirao, Hideyuki Nishizawa, and Masami Sugiuchi. Diffusion and drift of charge carriers in molecularly doped polymers. *Physical review letters*, 75(9):1787, 1995.

[110] Luca Fumagalli, Maddalena Binda, D Natali, Marco Sampietro, E Salmoiraghi, and P Di Gianvincenzo. Dependence of the mobility on charge carrier density and electric field in poly (3-hexylthiophene) based thin film transistors: Effect of the molecular weight. *Journal of Applied Physics*, 104(8):084513, 2008.

[111] WF Pasveer, Jeroen Cottaar, C Tanase, Reinder Coehoorn, PA Bobbert, PWM Blom, DM De Leeuw, and MAJ Michels. Unified description of charge-carrier mobilities in disordered semiconducting polymers. *Physical review letters*, 94(20):206601, 2005.

[112] Nguyen Van Lien and BI Shklovskii. Hopping conduction in strong electric fields and directed percolation. *Solid State Communications*, 38(2):99–102, 1981.

[113] EI Levin, VL NUGEN, and BI Shklovskii. Hopping electrical conduction in strong electric fields-anumerical machine experiment. *Sov Phys Semicond*, 16(5):523–527, 1982.

[114] DI Aladashvili, ZA Adamiya, KG Lavdovskii, EI Levin, and BI Shklovskii. Negative differential resistance in the hopping conductivity region in silicon. *JETP Letters*, 47(8):466–469, 1988.

[115] AV Nenashev, F Jansson, SD Baranovskii, R Österbacka, AV Dvurechenskii, and F Gebhard. Hopping conduction in strong electric fields: negative differential conductivity. *Physical Review B*, 78(16):165207, 2008.